

# Methods and results of an automatic analysis of a complete sample of *Swift*-XRT observations of GRBs.

P.A. Evans<sup>1\*</sup>, A.P. Beardmore<sup>1</sup>, K.L. Page<sup>1</sup>, J.P. Osborne<sup>1</sup>, P.T. O’Brien<sup>1</sup>,  
 R. Willingale<sup>1</sup>, R.L.C. Starling<sup>1</sup>, D.N. Burrows<sup>2</sup>, O. Godet<sup>1</sup>, L. Vetere<sup>2</sup>,  
 J. Racusin<sup>2</sup>, M.R. Goad<sup>1</sup>, K. Wiersema<sup>1</sup>, L. Angelini<sup>3</sup>, M. Capalbi<sup>4</sup>,  
 G. Chincarini<sup>5,6</sup>, N. Gehrels<sup>3</sup>, J.A. Kennea<sup>2</sup>, R. Margutti<sup>5,6</sup>, D.C. Morris<sup>3,7</sup>,  
 C.J. Mountford<sup>1</sup>, C. Pagani<sup>1</sup>, M. Perri<sup>4</sup>, P. Romano<sup>8</sup>, N. Tanvir<sup>1</sup>

<sup>1</sup> *X-ray and Observational Astronomy Group, Department of Physics and Astronomy, University of Leicester, LE1 7RH, UK*

<sup>2</sup> *Department of Astronomy and Astrophysics, Pennsylvania State University, 525 Davey Lab, University Park, PA 16802, USA*

<sup>3</sup> *NASA/Goddard Space Flight Center, Greenbelt, MD 20771, USA*

<sup>4</sup> *ASI Science Data Center, ASDC c/o ESRIN, via G. Galilei, 00044 Frascati, Italy*

<sup>5</sup> *INAF, Osservatorio Astronomico di Brera Via E. Bianchi 46, I-23807, Merate (LC), Italy*

<sup>6</sup> *Università degli Studi di Milano-Bicocca, Dipartimento di Fisica, Piazza della Scienza 3, 20126, Milano, Italy*

<sup>7</sup> *Center for Nuclear Studies, Department of Physics, The George Washington University, Washington, DC 20052, USA*

<sup>8</sup> *INAF, Istituto di Astrofisica Spaziale e Fisica Cosmica, Via U. La Malfa 153, I-90146 Palermo, Italy*

Accepted Received

## ABSTRACT

We present a homogeneous X-ray analysis of all 318 Gamma Ray Bursts detected by the X-ray Telescope on the *Swift* satellite up to 2008 July 23; this represents the largest sample of X-ray GRB data published to date. In Sections 2–3 we detail the methods which the *Swift*-XRT team has developed to produce the enhanced positions, light curves, hardness ratios and spectra presented in this paper. Software using these methods continues to create such products for all new GRBs observed by the *Swift*-XRT. We also detail web-based tools allowing users to create these products for any object observed by the XRT, not just GRBs. In Sections 4–6 we present the results of our analysis of GRBs, including probability distribution functions of the temporal and spectral properties of the sample. We demonstrate evidence for a consistent underlying behaviour which can produce a range of light curve morphologies, and attempt to interpret this behaviour in the framework of external forward shock emission. We find several difficulties, in particular that reconciliation of our data with the forward shock model requires energy injection to continue for days to weeks.

**Key words:** Gamma rays: bursts – X-rays: observations – Methods: data analysis – Catalogues

## 1 INTRODUCTION

The *Swift* satellite (Gehrels et al. 2004) has revolutionised our understanding of Gamma Ray Bursts (GRBs), and the X-ray telescope (XRT, Burrows et al. 2005) has played a major role in this process. For example, XRT data have shown that the early X-ray light curve is much more complex than originally thought, often containing a shallow-decay ‘plateau’ phase interpreted variously as energy injection in a forward shock (Zhang et al. 2006), reverse shock emis-

sion (Uhm & Beloborodov 2007) and dust-scattering of the prompt GRB emission (Shao & Dai 2007; although this has recently been ruled out by Shen et al. 2008). The high impact of the XRT has been made possible by *Swift*’s unique rapid slewing capability: the large field-of-view Burst Alert Telescope (BAT, Barthelmy et al. 2005a) detects GRBs, and *Swift* then automatically repoints itself so that the narrow-field XRT and UV/Optical Telescope (UVOT; Roming et al. 2005) can observe the new burst within  $\sim 60$ – $90$  seconds of the trigger. The XRT has detected  $\sim 95\%$  of *Swift*-BAT triggered GRBs, most of those within minutes of the trigger, usually providing the most accurate rapidly available

\* pae9@star.le.ac.uk

localisation of the GRB and enabling early follow up with ground telescopes. *Swift*'s X-ray afterglow light curves and spectra, starting at typically <100 s have been crucial to the discoveries made by *Swift* (see Zhang et al. 2007; O'Brien et al. 2006; Willingale et al. 2007, for reviews of the impact of *Swift* on GRB science).

Because GRBs fade rapidly, follow-up observers need to make quick decisions about whether or not to invest observing time on a given burst. This is especially true of potentially unusual bursts, such as high-redshift candidates or under-luminous GRBs. Thus it is desirable for GRB data to be rapidly available and analysed quickly, reliably and ideally in a uniform manner. *Swift* data are downlinked many times per day and are immediately processed by the Swift Data Center (SDC) at Goddard Space Flight Center and made available to the public via the SDC and data centres in the UK and Italy, minutes to hours after the downlink. We (the *Swift*-XRT team) have developed software which, when data arrive at the UK Swift Science Data Centre (UKSSDC), automatically determines the best possible XRT GRB position and builds X-ray light curves and spectra; the results are then published on the internet. This provides a homogeneously generated catalogue of data, which we detail and discuss in this paper (Section 4), following a description of the software.

There are two types of GRB follow-up data telemetered from *Swift*: TDRSS and Malindi data (described below). Initially, our software only worked with Malindi data, however in 2008 February we modified our ground-based software to work with TDRSS data as well (Evans et al. 2008a); this provides better positions, positions of fainter GRBs, and more reliable light curves and spectra than those produced on board (although these should not be used for scientific analysis).

### 1.1 TDRSS data

When *Swift* first detects and observes a GRB, some data are immediately telemetered to the ground via NASA's Tracking and Data Relay Satellite System (TDRSS). Among these 'TDRSS data' are the XRT Single Pixel Event Report ('SPER') data. *Swift*'s XRT selects between Windowed Timing (WT, high time resolution but only 1-D spatial information) and Photon Counting (PC, lower time resolution but full spatial information) modes automatically, based on the count rate in the central portion of the CCD (Hill et al. 2005). When the XRT enters PC mode during the first look at a new GRB, event lists containing every single-pixel (grade 0) event above 0.55 keV detected within the central 200×200 pixel region, the SPER data, are delivered to the XRT team via the GCN system every 2 minutes until *Swift* slews away from the burst (up to  $\sim 2$  ks after the trigger). It must be noted that while we have made our products as reliable as possible, SPER data are not fully calibrated and the light curves and spectra are intended as quick-look products; they should not be used for scientific analysis.

### 1.2 Malindi data

'Malindi data' are available several hours after a GRB trigger and comprise the full observation dataset. Nine or ten

times per day, *Swift* passes over the Malindi ground station in Kenya and downlinks the data buffered on board. These are then processed at the SDC and delivered to archives in the US, UK and Italy, typically 90–120 minutes after the Malindi downlink. *Swift* also observes GRBs which did not trigger the BAT, but are uploaded as Targets of Opportunity (ToOs). For these bursts only Malindi data are telemetered.

Malindi data are grouped into *observations*, usually one per day, each with a unique ObsID. A single observation may contain many *snapshots*; that is, pointings toward the source, since *Swift* is in a low Earth orbit and thus its targets get occulted by the Earth once per orbit. The terminology *observations* and *snapshots* is standard *Swift* parlance<sup>1</sup>, and will be used throughout this paper.

### 1.3 GRB afterglow models

In this paper we introduce tools to produce high-precision positions, light curves and spectra from XRT data, and describe the automatic application of these tools to GRBs. This gives us a catalogue of results for all 318 GRBs detected by the *Swift*-XRT up to GRB 080723B, and we discuss the implications for afterglow science from this analysis. While our dataset can be used to test any models for GRB emission, we do this in the context of the fireball model (e.g. Rees & Mészáros 1994, Sari, Piran & Narayan 1998), which is the current consensus model.

In this model the GRB progenitor launches highly relativistic jets of material in a series of shells, of differing bulk Lorentz factors. Internal collisions (i.e. within the jet) between shells cause shocks which radiate the GRB 'prompt emission'. The X-ray data presented in this paper may contain the tail of this prompt emission, however it is thought to arise predominantly from the afterglow. This is emission from an external shock which forms where the jet is decelerated by the circumburst medium, and which propagates into that medium, cooling by synchrotron radiation as it does so. See Piran (2005) for a comprehensive review of the fireball model.

### 1.4 Layout of the paper

This paper is laid out thus:

- §2 (pp 3–10): XRT automatic analysis tools:
  - §2.1 (pp 3–5): Spectra.
  - §2.2 (pp 5–7): Positions.
  - §2.3 (pp 7–10): Light curves & hardness ratios.
- §3 (pp 10–12): Web tools to analyse any XRT source
- §4 (pp 12–17): Results of XRT GRB analysis
- §5 (pp 17–22): A canonical X-ray light curve?
- §6 (pp 22–23): Understanding the X-ray afterglow

Throughout this paper, errors quoted in all tables are at the 90% confidence level. Error bars on data in all figures are 1- $\sigma$  uncertainties.

<sup>1</sup> <http://heasarc.gsfc.nasa.gov/docs/swift/archive/archiveguide1/node3.html>

## 2 AUTOMATED DATA PRODUCTS

We have developed software to produce three types of data products: ‘enhanced’ positions, light curves and spectra. The spectra were announced in Evans et al. (2008b), and are presented in Section 2.1. The method of enhancing XRT positions has been previously documented (Goad et al. 2007; hereafter G07), however we have improved the algorithm, resulting in a factor of  $\sim 2$  improvement in precision (Section 2.2). The light curve code has been published by Evans et al. (2007) and only minor modifications are described here (Section 2.3) along with details of new functionality which has been made available to the user. We also describe automatic light curve fitting, in Section 2.4.

For GRBs which trigger the BAT, these products are created automatically while GRBs observed as ToOs by *Swift* must be manually registered for automatic analysis. This is usually done at the time of the ToO upload, so the data products are available as rapidly as for BAT-detected bursts. Before any of these products are produced, the XRT data are reprocessed at the UKSSDC using the latest release of the XRTPIPELINE tool<sup>2</sup>. This may differ from the version used at the SDC to create the cleaned event lists available from the quick-look and archive sites. When a new version of the *Swift* software or calibration is released, we carry out some tests to confirm our product-generation code works reliably with the new release and then switch to using the latest version. We do not however reprocess earlier GRBs with the new release of the software.

### 2.1 Spectra

To create a spectrum from Malindi data, an image is formed from the first available PC mode event list, and XIMAGE is used to identify any sources. The brightest source within the BAT error circle (or equivalent for bursts detected by other missions) is assumed to be the GRB, and the sky-coordinate point-spread-function (PSF) fit routine developed for the position enhancement (Section 2.2) is used to determine the source position in the XRT astrometric frame. We use only observations which begin within 12 hours of the first one. Each observation is subdivided into snapshots, and these may be further subdivided into times where pile up – in which multiple photons are registered as single events – is or is not an issue. To identify intervals affected by pile up we first search for times where the count rate within a 30 pixel radius circular region centred on the source is above 0.6 counts  $s^{-1}$  in PC mode or 150 counts  $s^{-1}$  in WT mode. In PC mode we then obtain the PSF profile of the source and compare it to the calibrated, non-piled-up PSF (Moretti et al. 2005). This indicates not only whether the source is piled up, but the radius out to which pile up is a factor,  $R_p$ . If the source is piled up, we use an annular extraction region to obtain source data, with an inner radius  $R_p$ . For WT mode data we assume the data are piled up whenever the count rate exceeds 150 counts  $s^{-1}$  and use a box annulus extraction region, where the inner radius is that necessary to keep the measured count rate below this level. For alternative

methods of identifying and eliminating pile up, see Vaughan et al. (2006) or Romano et al. (2006). Where the data are not piled up, we use a circular (rectangular) extraction region for PC (WT) mode. For each snapshot we determine the mean source count rate and use this to choose the radius of the source extraction region, according to Table 1; this maximises the signal-to-noise ratio of the spectrum and is identical to the method used for light curves.

Once the data have been divided into time intervals – each with a source extraction region – we generate a source spectrum, source event list and full frame event list for each one. Using the full frame event lists we create an exposure map and (using this and the source spectrum) an Ancillary Response File (ARF) per interval. We then combine the source event lists from each time interval using EXTRACTOR to get a single source spectrum. We similarly combine the ARFs, using the ADDARF tool; each ARF is weighted according to the proportion of counts in the total source spectrum which came from this time interval. This is not the same as extracting a single spectrum, exposure map and ARF from an event list spanning multiple snapshots, since in that case the weighting of the snapshots is determined by the exposure map (hence exposure in each orbit), but GRBs are not of constant brightness. The ARFs must be correctly weighted since the proximity of the source to the bad columns on the CCD, and hence the effective detector area, will change from one snapshot to the next. That weighting by counts is the correct approach is readily demonstrated: the true number of counts from the source ( $C_t$ ) is simply the measured counts ( $C_m$ ) multiplied by some correction factor ( $Q$ , implicit in the ARF) which reflects counts lost to (for example) the bad columns. If there are multiple snapshots, the true total number of counts is  $C_t = \Sigma(C_m Q) = \Sigma C_m \times \frac{\Sigma(C_m Q)}{\Sigma C_m}$ , i.e. a the overall correction factor (or ARF) is the count-weighted mean of the individual ARFs.

The BACKSCAL keyword must be set for the source spectrum, for use by XSPEC (Arnaud 1996). Since this can be different for each time interval included (the source region size is variable), this is taken as the weighted mean of the BACKSCAL values from the individual source spectra extracted per time interval, weighted according to the number of counts in those spectra.

A background spectrum is also produced. In WT mode background data are extracted from the entire window, excluding a 120-pixel (283'') wide box centred on the source. In PC mode the background region is an annulus with an inner radius of 60 pixels (142'') and an outer radius of 110 pixels (260''); if this extends beyond the edge of the detector window it is shifted accordingly; the inner circle of course remains centred on the source. To create the background spectrum we do not subdivide the data more finely than the observations. For each observation we identify any sources in the background region using XIMAGE and exclude those areas from the extraction region. The individual observations’ background spectra are then combined as for the source spectra.

The spectra thus produced were extensively verified by the *Swift*-XRT team. Our test procedure consisted of producing spectra both manually and using this software. These were both fitted with the same model and the best-fitting parameters compared. We did this for more than thirty spectra and in every case, the difference between the parameters

<sup>2</sup> Part of the XRT software, distributed with the HEASOFT package: <http://heasarc.gsfc.nasa.gov/lheasoft/>

Count rate $R$ (counts $\text{s}^{-1}$ )	Source radius in pixels ( $''$ )
$R > 0.5$	30 (70''8)
$0.1 < R \leq 0.5$	25 (59''0)
$0.05 < R \leq 0.1$	20 (47''2)
$0.01 < R \leq 0.05$	15 (35''4)
$0.005 < R \leq 0.01$	12 (28''3)
$0.001 < R \leq 0.005$	9 (21''2)
$0.0005 < R \leq 0.001$	7 (16''5)
$R \leq 0.0005$	5 (11''8)

**Table 1.** Source extraction radii used for given PC-mode count rates.  $R$  is the measured, uncorrected count rate. This table is reproduced from Evans et al. (2007). Values are given in XRT pixels and arcseconds: one XRT pixel corresponds to 2.36''.

from the automatic and manual spectra were much less than the uncertainties on those parameters. We therefore conclude that the automatic generation of spectra is reliable.

Spectra are automatically created for each new GRB observed by the XRT, and are updated as new data are received. The results are posted online at [http://www.swift.ac.uk/xrt\\_spectra](http://www.swift.ac.uk/xrt_spectra) in postscript and GIF format. We also provide a tar archive for download which contains the source and background spectra and the ARF file necessary for users to fit the data themselves<sup>3</sup>. The results of automatic spectral fitting (below) are available from the same website.

Since the creation of an XRT spectrum is useful for any target observed by *Swift*, not just GRBs, we have created a tool to allow users to build spectra using our software for any object observed by the XRT, see Section 3.

### 2.1.1 Automatic spectral fitting

After creating the spectra, our software automatically models them with an absorbed power-law. Fitting is performed using the  $X$ -statistic in XSPEC 12; we first apply a `group min 1` command in GRPPHA (necessary for XSPEC to correctly calculate the  $C$ -statistic, Arnaud, private communication). A Response Matrix File (RMF) must also be used to fit the data; the XRTMKARF task used to create the ARF files when compiling the spectrum selects the appropriate RMF from the Calibration Database (CALDB), and we supply this file to XSPEC. For a review of the XRT spectral response see Godet et al. (2009).

The `NH_FTOOL`<sup>4</sup> is used to determine the Galactic column density in the direction of the burst using the map from Kalberla et al. (2005), and the spectrum is fitted in with the model `phabs*phabs*pow`. The first absorption component is frozen at the Galactic value and the second is free to vary. The abundances are fixed at those from Anders & Grevesse (1989). A tcl script (SHAKEFIT) developed by Simon Vaughan (Hurkett et al. 2008; see their section 3.2.2), which uses the `ERROR` command to detect and recover from local minima is then used to find the true global best fit. If

a spectroscopic redshift has been reported in the literature, the XRT team can supply this and the second absorption component in the model is replaced with a `zphabs` component, with the redshift frozen at that reported. The 90% confidence intervals of each free parameter are found using the `ERROR` command in XSPEC which steps the parameter of interest and repeats the fit until the  $C$ -statistic has worsened by 2.706 compared to the best fitting value. The observed and unabsorbed 0.3–10 keV flux for the model are also obtained from XSPEC, and the former of these is used to determine the count-rate to flux conversion factor for the GRB. This is then automatically applied to the count-rate light curve to produce a flux units version.

Very occasionally (< 1% of the time) XSPEC finds a local minimum of the  $C$ -statistic rather than the best fit. This is usually immediately obvious from the plot presented on the web pages, or because the best-fitting values are unusual (the probability distributions in Section 4 give a quantitative definition of ‘unusual’). In this case a member of the XRT team will determine fitting parameters and supply these to the software, which will then repeat the fit, using these parameters as the initial values. When new data arrive and the spectrum is updated, the manually-supplied values will again be used as the initial values for the fit. All of the results presented in this paper have been verified by visual inspection, and the few with poor fits corrected.

The results of these fits are presented in a table on the web page for each GRB, accessible via [http://www.swift.ac.uk/xrt\\_spectra](http://www.swift.ac.uk/xrt_spectra).

### 2.1.2 Time resolved spectra

Only time-averaged GRB spectra are produced automatically, however the software allows for arbitrary time intervals to be specified, over which the spectra can be compiled: on the web page presenting the spectra for each GRB is an option to ‘Build time-sliced spectra’. Following this link users can specify times of interest and their spectra will be built. If a member of the XRT team decides that a particular time-resolved spectrum should be made available along with the time-averaged spectra for a GRB they will add that spectrum to the main spectrum results page of the burst.

### 2.1.3 Application to SPER data

Spectra can also be obtained from the rapidly available SPER data using this software. Note however that the SPER data have not been fully calibrated and SPER spectra should be used as a quick-look product, rather than for scientific analysis. Additional processing of the SPER data is necessary to prepare them for spectral extraction. All SPER messages are combined into a single file and a value of 100 is subtracted from the PHA (uncalibrated event energy) column, (this was added on board to avoid negative values being obtained after bias subtraction). A ‘Grade’ column is then added (all events in SPER are grade 0). The tool XRT-CALCPI is executed to create a PI (calibrated event energy) column from which spectra can be built. At this point a spectrum can be extracted. For SPER data we do not subdivide the data into intervals since they only cover a single snapshot. If the data are piled up at any point an annular

<sup>3</sup> Users also require an RMF file, which can be found in the Calibration Database (CALDB, <http://swift.gsfc.nasa.gov/docs/heasarc/caldb/swift/>).

<sup>4</sup> <http://heasarc.gsfc.nasa.gov/lheasoft/ftools>

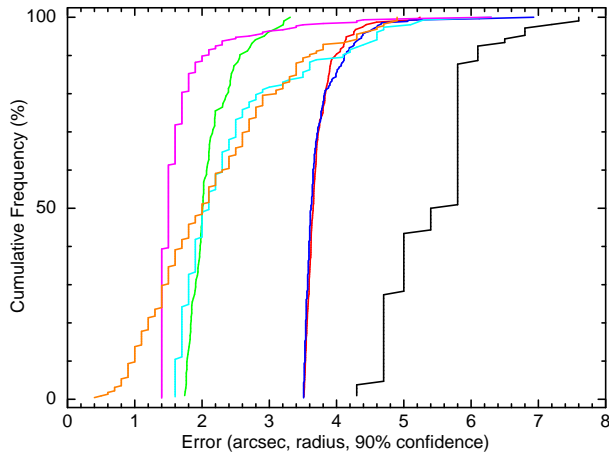


**Figure 1.** The cumulative frequency of the 90% confidence error radius for XRT GRB positions determined using different techniques.

*Black:* on-board positions, *Red:* positions from SPER data derived using a PSF fit, *Green:* enhanced SPER positions *Blue:* ‘refined’ positions obtained from Malindi data using `XRTCENTROID`, *Cyan:* enhanced Malindi positions using the G07 algorithm, *Magenta:* The enhanced Malindi positions using the algorithm presented here, *Orange* positions from Butler et al. (2007). For the latter, we have removed positions with errors  $> 5''$  before calculating the distribution since these occur when there is insufficient data to correct the position and bias the plot towards larger uncertainties than are found when positions are successfully improved.

source region is used for all of the SPER data. This means that we have only one source spectrum and ARF. Fitting is performed as for Malindi data (see Section 2.1.1). Because SPER data only include events above 0.55 keV, it is harder to constrain the absorbing column.

## 2.2 ‘Enhanced’ positions

The technique of ‘enhancing’ XRT positions from Malindi data by determining the spacecraft attitude from images taken with the Ultra-violet/Optical Telescope (UVOT) was first presented in G07. This technique produced positions with error radii typically 40% smaller than the ‘standard’ positions determined using the spacecraft attitude information determined from the on-board star trackers. With all available data, the G07 positions were a little less precise than those determined by Butler et al. (2007) using serendipitous X-ray sources to find the correction; but while the latter typically have large initial errors and only offer improvement over the ‘standard’ positions  $\sim 1$  day after the trigger, the G07 positions were available within hours of a trigger.

We have made significant revisions to the enhancement process, reducing the error radii by a further 30–50%. These positions are still available within hours of a trigger, and now in  $\sim 75\%$  of cases give better precision than those of Butler et al. (2007), and are the most accurate XRT positions available. Furthermore, we have developed a version of this algorithm applicable to the SPER data, reducing the error radius of the prompt localisations by up to 60%. These positions are typically available 10–20 minutes after a GRB trigger. The relative precisions of the different XRT positions is shown in Fig. 1.

Although we concentrate here on the improvements made since G07, it is necessary to briefly summarise the algorithm used there, to give the context for the improvements. For full details, see G07.

To produce an enhanced XRT position using the G07 method, the available data are first split into ‘overlaps’ – times of simultaneous XRT (PC mode) and UVOT ( $v$ -band) data. For each such overlap a detector co-ordinate X-ray image is produced and the GRB localised therein. This is done using a PSF-fit which corrects for the effects of the bad columns on the CCD. The position is then transformed into an equivalent position in UVOT detector co-ordinates, and thence into UVOT sky co-ordinates, using the attitude information from the star trackers on-board *Swift*. An image of the UVOT field of view is also constructed, with the sky co-ordinates calculated using the same attitude information. Serendipitous sources in the UVOT image are matched to the USNO-B1 catalogue, giving the quaternion needed to correct the image’s attitude. This quaternion is then applied to the previously calculated XRT GRB position in UVOT sky co-ordinates, to give the ‘enhanced’ XRT position for that overlap. This process is performed for every available overlap, the weighted mean of all overlaps is then calculated and systematic errors are added to give the enhanced XRT position of the GRB. Since G07, this process has been improved in the following ways:

- 1) The XRT-UVOT map, originally only derived for the UVOT  $v$  filter, has been extended to all UVOT filters. We have found, however, that limiting the software to use just  $v$ ,  $b$  and white filters gave the best results<sup>5</sup>.

- 2) Multiple observations can now be used, whereas originally only a single one was used (recall that a single observation can still contain many snapshots). We do not include all available observations as the X-ray afterglow will generally be too faint to detect in a single overlap after  $\sim 12$ –24 hours and the inclusion of more observations slows the enhancement process significantly. Instead we use any observation which began within 12 hours of the first. Since *Swift*’s automatic response to a new GRB is a 60-ks observation, in many cases this still means only the first observation is used and this change to the code then has no impact. It is not uncommon however, for the automatic observations to be interrupted, either manually (to avoid overheating the XRT, Kennea et al. 2005) or automatically (i.e. *Swift* detects another GRB), in which case multiple observations are suitable for use in the enhancement process.

- 3) We have substantially re-written the PSF fitting code used to determine the position of the object on the XRT. The  $C$ -statistic was previously calculated by comparing the number of counts expected under the PSF with those in the data (Cash 1978). It is now calculated by comparing the value of each pixel in the image with that predicted by the model PSF. Additionally, the fit was previously performed in XRT detector co-ordinates (so that the positions of the bad columns on the CCD caused by the micrometeoroid impact, [Abbey et al. 2005], were known), but it is now performed in sky co-ordinates, using exposure maps to compensate for bad columns or hot pixels.

<sup>5</sup> This is probably because the USNO-B1 catalogue is an optical catalogue so matching UV images to it is error prone.

These changes improve the enhanced positions for several reasons:

(i) Although *Swift* does not remain perfectly steady while on-source, the star trackers provide precise *relative* attitude information. Thus, while the detector-coordinate image may be distorted by spacecraft motion, the sky image will not be, and the PSF fit in this co-ordinate system will be more precise.

(ii) UVOT data are corrected for the spacecraft movement before being downlinked. Every photon detected is shifted to the position it would have had if the spacecraft had not moved since the image exposure began. As a result, the effective time of the UVOT image is the start of the exposure. In contrast, a detector-coordinate XRT image has no such correction and its effective time is the mean photon arrival time within the image. Thus the aspect solution determined from the UVOT image is actually for a different time, and possibly slightly different attitude, than that at which the GRB position was measured on the XRT detector. This was a contributor to the empirically-derived systematic error in G07, see their section 6. XRT sky-coordinate images are built using the sky-coordinate position of each event in the event lists which were calculated on an event-by-event basis using the spacecraft attitude information, and are thus analogous to the UVOT sky images. The sky co-ordinate position of an object is therefore stable through a snapshot, allowing the POINTXFORM tool to be used to convert the measured sky-coordinate position into XRT detector co-ordinates at the start of the UVOT exposure, so the aspect solution and corrected position can be made contemporaneous.

(iii) Because the GRB position in XRT sky co-ordinates is stable within a snapshot, we no longer need strictly simultaneous XRT and UVOT data. Instead, we use the longest XRT exposure possible without using the same data in multiple overlaps, up to a maximum duration of an entire snapshot. For example, if a snapshot contains two UVOT images, one in the *v* filter and one in white, the XRT data will be split in two – the division occurring between the UVOT exposures. An XRT position will be found for each part of the snapshot and enhanced using the approximately contemporaneous UVOT data. On the other hand, if the snapshot contains *v* and uvm2 filter UVOT images, the XRT position will be determined using the entire snapshot of data, and then enhanced using the *v* image (we do not use the UV filter images to enhance positions, see above). This means that overlaps can be used where the XRT source is fainter than was possible in the previous version.

4) We have supplemented the improvement to the PSF fitting code by deducing PSF profiles of piled up sources, in addition to the profile in the CALDB (Moretti et al. 2005). For each XRT image we perform the PSF fit 6 times; once with each PSF profile. The fit with the lowest *C*-statistic is then assumed to give the most accurate position of the GRB.

To determine the piled-up PSF profiles we identified objects observed by *Swift* in PC mode which were piled up, away from the bad columns on the detector and approximately constant in brightness. We then obtained the PSF profile using XIMAGE and modelled it with a King–Gaussian function; the latter component reflecting the counts lost to pile up. The centre of the Gaussian profile was frozen at zero

Count rate (counts s <sup>-1</sup> )	King $R_c$ ( $''$ )	King $\beta$	$N_{\text{gaus}}$	Gaus $\sigma$ ( $''$ )
0.90	4.654	3.321	0.522	3.019
1.36	6.578	3.627	0.504	4.139
2.59	6.620	3.606	0.634	3.990
5.15	12.790	3.505	1.039	6.411
8.58	19.880	3.889	1.245	6.682

**Table 2.** PSF profiles for piled-up sources of different count rates. The profile is defined as  $\text{King}(R_c, \beta) - N_{\text{gaus}}\text{Gaus}(\sigma)$ .

(i.e. the centre of the PSF). The PSF profiles thus deduced are given in Table 2, defined as  $\text{King}(R_c, \beta) - N_{\text{gaus}}\text{Gaus}(\sigma)$ , where  $N_{\text{gaus}}$  represents the relative normalisation of the Gaussian component compared to the King component.

5) *Swift* data are normally delivered to the data centres when the data from all three instruments have been processed. However, during the first observation of a new GRB special obsIDs are created which contain just the XRT or UVOT data. These obsIDs – which end with ‘991’ for XRT or ‘992’ for UVOT – are usually available before the instrument-combined dataset. We have modified our software to use these special obsIDs, rather than waiting for the ‘all-in-one’ obsID data. This means that the positions are available up to half an hour earlier than previously.

After implementing these changes, we ran the code for every GRB observed by *Swift*, obtaining positions for 83%. Following G07, we compared these positions to the UVOT positions for those GRBs which were detected by that instrument (taken from the GCN circulars). For each burst with an enhanced XRT position and a UVOT position, we calculated the angular distance between these positions,  $R$ . We also calculated the combined 90% confidence error in the enhanced XRT and UVOT positions  $E_t = \sqrt{E_{\text{xrt\_enh}}^2 + E_{\text{uvot}}^2}$ . If  $R/E_t \leq 1$  the positions agree. If we included only the statistical errors and the systematic uncertainty arising from the XRT-UVOT map (1.3 $''$ ), we found that fewer than 90% of enhanced positions agreed with the UVOT positions, as G07 did. However, we needed to increase our systematic only marginally, to 1.36 $''$ , to achieve 90% agreement, whereas in G07 we needed a systematic of 1.5 $''$ . Our error radii are now  $\leq 1.5''$  50% of the time, and  $\leq 2.0''$  90% of the time. As Fig. 1 shows, these represent the best available XRT positions for the majority of GRBs.

The enhanced positions of all GRBs observed by *Swift* are available online at [http://www.swift.ac.uk/xrt\\_positions](http://www.swift.ac.uk/xrt_positions). When a new GRB is observed by *Swift*, an enhanced position is automatically produced and added to this page as soon as the necessary data are available. A GCN circular is also dispatched to advise the community of the position, since in the majority of cases this represents the best available position at this time and its rapid dissemination helps follow-up astronomers. If no XRT counterpart was identified in the TDRSS data this circular is not automatically dispatched. Under such circumstances, the software enhances the position of the brightest source within the BAT error circle; experience has shown that this is not always the GRB. Positions will nonetheless be posted online even in these circumstances. As *Swift* continues to observe the new GRB, the position

is updated with each new delivery of data. These updates appear at the above URL, but are not disseminated by other means.

Enhanced positions cannot be produced for all GRBs. If the burst is too faint to be seen by XRT in a single snapshot the position cannot be found. Also, sometimes the UVOT-SKYCORR tool is unable to find sufficient matches between UVOT field stars and USNO-B1 entries to return an aspect solution. Full details of other, less common, reasons a position is not produced were given in G07. To date 83% of GRBs detected by the XRT have enhanced positions. If we consider only BAT-triggered GRBs and exclude those where the UVOT was not in operation, this number rises to 90%.

Since many *Swift* non-GRB observations use the XRT to determine the position of a newly-discovered (or known, but poorly localised) object, we have developed a web tool to apply the position enhancement to user-selected non GRB objects. See Section 3 for details.

### 2.2.1 Application to SPER data

We can also apply the enhancement software to the SPER data. This was not previously possible because the XRT and UVOT data had to be simultaneous – for the limited TDRSS data this is often not the case, or requires the XRT SPER data to be filtered on time; given that SPER data contain substantially fewer events than Malindi data this made determining the XRT position unreliable. Since the modification to the PSF fit (point 3 above) removed the simultaneity requirement, we can enhance positions using TDRSS data. The process is almost identical to the Malindi data process described above, with the following differences:

(i) Since we always have just one snapshot, the XRT position is determined once, using all available data, and corrected multiple times; the statistical uncertainty in the XRT position is thus only applied once, at the end of the process.

(ii) We use the UVOT source lists telemetered via TDRSS, rather than the UVOT images, to determine the aspect solution.

Point (ii) arises because the TDRSS source lists are calculated on board from the full field-of-view image, however only a sub-image is downlinked; thus the on-board source list provides more matches to the USNO-B1 catalogue and a solution can be found more frequently. The source localisation performed on board is less sophisticated than is done on the ground, increasing the systematic uncertainty needed to achieve 90% agreement between our ‘enhanced SPER’ positions and the UVOT positions to  $1.7''$ , compared to  $1.36''$  for Malindi data. In 2008 October the filter sequence followed by UVOT in its initial burst response was changed to use the *U* filter for the second exposure rather than the White filter (the *U* filter has a lower background rate and is thus expected to find more afterglows than the White filter). We do not currently have sufficient data to evaluate the effect of this change on the enhanced SPER positions directly, however using historical Malindi data and *U*-filter images taken later in the observations, we determined that our systematic error needed to increase from  $1.7''$  to  $1.9''$  if the *U* filter images were to be used. On the other hand, not using the *U* filter TDRSS data would mean most enhanced SPER positions would be based on only one UVOT aspect

solution and consequently have errors typically  $0.2''$  larger than hitherto. They would also be produced longer after the burst as they would need to wait for the third UVOT exposure. Thus, on 2008 November 13 we modified the SPER position enhancement to use the *U* filter images and a  $1.9''$  systematic error.

## 2.3 Light curves and hardness ratios

The software we used to generate automatic XRT light curves and hardness ratios of GRBs was previously presented in Evans et al. (2007). This software has received minor revision, which we describe briefly below, along with a significant increase in functionality (Evans et al. 2008b).

### 2.3.1 Modifications to the software

1) Originally, the XRTCENTROID tool was used to determine the source position in XRT co-ordinates. When the bad columns on the CCD intersected the source PSF, this could result in an inaccurate position. This in turn could cause the pile-up or bad column correction factors to be incorrect. We have altered the software to use the PSF fit instead, since this gives accurate positions despite the bad columns. This made small changes to a few light curves.

2) In the original version of the software, the final bin was always plotted as an upper limit if it contained fewer than 15 counts (i.e. the errors could not be considered Gaussian). In many cases the source is clearly detected at these times and an upper limit is inappropriate. In 2007 June we modified the software such that, if the final bin contains fewer than 15 counts, the Bayesian approach of Kraft, Burrows & Nousek (1991) is used to determine whether the source is detected at the  $3\text{-}\sigma$  level. If it is, the Bayesian method is then used to determine the  $1\text{-}\sigma$  confidence interval on the count rate, and this is plotted as a point on the light curve. Otherwise an upper limit is plotted as previously. Subsequent data deliveries are still included in this final bin until it contains at least 15 counts, at which point the errors on the bin are calculated using Gaussian statistics and a new bin is begun.

3) In 2008 July we fixed a minor bug in the software, which occasionally caused Good Time Intervals (GTIs: times during which XRT was collecting data) containing no events and lying between light curve bins to be ignored. This fix made almost no difference to the light curves.

4) We made two other minor changes in 2008 July, of a cosmetic nature. First, we amended the definition of the actual ‘time’ value of a bin to be ten to the power of the mean of the logarithms of the event times within the bin, rather than the linear mean. This makes light curve plots reflect more accurately the distribution of counts in a bin<sup>6</sup>. Second, at the end of an observing snapshot, any events which are not yet sufficient to form a light curve bin are either appended to the previous bin or carried forward to the next bin, whichever maximises the fractional exposure.

<sup>6</sup> For example, a bin with 4 events at  $2 \times 10^4$  s and a single event at  $2 \times 10^6$  s has a ‘time’ of  $3.2 \times 10^4$  s using the new method, but  $4.2 \times 10^5$  s using the standard mean.

Previously, these events could not be appended to the previous bin if this meant spanning gaps in observations. This change reduces the number of low fractional exposure bins in light curves.

5) Now that we are producing automatic spectra of GRBs (Section 2.1), the counts-to-flux conversion factor determined from this is automatically used to create a flux-units light curve. We still use a single conversion for the entire light curve. This conversion factor is taken from the PC mode data unless there are fewer than 200 events in the PC spectrum and more than 200 in the WT spectrum, in which case the WT-mode conversion factor is used.

6) Four event lists are also now available for download: the source and background event lists in WT and PC mode. As well as containing the events used in the light curve, these contain the GTIs (which are used in the light curve fitting, Section 2.4.2) and the columns SRCRAD – the radius of the source extraction region, and PUPRAD – the radius of the data excluded to counter pile up. The former is in units of XRT pixels and the latter in arcseconds, as required by the light curve software. One XRT pixel corresponds to  $2.36''$ .

7) Evans et al. (2007) stipulated that, if  $C$  is the number of counts needed to complete a bin in the main light curve, there should be  $2C$  counts in each band of the hardness ratio to complete a bin. This has been relaxed to  $C$  counts in each bin, giving significantly better time resolution in the hardness ratio.

As with the positions, we have also produced a web-based tool to create light curves for non-GRB objects. This tool allows ‘conventional’ binning, i.e. bins of fixed duration, and is described in Section 3.

### 2.3.2 User-defined data binning

In order to fully automate the light curve creation, the binning criteria defined in Evans et al. (2007) are applied to all light curves, and these give a useful, valid representation of the XRT data; but not necessarily the ‘best’ representation.

We have therefore produced a web-based tool to allow users to change the binning criteria for a GRB. On the results page for each GRB<sup>7</sup> there is a link entitled ‘rebin this GRB’. Following this link the user can specify the minimum number of counts per bin in each XRT mode and whether this is to be used for all bins or is ‘dynamic’ (i.e. it varies with source brightness). On this page there is a link to the ‘advanced’ rebinning interface, which allows the user to choose which event grades and energy bands are used in light curve creation. The bands used for the hardness ratio can also be adjusted here.

### 2.3.3 SPER light curves

This software can be easily applied to SPER data to produce light curves within minutes of a trigger. These are of greater reliability than the light curves telemetered via TDRSS, as the SPER light curves are background subtracted and binned with the same method as used on Malindi data (Evans et al. 2007). However, SPER data were originally designed purely for source detection and localisation, and

thus do not contain GTI information; we are forced therefore to assume that there is no dead-time in the light curve. Since SPER data only cover the first snapshot this is a safe assumption unless the XRT switches back into WT mode<sup>8</sup>.

## 2.4 Automatic light curve fitting

We have produced software to automatically fit broken power-law models to the light curves. Note that this is not currently routinely applied to new data. The fitting was performed using the least-squared approach implemented via the MINUIT2 minimisation routines produced at CERN<sup>9</sup>, using the  $\chi^2$  statistic. Only light curves containing at least 3 bins were fitted (i.e. only fits with at least 1 degree of freedom were attempted).

The procedure can be described as a four-step process:

- (i) Identify ‘deviations’ in the light curve
- (ii) Ignore the times of flares, and fit a series of power-laws to the light curve
- (iii) Use the F-test to determine the best, justifiable fit
- (iv) Check the results and repeat manually if necessary

These steps are discussed in detail below. Steps i–iii are automated, however in step iv) a human can decide that the automatic results were incorrect, and repeat those steps manually.

### 2.4.1 Identifying ‘deviations’

For this paper we aim to characterise the light curves in terms of power-law decays (see Nousek et al. 2006). However, many light curves show deviations from such behaviour which must first be removed. The most common deviations are flares, but other phenomena, such as the slow, curved rise seen in GRB 060218 (Campana et al. 2006) must also be ignored since they cannot be sensibly modelled as power-law decays. To ensure that readers can compare model predictions with the *Swift* data presented here, we list in Table 4 the times which were ignored from the fits. This should not be considered a statistical sample of flares since it includes other phenomena; also the times of the flare are based on when the count rate in the light curve begins to rise (see below) rather than on fitting a flare model to the light curve. For studies of flares in XRT light curves, see for example Falcone et al. (2007); Chincarini et al. (2007); Kocevski, Butler & Bloom (2007).

Our automatic script to identify deviations first searches the light curve for any interval where the count rate rises for at least two consecutive bins. If this leads to an increase in count rate of at least  $2\sigma$  a possible deviation is deemed to have started.

To determine when this potential deviation ends we look for a shallowing of the decay. We first identify the peak of the potential deviation as the highest intensity bin before the count rate systematically drops again. Beyond this peak, the software steps through each bin, calculating two decay

<sup>8</sup> This rarely occurs unless the GRB emits a strong flare, in which case this is obvious from the SPER light curve.

<sup>9</sup> <http://project-mathlibs.web.cern.ch/project-mathlibs/sw/Minuit2/html/index.html>

<sup>7</sup> [http://www.swift.ac.uk/xrt\\_curves/<target ID>](http://www.swift.ac.uk/xrt_curves/<target ID>)

indices for each bin. If the current bin is bin  $n$ , these indices are:  $\alpha_1$ : the index of the decay from the peak of the deviation to bin  $n$ , and  $\alpha_2$ : the index of the decay from bin  $n - 1$  to bin  $n$ . A deviation is deemed to have ended if at least one of the following conditions is met: a) There is a gap of at least 1 ks between light curve bins, and prior to the gap the time was  $< 2$  ks since the trigger (i.e. they cannot begin in the first *Swift* snapshot and extend into the second), or b) Two out of three consecutive bins are found with  $\alpha_2 < \alpha_1$  and both  $\alpha_1$  and  $\alpha_2$  decrease from one bin to the next.

The first condition exists because occasionally a flare starts towards the end of the first *Swift* observing snapshot, and during the gap in observations the flare ends and the light curve enters its final decay; thus the end of the flare using the second test is never found. Chincarini et al. (2007) found that flares tend to have duration:midpoint ratio of  $\sim 0.1$ , so we allow later time flares to span snapshots.

Any time identified above is only confirmed as a genuine deviation, and hence ignored for power-law fitting, if it contains fewer than 10 changes in XRT mode (so is not an artefact of mode switching), contains at least 2% of its component bins before the peak and has a ‘significance’ (defined below) of 1.8. If the potential deviation occurs in the first snapshot (i.e. within 2 ks of the trigger), the ‘significance’ must be at least 3 for it to be confirmed. These numbers were arrived at by trial and improvement to minimise the numbers of false positives and negatives. The significance of a deviation is defined as the peak count rate minus the pre-deviation count rate, divided by the errors in these values added in quadrature.

### 2.4.2 Fitting power laws

Once the deviations have been identified and removed, we fitted the remaining count-rate light curve with power-law segments separated by zero to five breaks. Note that these breaks are not smoothed. Upper limits were excluded from the fit. To fit the light curves correctly is non-trivial because of two, interconnected factors: the bins have a finite duration, and many bins have a fractional exposure less than 1. The normal way to calculate  $\chi^2$  – comparing model and data at the ‘time’ of the bin – does not account for the finite (and sometimes very large) duration of the bin and the evolution of the light curve through this. Instead, one should compare the number of counts detected in each bin to the number predicted by the model. Determining the number of counts predicted by the model in a given bin is non-trivial. The simplest approach (method 1) is to integrate the model across the light curve bin. However if the fractional exposure in the bin is not unity this technique fails, since the model has been integrated over a longer time interval than that during which counts were being collected. Renormalising the model by the fractional exposure is not a valid solution: this assumes that the source count-rate is the same during the dead-times and live-times within the light curve bin; for GRBs, which fade, this is clearly untrue.

A better fitting technique (method 2) is to use the Good Time Interval (GTI) information available with the light

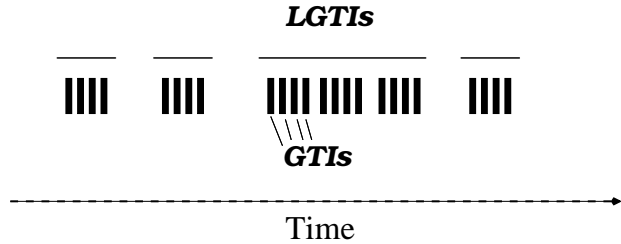


**Figure 2.** An illustration of the long good time interval (LGTI) concept. The vertical rectangles represent individual GTIs. The lines above show the LGTIs – groups of GTIs with less than 30 s of dead-time between consecutive intervals.

curves<sup>10</sup> and to integrate the model across the times during which the XRT was collecting data. Unfortunately, it has not been uncommon for the XRT to ‘mode switch’ (to toggle rapidly between PC and WT modes). This creates a large number of short GTIs. Integrating the model over each of these GTIs dramatically slows down the fit, especially for well-observed bursts, rendering this method impractical. Although recent software and operational changes mean that mode-switching is now a rare occurrence, it has been sufficiently common in the past that to fit all XRT light curves using method 2 would take several months.

We thus tried a compromise (method 3), whereby within a light curve bin we group GTIs together into ‘long GTIs’ (LGTIs). An LGTI is defined as a cluster of GTIs with less than 30 s of dead-time between consecutive GTIs. This is illustrated in Fig. 2. The model value for a given bin is found by integrating the model across each LGTI, multiplying by the fractional exposure in the LGTI to correct for dead-time and then summing this integration for all LGTIs within the light curve bin. This method, like method 1, contains a simplifying assumption; in this case, that during the dead-time within an LGTI the model can be assumed to be constant and at its mean value for the LGTI. This is a much more defensible assumption from method 3 than that for method 1; The dead-time within an LGTI is generally very short compared to the duration of the LGTI, whereas the deadtime in a bin can be a substantial fraction of the bin duration. To check whether this assumption affects the fitted models, we chose 6 GRBs containing bins of non-unity fractional exposure, and modelled their light curves using both methods 2 and 3. We found that almost all the fitted parameters and errors agreed to at least three significant figures; where they only agreed to two, the parameter errors were large.

For each light curve our automatic script first fitted an unbroken power-law and then added breaks and refitted with up to a maximum of five breaks (fewer if there was less than one degree of freedom before this). Although break time is a free parameter, it was necessary to estimate the time at which a break would most improve the  $\chi^2$  before adding it, to reduce the likelihood of the fit converging on a local minimum. To achieve this, the software compared the data with the previous model and identified time intervals where the data lie systematically above or below the model.

<sup>10</sup> This is contained in the source event lists, available from the *Swift* light curve repository.

It calculated the  $\chi^2$  contribution from each such interval and added the break at the end of the interval with the greatest  $\chi^2$  contribution, or the start of the interval if it extended to the end of the observation.

#### 2.4.3 F-test

For each broken power-law fit performed in the previous step,  $\chi^2$  is compared to that from the fit with one fewer break, and an F-test used to determine whether the break is significant. We define a break as significant if the F-test returns a probability of the  $\chi^2$  improvement as  $< 0.3\%$ . Note that we don't interpret this quantitatively as confirming the break at the  $3\sigma$  level, rather we use it as a convenient means of determining how many breaks to use. Even if the break is not deemed significant in this way, the software still adds a further break; sometimes the 'true' best fit requires 2 breaks, but the  $\chi^2$  improvement from a no-break fit to a one-break fit is not significant. The fit with the most breaks which is deemed significant by the test above is taken as the 'best' fit.

#### 2.4.4 Human intervention

For each GRB, we checked the results of the automated steps above. In 23% of cases flares were misidentified; occasionally genuine flares were missed, but most of the failures were false positives. In these cases we manually defined the times to be excluded and re-ran the automatic power-law fitting.

In  $\sim 5\%$  of cases visual inspection suggested that use of the F-test had not identified the true best fit. Sometimes this was because one of the fits had found a local minimum of  $\chi^2$  rather than the best fit. In these cases we manually adjusted the parameters and refitted until the true best fit was found and re-performed the F-test. In other cases ( $\sim 1\%$  of light curves), the F-test deemed a break necessary only at the 90–99% level, however, knowing that light curves often show a 'steep-shallow-steep' behaviour (Nousek et al. 2006; Zhang et al. 2006) allowed us to confirm that the break was genuine – an example of this is given in Fig. 3, along with several examples of good automatic fits.

## 3 NON-GRBS

So far we have only discussed GRBs, since it is for these that we create products automatically, and present results below. However, *Swift* regularly observes other types of source, with the XRT data often being crucial to the science goals of the observation. We have thus adapted the three tools discussed in Section 2 for use with non-GRB sources, and created a web interface to execute them on-demand. This is available at [http://www.swift.ac.uk/user\\_products](http://www.swift.ac.uk/user_products). In this section we briefly detail the differences between the 'non-GRB' versions of the software and those described in Section 2. While these tools are public, we refer users to the usage policy at the end of this paper.

### 3.1 Spectra

The spectrum creation and fitting software for non-GRBs is almost identical to that used for GRBs, except that the

user can choose which observations are used to form the spectrum. The user can also specify up to 4 time intervals rather than creating a single time-averaged spectrum (for GRBs this is possible as well, but only after the average spectrum has been automatically produced). As with GRBs, the spectra are automatically fitted with absorbed power-law models, and the spectral files are provided for download so users can fit other models and interact with the data as required.

### 3.2 Positions

As noted in Section 2.2, if UVOT images taken in the UV filters are used to enhance XRT positions, we tend to find larger errors, thus for GRBs we use only the *v*, *b* and white filters. However, many non-GRB observations are performed using the 'filter of the day' (to prolong the life of *Swift*'s filter wheel), which is usually one of the UV filters. Thus the non-GRB position enhancement tool works in two passes: first it tries to find observations containing PC mode XRT data and UVOT images obtained in the optical filters; if successful, it uses these data to enhance the position. If no such observations can be found, it reverts instead to using the UV filters, and the systematic error is accordingly increased from  $1.36''$  to  $1.9''$ .

For GRBs, only observations which begin within 12 hours of the first one are included; this is because the GRB is generally too faint to detect after this point. Although this is not necessarily true for non GRB sources, this behaviour is kept by default because using more observations increases the length of time taken to produce the position, and our GRB experience shows that most positions produced with this selection criteria are limited by systematics, not statistics. This can be changed by the user, or the user can explicitly state which observation(s) should be used. In the case of an object which was monitored for some time in quiescence by *Swift* before undergoing some outburst, it is particularly recommended that users specify the obsID to use, since the brighter data from the outburst would not be included by default but are more likely to give a good position (unless the outburst pushes XRT into WT mode).

### 3.3 Light curves

For most non-GRB objects the binning method used for GRBs – defining bins by the number of counts they contain – is not ideal. We have thus produced a version of the software which bins in a conventional way: the user specifies the duration of the bins (the method used for binning GRB light curves is however still available for non-GRB sources; alternatively users can choose to produce one bin per snapshot, or per observation). After a gap in the data (for example, between snapshots) a new bin begins at the start of the next GTI which is not necessarily an integer number of bin widths after the last bin ended. There are several caveats about this binning method:

- 1) The software uses Gaussian statistics to calculate the uncertainty after background subtraction. If there are fewer than 15 counts in a bin, this may not be accurate. It is the user's responsibility to choose a bin size which ensures sufficient counts per bin. A warning is given if any bins contain fewer than 15 counts.

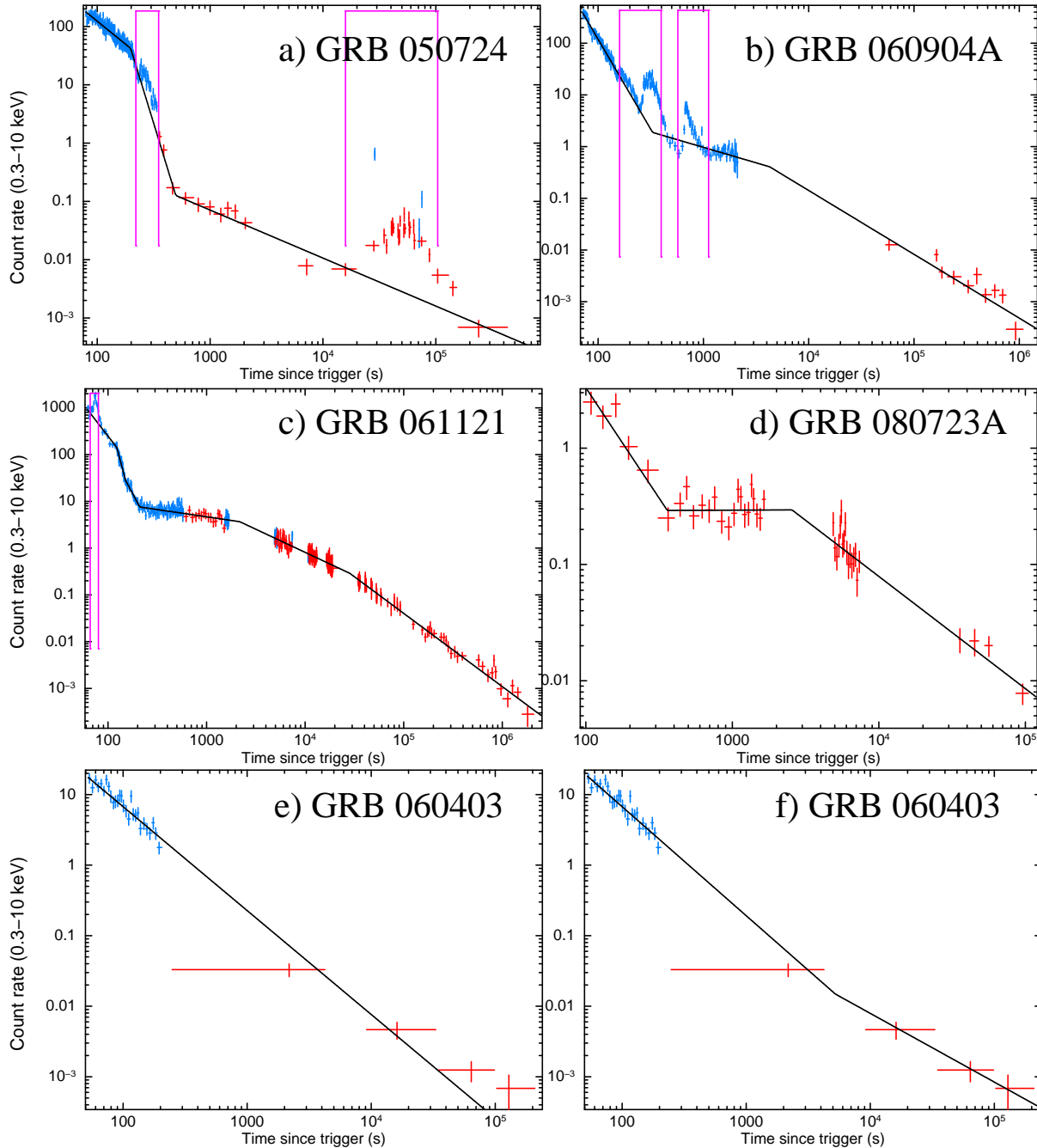


**Figure 3.** Examples of automatically fitted light curves. WT data are shown in blue, PC data in red. The purple boxes mark times identified as deviations from power-law behaviour and excluded from the fit. Panels a)-d) show cases where no human intervention was needed. Panels e) and f) illustrate a case where we overruled the automatic determination of the ‘best’ model. The break added in f) is only significant at the 96% level according to an F-test, so the automatic software suggested e) as the best fit. However, given that we know that GRB light curves tend to flatten in the first few kiloseconds, we believe that the automatic fit with a break shown in f) is the most appropriate fit.

2) Sometimes the XRT enters WT mode for reasons other than the source being bright. This can produce spurious light curve points with large error bars (both are invalid), and disrupt the scaling of the plots. By default any WT mode bin with fewer than 15 counts is assumed to be spurious and is not included in the light curve produced. The web interface allows the user to change the minimum

number of WT counts necessary for a valid bin – setting it to 0 will include all WT data points.

3) The last bin in a snapshot may have a low fractional exposure, in which case any statistical fluctuations in the data will be exaggerated. We recommend that users check any such points and consider rejecting any point with a low fractional exposure; an option to do this automatically is provided by the interface.

When the fixed bin-width binning method is used, an OGIP compliant FITS file is produced containing the light curve, in addition to the standard products created for GRBs.

## 4 RESULTS

In Section 2 we presented details of how enhanced positions, light curves and spectra are produced. These methods have been applied to every GRB detected by the XRT, and will run automatically on all new GRBs. The results are posted online and are available via:

- Index: [http://www.swift.ac.uk/xrt\\_products](http://www.swift.ac.uk/xrt_products)
- Positions: [http://www.swift.ac.uk/xrt\\_positions](http://www.swift.ac.uk/xrt_positions)
- Light curves: [http://www.swift.ac.uk/xrt\\_curves](http://www.swift.ac.uk/xrt_curves)
- Spectra: [http://www.swift.ac.uk/xrt\\_spectra](http://www.swift.ac.uk/xrt_spectra)

For SPER data the results are available via: <http://www.swift.ac.uk/sper>. Each page contains detailed documentation, including a log of any changes made after publication of this paper. All of these pages are interlinked and an index of these results, and those from the BAT, is available via the GCN ground analysis web page at: [http://gcn.gsfc.nasa.gov/swift\\_gnd\\_ana.html](http://gcn.gsfc.nasa.gov/swift_gnd_ana.html).

In Tables 5–8 we list the enhanced positions, best-fitting light curve parameters, and best-fitting spectral fit results for all GRBs observed by the XRT up to GRB 080723B<sup>11</sup>. In Table 6 we also give the *Swift* target ID and the BAT  $T_{90}$  (from the Swift data table<sup>12</sup>) for reference. Although our automated processing only produces time-averaged spectra, in this compilation of results it is interesting to consider possible spectral evolution. So, for each GRB with a break in its light curve we extracted and fitted spectra for each light curve segment (delimited by the breaks). These results are presented in Tables 9 and 10<sup>13</sup>. The tables are also available online, through the Virtual Observatory ([ivo://uk.ac.le.star.swift/dsa\\_grb\\_aux/SwiftXRTGRBCat](http://ivo://uk.ac.le.star.swift/dsa_grb_aux/SwiftXRTGRBCat)), and via CDS (<http://cdsweb.u-strasbg.fr/cgi-bin/qcat?J/MNRAS/>

### 4.1 Validation of SPER results

The analysis of SPER data is intended to give users an indication of a GRB's properties extremely rapidly; they are not intended for scientific analysis. Since these data are in every case superceded by Malindi data, we do not list the SPER results in this paper; however we demonstrate their veracity and the limits thereof.

As with the enhanced Malindi positions, we determined the offset between the enhanced SPER position and the UVOT position of every GRB with both of these positions, and confirmed that they agreed 90% of the time, i.e. the enhanced SPER 90% confidence error radius is correctly calibrated.

<sup>11</sup> In order to fit the table within an A4 page it is necessary to tabulate the decay indices and break times separately. The online data contain these together in a single file.

<sup>12</sup> [http://heasarc.gsfc.nasa.gov/docs/swift/archive/grb\\_table.html](http://heasarc.gsfc.nasa.gov/docs/swift/archive/grb_table.html)

<sup>13</sup> We have separated  $\beta$  and  $N_H$  for the paper, however these are in a single table online.

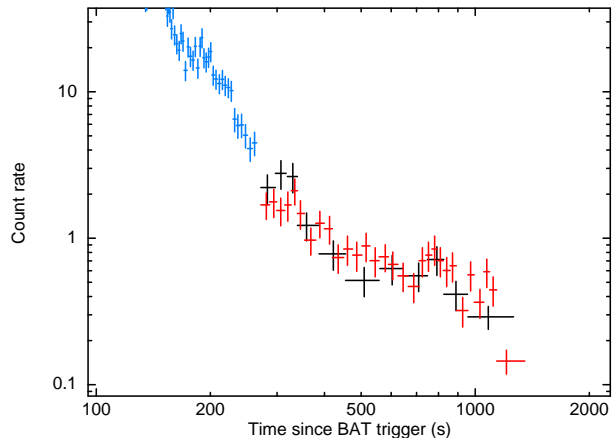


**Figure 4.** An example SPER light curve (black) plotted with the Malindi-data light curve (red – PC and blue – WT). The SPER data clearly give a good representation of the true light curve.

We chose not to fit the SPER light curves as they typically have few bins. Instead we compared SPER and Malindi curves by eye, an example is given in Fig. 4. We found good agreement between SPER and Malindi light curves.

To test the spectra, we created spectra from Malindi data covering the same time region as the SPER data, and fitted them. We then compared the column density, spectral index and observed flux between these fits and those from the SPER spectra. The first two parameters were in good agreement, however the fluxes only agreed within their 90% errors 70% of the time. This discrepancy probably reflects the lack of GTI information for SPER data, and may also suggest that using the covariance matrix from the fit to estimate the flux errors (as we do) underestimates the errors.

### 4.2 ‘Malindi’ data

The large volume of uniformly analysed Malindi data presented in Tables 6–Table 10 (i.e. temporal and spectral analyses) allow us to consider the sample properties of the GRBs observed by *Swift*'s XRT.

We have created probability distribution functions (PDFs) for the temporal and spectral indices and temporal break times. We prefer these to histograms as the latter neglect uncertainties on the parameters; a PDF accounts for them and so gives a better representation of the data. The sample PDFs were obtained by treating the PDF of any single parameter as two halves of normal distributions with widths set by the measured uncertainties, each half normalised so as to form a continuous function, as done by Starling et al. (2008), i.e.

$$P(x|\bar{x}, \sigma_1, \sigma_2) = \frac{\sqrt{2}}{\sqrt{\pi}(\sigma_1 + \sigma_2)} \begin{cases} e^{-(x-\bar{x})^2/2\sigma_1^2} & (x \leq \bar{x}) \\ e^{-(x-\bar{x})^2/2\sigma_2^2} & (x > \bar{x}) \end{cases} \quad (1)$$

where the 1- $\sigma$  errors on each parameter are taken as the calculated 90% confidence error divided by 1.6. We then created overall PDFs of the temporal index ( $\alpha$ ) and spectral index ( $\beta$ ) by summing the PDFs of each individual  $\alpha$  or  $\beta$  parameter and dividing the merged PDF by the number of contributing values. The peak and FWHM of the various PDFs are given in Table 3; these were calculated by fitting

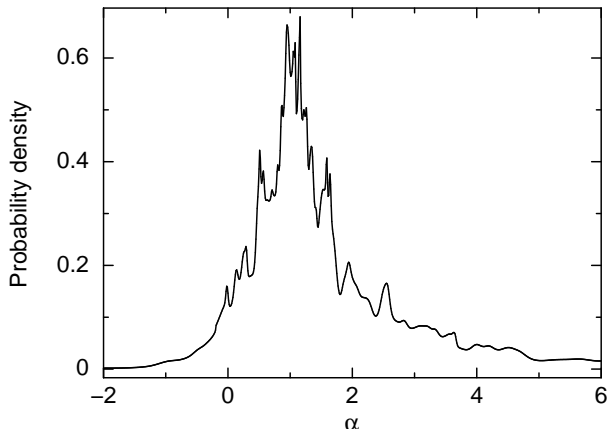


**Figure 5.** Probability distribution function of the light curve power-law decay indices tabulated in Table 6.

Gaussians to the PDFs; note that many distributions are clearly more complex than a simple Gaussian, in which case the values in Table 3 should be taken as indicative, rather than precise.

The  $\alpha$  PDF is given in Fig. 5, and shows a fairly tight distribution of values. There are a total of 665 values suggesting that the steep drops in probability around  $\alpha = 0.5, 1.5$  are real. This is perhaps not surprising, the ‘canonical’ X-ray light curve (Nousek et al. 2006; Zhang et al. 2006) contains four phases, and as discussed below there are several other light curve morphologies observed, with one or more distinct phases. Each phase has its own  $\alpha$  distribution corresponding to the peaks in Fig. 5. See Section 5 for more details.

The PDF of observer-frame break times is given in Fig. 6; we lack the redshift information necessary to translate to the rest frame for most bursts. Since GRB light curves span many decades, the probability density is defined here as probability per unit  $\log(\text{time})$ , rather than per unit time. The two peaks around  $\sim 1\text{--}300$  s and  $10^4$  s arise from the ‘canonical’ light curves and reflect the most common start and end times of the plateau phase, however there is significant probability of a break at all times between  $\sim 100\text{--}10^5$  s. This is likely the result of two effects: the redshift distribution of GRBs, and an intrinsic scatter of GRB light curve morphology. There are also selection effects which may affect this distribution: to tightly constrain a break requires good sampling of the decay on either side of the break, thus towards the end of the light curve breaks are much harder to constrain and will have broader PDFs, or not be seen at all (Curran et al. 2008; Racusin et al. 2009). Also, there is usually a gap in *Swift* observations between  $\sim 2\text{--}4$  ks after the trigger (while *Swift* is the far side of the Earth from the GRB) making it harder to tightly constrain breaks in this interval.

Turning to the spectra, the PDF of the spectral index ( $\beta$ ) is shown in Fig. 7 (panel a). Here, and in Tables 8 and 9, we give the spectral index  $\beta$  (i.e.  $F_\nu \propto E^{-\beta}$ ). Some authors prefer the photon index  $\Gamma$  (i.e.  $N_E(E) \propto E^{-\Gamma}$ , this is the value used in the XSPEC power-law model). These are very simply linked:  $\beta = \Gamma - 1$ .

In creating the spectra we made no attempt to exclude times of flares, preferring to maximise the number of counts

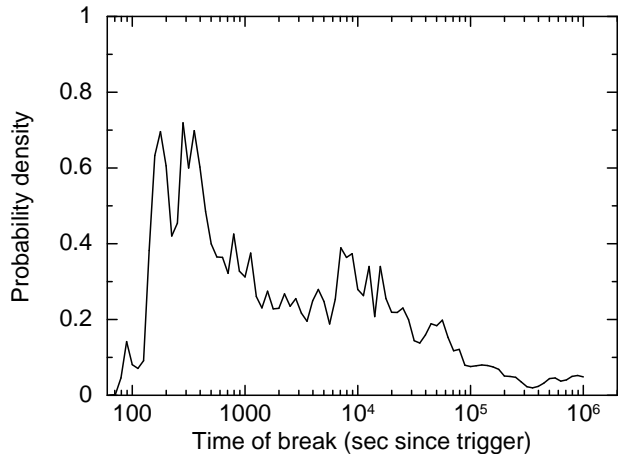


**Figure 6.** Probability distribution function of the break times [probability per unit  $\log(\text{time})$ ] between the power-law decay segments, tabulated in Table 7.

in the spectra. Previous studies (e.g. Falcone et al. 2007) and the X-ray hardness ratios on the XRT light curve repository, show that flares tend to have harder spectra than the underlying afterglow emission. Table 4 shows that 81 of the GRBs in our sample contained ‘deviations’ from power-law decays, many of which were flares. To determine whether this has biased our results, we regenerated the spectra excluding the times of any deviations from power-law behaviour, as identified in the light curve fitting phase (Table 4). In panel b) of Fig. 7 we show the PDF of the spectral index from these data (this includes all the GRBs with no deviations, as well as those where deviations were removed), this is almost identical to that in panel a). In panel c) we show the PDF of the change in  $\beta$  caused by ignoring the times of deviations (derived only from the 81 GRBs listed in Table 4). This shows the mean change to be  $0 \pm 0.2$ ; for comparison, the median uncertainty in  $\beta$  in Table 8 is  $\pm 0.16$ . We thus conclude that the presence of flares has a negligible effect on our time-averaged spectra.

Another factor which may affect the spectral index is the redshift ( $z$ ) of the burst; if the redshift used in the fit is incorrect and there is significant absorption in the GRB host galaxy, the absorption will not be correctly modelled – this is most notable around the neutral oxygen edge at 0.525 keV (rest frame). This in turn affects the spectral index. For example, for GRB 050904 ( $z = 6.29$ , Cusumano et al. 2007) the fit reported in Table 8 has  $\beta = 0.927^{+0.048}_{-0.049}$ . If we set the absorption above the Galactic value to be at  $z = 0$  we find  $\beta = 0.964^{+0.062}_{-0.060}$ .

In our default approach (Section 2.1), unless the redshift of the GRB has been spectroscopically determined, we use an unredshifted absorber to model the excess absorption, as well as the Galactic component. Since this is clearly incorrect, we tried refitting all these GRBs, using  $z = 2.23^{14}$  for the excess absorption if the redshift was not known. In panel (d) of Fig. 7 we show the PDF of spectral indexes where  $z$  was taken from the literature, where available, and

<sup>14</sup> the mean reported redshift for *Swift*-detected GRBs to date, calculated from Table 8.

Parameter	Peak of PDF	FWHM
$\alpha$	1.1	1.5
$\beta$	0.98	0.66
$\log(N_{\text{H}})$ $\text{cm}^{-2}$	21.3	1.2
Counts-to-flux factor (observed)	$3.8 \times 10^{-11}$ ( $\text{erg cm}^{-2} \text{ ct}^{-1}$ )	$1.4 \times 10^{-11}$ ( $\text{erg cm}^{-2} \text{ ct}^{-1}$ )
$\alpha_{\text{plat}}^a$	0.32	0.79
$\alpha_{\text{norm}}^a$	1.2	0.5
$\beta_{\text{plat}}^a$	1.0	0.53
$\beta_{\text{norm}}^a$	1.1	0.65
$\log(T_{\text{rmplat,start}})$	2.5	0.7
$\log(T_{\text{rmplat,end}})$	4.0	1.2
$\alpha_{\text{steep}}^b$	$\sim 2.7$	$\sim 2.1$
$\alpha_{\text{shallow}}^b$	0.82	0.46
$\beta_{\text{steep}}^b$	$\sim 1.1$	$\sim 1.3$
$\beta_{\text{shallow}}^b$	1.21	0.68
$\log(T_{\text{break}}^b)$	2.8	0.75
$\alpha_{\text{steep}}^c$	$\sim 1.2$	$\sim 0.9$
$\alpha_{\text{shallow}}^c$	$\sim 0.7$	$\sim 0.8$
$\beta_{\text{steep}}^c$	1.1	0.6
$\beta_{\text{shallow}}^c$	0.98	0.38
$\log(T_{\text{break}}^c)$	$\sim 4.0$	$\sim 2.8$
$\alpha_{\text{steep}}^d$	1.1	0.7
$\beta_{\text{steep}}^d$	1.1	0.6

**Table 3.** The peak and FWHM of the PDFs plotted in this paper, where the PDFs have been approximated as Gaussians.  $a-d$  refers to the different classes of GRB illustrated in Fig. 9, e.g.  $\alpha_{\text{steep}}^b$  refers to the decay index of the steep-decay phase of those light curves which begin steep and then flatten.

Note: the underlying distributions are not always Gaussian, or are poorly sampled so the values herein are indicative.

otherwise set to 2.23. Panel (e) shows the PDF of the change in  $\beta$  caused by assuming  $z = 2.23$  instead of  $z = 0$  for those GRBs with no spectroscopic redshift. The latter is  $0 \pm 0.2$ , suggesting that it is acceptable to assume no redshift if no spectroscopic determination has been made.

In Fig. 8 we present the PDF of the ‘excess’ absorption: that is, the value of the second absorption component in the fit (the first being frozen at the Galactic value from Kalberla et al. 2005, see Section 2.1 above). The panels are as in Fig. 7.

#### 4.2.1 Time-resolved analysis

It is interesting to consider how the sample of *Swift* GRBs presented here compare to theoretical predictions. In this paper we limit ourselves to comparison with the fireball model (e.g. Sari et al. 1998), introduced in Section 1.3. We do this using the ‘closure relationships’ which related the temporal index ( $\alpha$ ) and the spectral energy index ( $\beta$ ), see, e.g. Zhang et al. (2006) for a table of such relationships. These are simplifications of the complete model; in particular they assume that the electron distribution  $p \sim 2.2$ , and that the microphysical parameters such as the proportion of blastwave energy stored in magnetic fields are not evolving through the outburst.

Since the ‘canonical’ afterglow (Nousek et al. 2006;

Zhang et al. 2006) contains 4 distinct phases – high-latitude emission (which is not afterglow emission), a plateau, a ‘normal’ decay phase, and post-jet-break decay – it is not sensible to compare all of the  $(\alpha, \beta)$  pairs we have derived *en masse*. Instead we classified each light curve segment to study the groups separately. To achieve this, we first classified each light curve either as ‘no break’, ‘one break’, ‘canonical’ or ‘oddball’. The first two are self explanatory. For the latter two: any light curve with at least two breaks was considered canonical if it contained one shallowing break, with  $\Delta\alpha \leq -0.5$ , and a later steepening break, with  $\Delta\alpha \geq 0.5$ , and an oddball otherwise [note that the canonical light curve, as defined by Nousek et al. (2006) does not contain this quantitative definition; we provide it for homogeneity]. We manually checked these classifications and reclassified 7 light curves from canonical to ‘oddball’ (for example GRB 060202 shows a steep-shallow-steep-shallow behaviour which is not canonical, but meets the criteria defined above). The list of light curves in each class is given in Table 11, and schematic diagrams of all classes except ‘oddball’ (which comprises a range of morphologies and cannot be shown schematically) are given in Fig. 9. The two types of singly-broken decay morphologies will be referred to as ‘type b’ and ‘type c’ morphologies hereafter, for brevity.

For each canonical light curve we defined any segment with a positive  $\alpha$  (i.e. decaying) before the break with  $\Delta\alpha \leq -0.5$  as belonging to the steep decay phase. Segments after this, but before the break with  $\Delta\alpha > 0.5$  were identified as the plateau phase. The next segment was identified as the ‘normal’ decay phase and any subsequent decay segments were assumed to be post-jet-break decays. These classifications were again checked by eye, and a small number of segments reclassified accordingly.

In Fig. 10 we plot  $(\alpha, \beta)$  from Tables 6 and 9 for each of these 4 segments of the canonical afterglow (panels a–d; PDFs of these are given in Fig. 11) We also show the regions covered by the standard afterglow closure relationships (from Zhang & Mészáros 2004); the thick grey band shows the range allowed by the pre-jet break emission in a slow cooling regime (i.e. the synchrotron peak frequency,  $\nu_m$  is below the cooling frequency  $\nu_c$ ). The two dark grey lines map the closure relationships for the fast cooling regime ( $\nu_m > \nu_c$ ). In panel (d) we also show the region covered by the post-jet break closure relationships (blue band). The points in panels a) and b) appear uncorrelated with the closure relationships, however this is unsurprising. In the standard interpretation, the steep decay phase (a) is not afterglow emission, and in the plateau phase (b) energy is being injected into the afterglow. What is perhaps surprising is that many of the ‘normal decay’ phase points (c) do not lie within the range predicted by afterglow theory. The post-jet-break points (d) are the only ones which agree well with afterglow theory, although they agree much better with the pre-jet break relationships than the post-break ones. We consider these facts in more detail below (Section 6).

For the bursts showing only one break, we show the  $(\alpha, \beta)$  values of the steeper decay in panel (e) of Fig. 10 and the shallower decay in panel (f). The black points are type b curves and the red ones type c (c.f. Fig. 9). Panel (g) shows the bursts with no breaks in their X-ray light curves. Overall, Fig. 10 shows similar results to those in Butler & Kocevski (2007a, fig 1), however they had a smaller

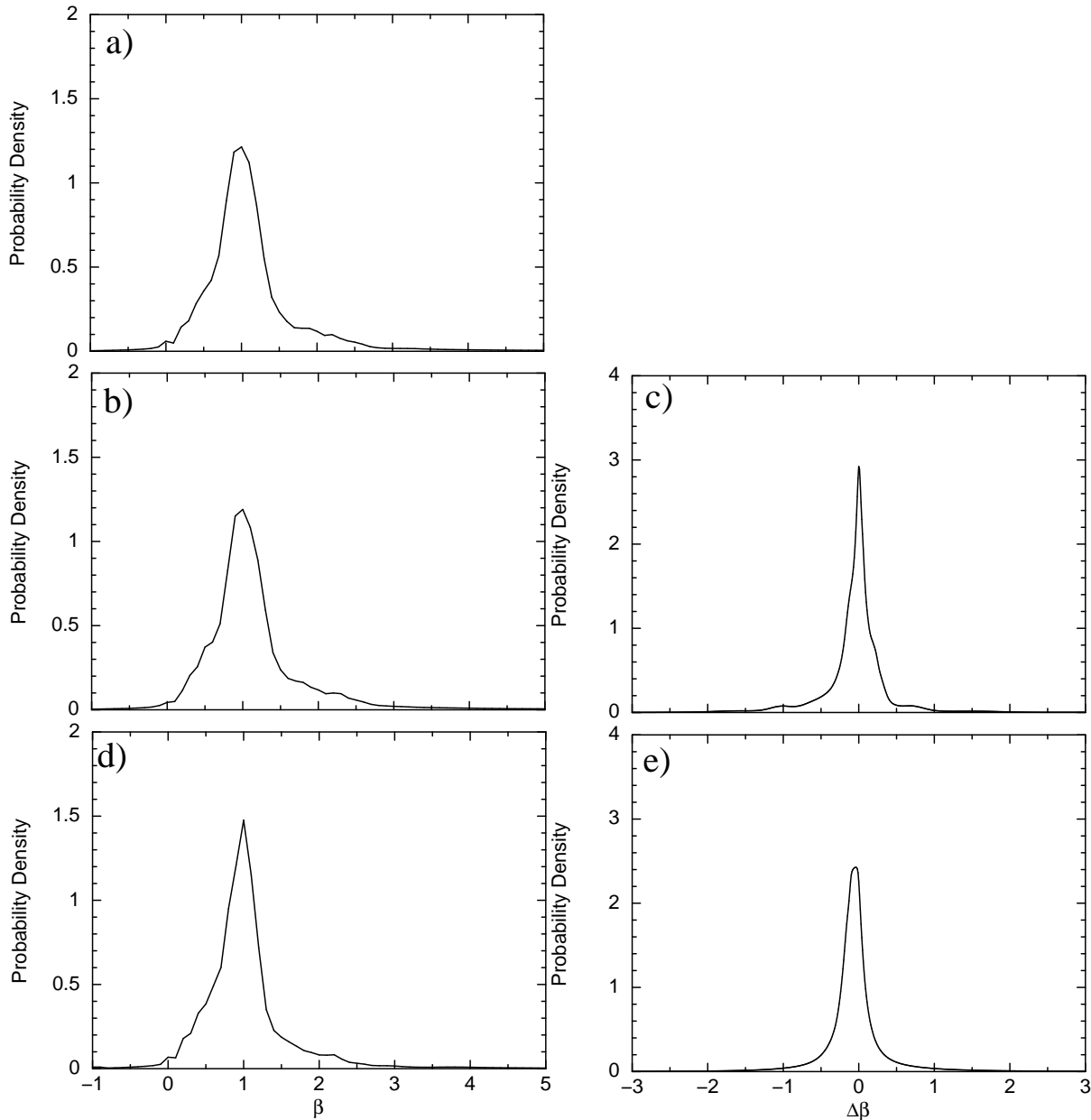


**Figure 7.** Probability density functions (PDFs) of the spectral index ( $\beta$ ) from the time-averaged spectra. Panel a) shows the overall distribution. b) shows this when times of flaring are excluded. Panel c) shows the PDF of  $\Delta\beta$  caused by removing flares. Panel d) shows the distribution when bursts with unknown redshift are assumed to be at 2.23, rather than 0, and e) shows the PDF of  $\Delta\beta$  resulting from this change.

sample and divided the light curves into segments based on a uniform time-slice rather than individual fits, thus our results are not directly comparable.

### 4.3 Other sample statistics

In the rest of this paper we will concentrate on the collection of light curves presented in this catalogue. These data can also be combined with other datasets such as the BAT

or UVOT catalogues (Sakamoto et al. 2008; Roming et al. 2009) or the online *Swift* data table<sup>15</sup>.

For example, Gehrels et al. (2008) compared  $E_{\text{iso}}$  with the X-ray luminosity 11 hours after the trigger and found a correlation with a slope of  $\sim 1$ . They thus suggested that the radiative efficiency of the blastwave is similar from GRB to GRB. In Fig. 12 we show the BAT fluence plotted against the X-ray flux at 11 hours (i.e. we have made no correction for distance, since only  $\sim 30\%$  of the GRBs in our catalogue

<sup>15</sup> <http://heasarc.gsfc.nasa.gov/docs/swift/results/>

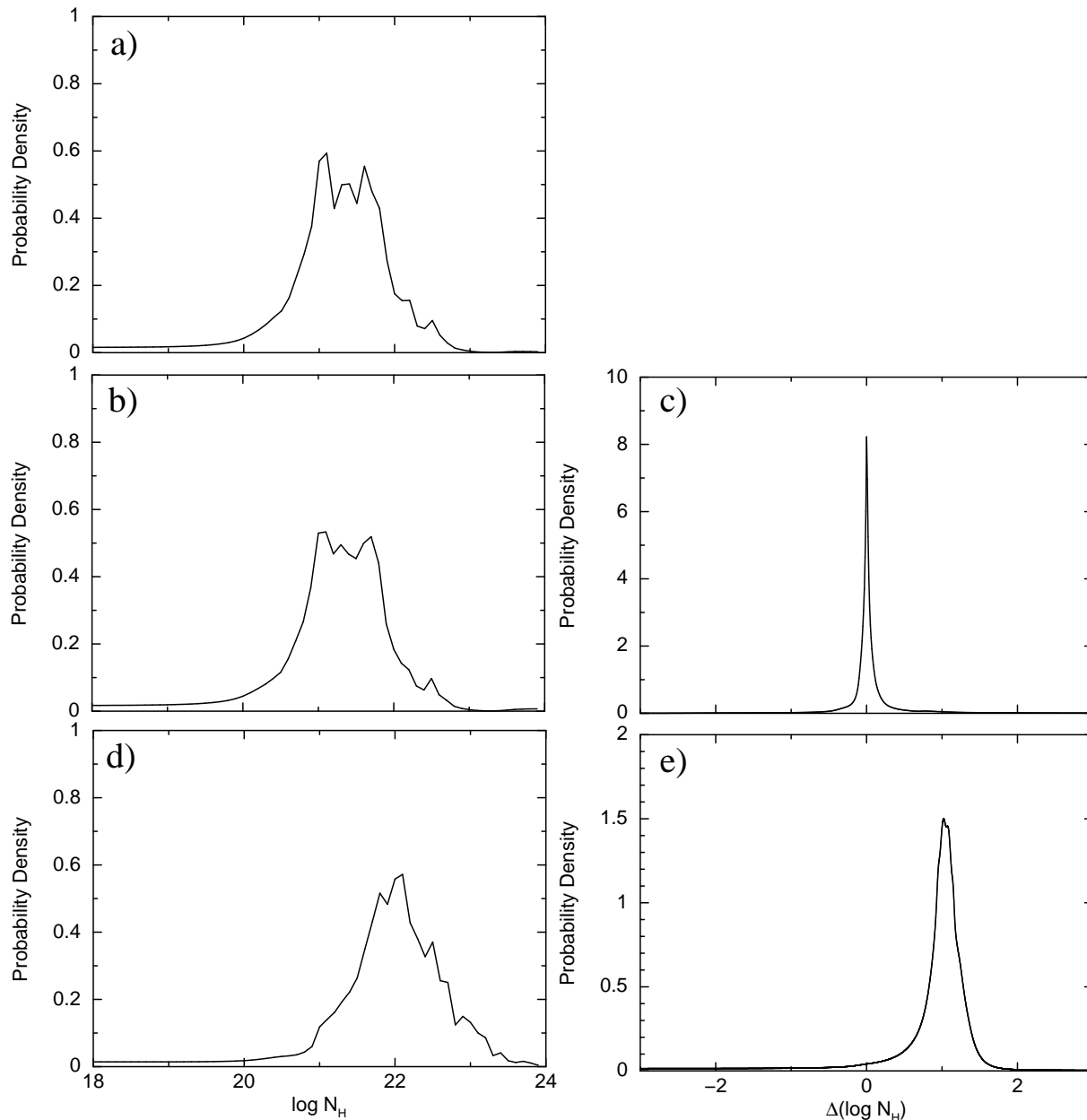


**Figure 8.** Probability density functions (PDFs) of the ‘excess’ column density, i.e. that above the Galactic value, from the time-average spectra. Panel a) shows the overall distribution. b) shows this when times of flaring are excluded. Panel c) shows the PDF of  $\Delta \log N_{\text{H}}$  caused by removing flares. Panel d) shows the distribution when bursts with unknown redshift are assumed to be at 2.23, rather than 0, and e) shows the PDF of  $\Delta \log N_{\text{H}}$  resulting from this change.

have known redshift) using the large sample of GRBs in this paper; the trend can still be seen.

As another example, Willingale et al. (2007) compared the fluence of their two emission components (prompt and afterglow), found a weak correlation and showed that that the afterglow fluence never exceeds the prompt fluence. We have performed an analogous analysis, comparing the 15–150 keV BAT fluence from the *Swift* data table with the fluence of the plateau phase in the canonical light curves (Fig. 13). Note that Willingale et al. (2007) determined the fluence over a wide energy band whereas we have only considered the 2 distinct bands covered by the data (i.e. 0.3–10 keV

for XRT and 15–150 keV for BAT). Our results are however consistent with those of Willingale et al. (2007). Considering the plateau further if it is caused by energy injection (see below) one may naïvely expect to see some relationship between  $T_{90}$  and the plateau duration, e.g. perhaps longer lived bursts also inject energy for longer. Combining our data with the *Swift* data table however reveals no correlation between these two parameters.

These are a few examples of the large-scale studies which our dataset enables; to aid in such studies all of our light curves, positions and spectra are online and the tab-

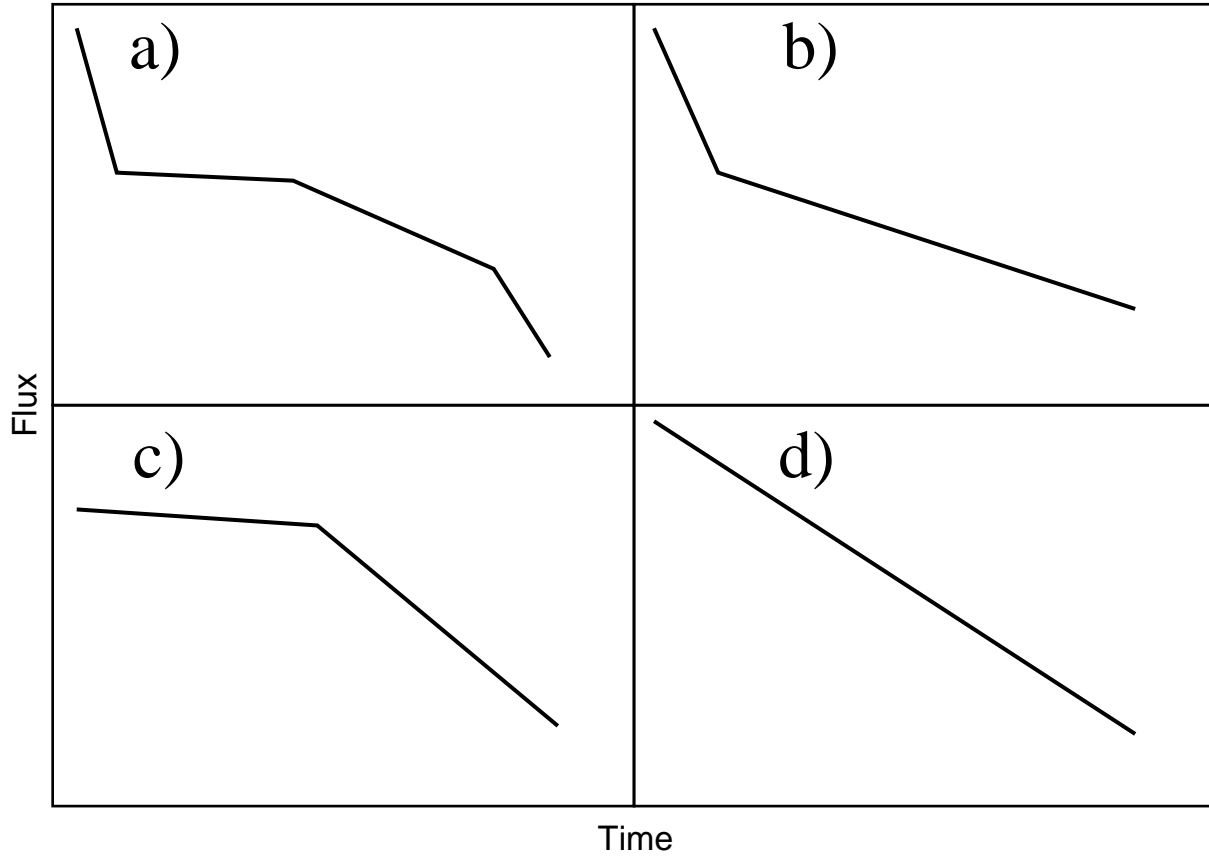


**Figure 9.** Schematic diagrams of the different light curve morphologies seen, excluding the ‘oddballs’. Panel a) shows the so-called ‘canonical’ light curves. Panels b)–c) are those with one break, either flattening (b) or steepening (c). Panel d) are those with no breaks.

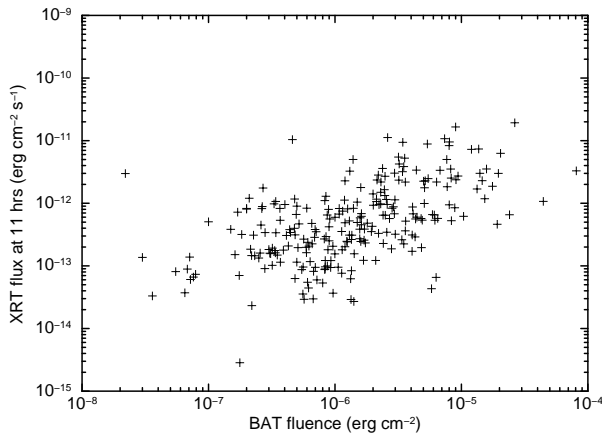


**Figure 12.** The X-ray flux at 11 hours post-trigger plotted against the BAT fluence. The correlation reported by Gehrels et al. (2008) is still present in our larger dataset. Note that Gehrels differentiated between long and short bursts (the correlation being more obvious for the former) which we have not done.

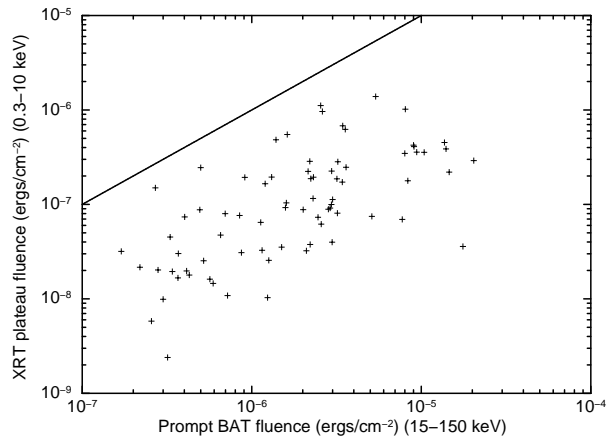


**Figure 13.** The fluence of the X-ray plateau phase plotted against the BAT fluence of the prompt emission, for the canonical light curves. The line shows where the two quantities are equal. This plot is analogous to fig. 6 of Willingale et al. (2006) but with a larger sample, and confirms their findings.

## 5 A CANONICAL LIGHT CURVE?

For the rest of this paper we consider the sample of GRB light curves, and specifically, the range of morphologies found, as demonstrated in Fig. 9. Nousek et al. (2006), Zhang et al. (2006) and Panaitescu et al. (2006) proposed

ulated data in this paper are available in machine readable format; details were given earlier in this section.

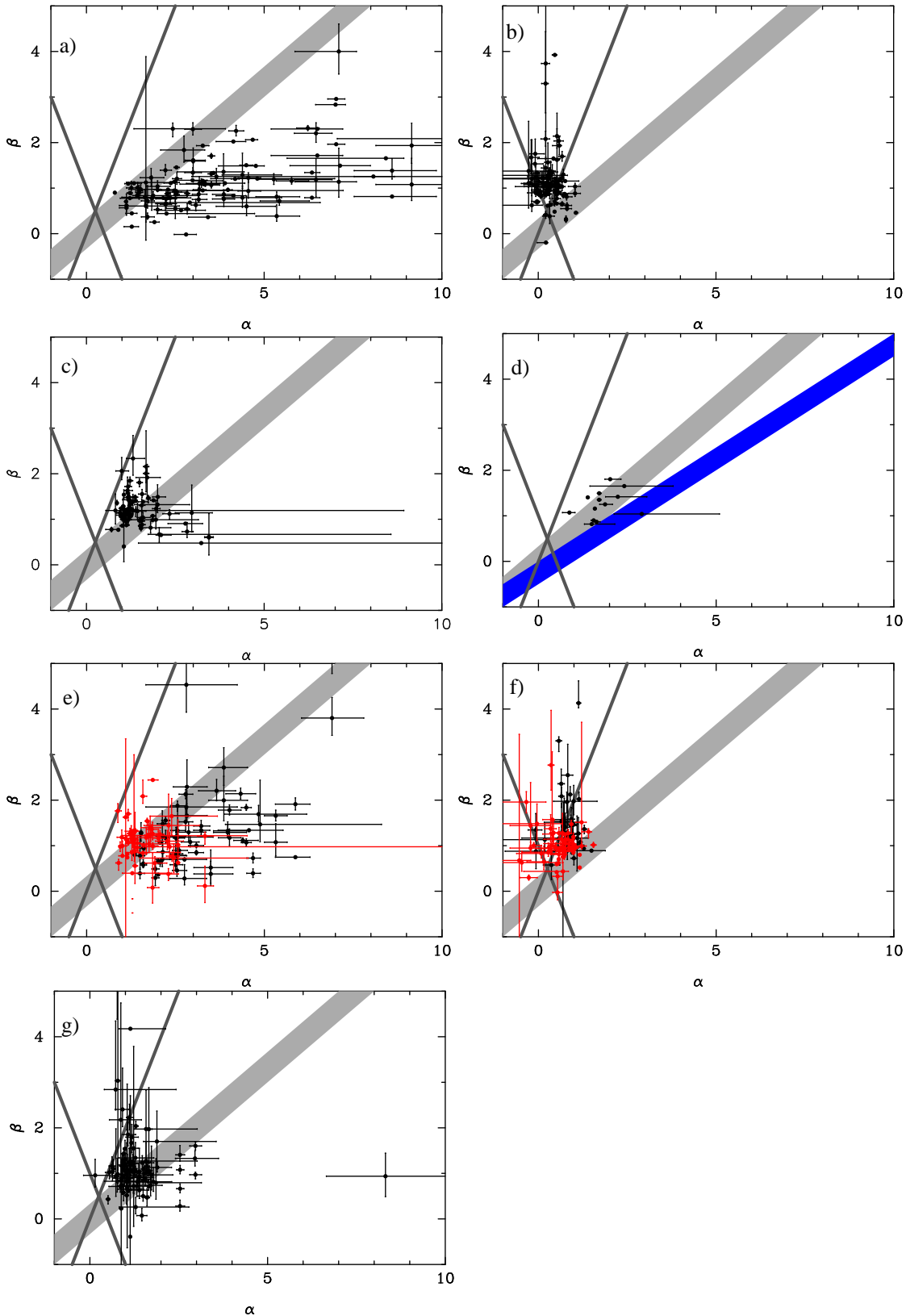


**Figure 10.** Spectral indices ( $\beta$ ) vs temporal indices ( $\alpha$ ) for different light curve phases; see Fig. 9. Panels a)–d) are for the ‘canonical’ light curves and show the values from the steep decay, plateau, ‘normal’ and ‘late break’ phases. Panels e)–f) show the values from those light curves showing a single break; the steeper of the segments are plotted in e) and the shallower in f). The black and red points indicate type b and c light curves respectively (see Fig. 9). Panel g) show the values for those light curves which do not contain a break. The grey bands mark the areas permitted by standard afterglow closure relationships; the narrow grey lines are for the fast-cooling regime. The blue band in panel d) marks the range permitted by post-jet-break closure relationships.

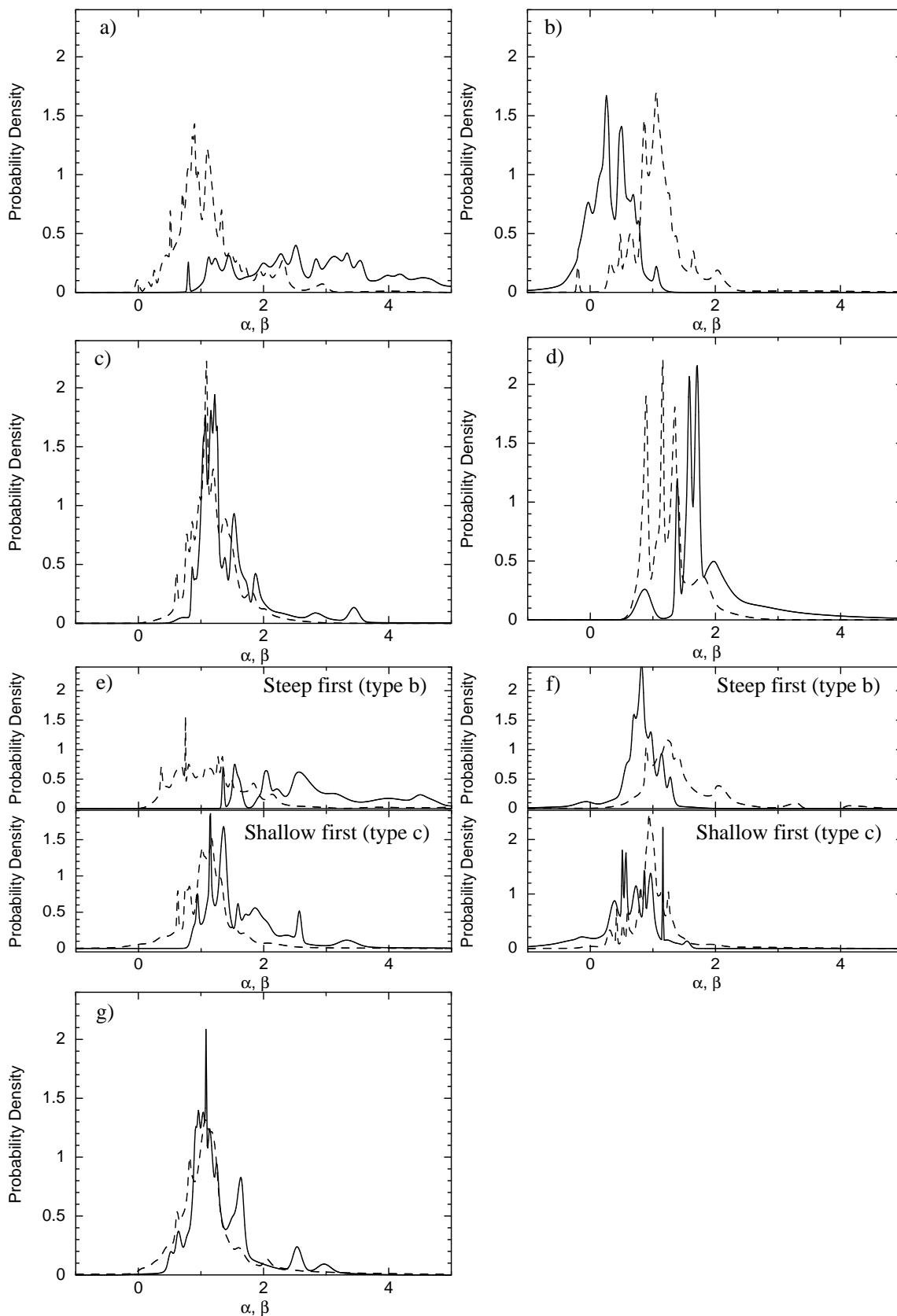


**Figure 11.** PDFs of the temporal (solid lines) and spectral (dashed lines) indices ( $\alpha$  and  $\beta$  respectively) for the different light curve phases. Panels a)–d) are for the ‘canonical’ light curves and show the values from the steep decay, plateau, ‘normal’ and ‘late break’ phases. Panels e)–f) show the values from those light curves showing a single break; the steeper of the segments are plotted in e) and the shallower in f). For clarity, these plots have been split into two panes to separate the type b and c cases. Panel g) show the values for those light curves which do not contain a break

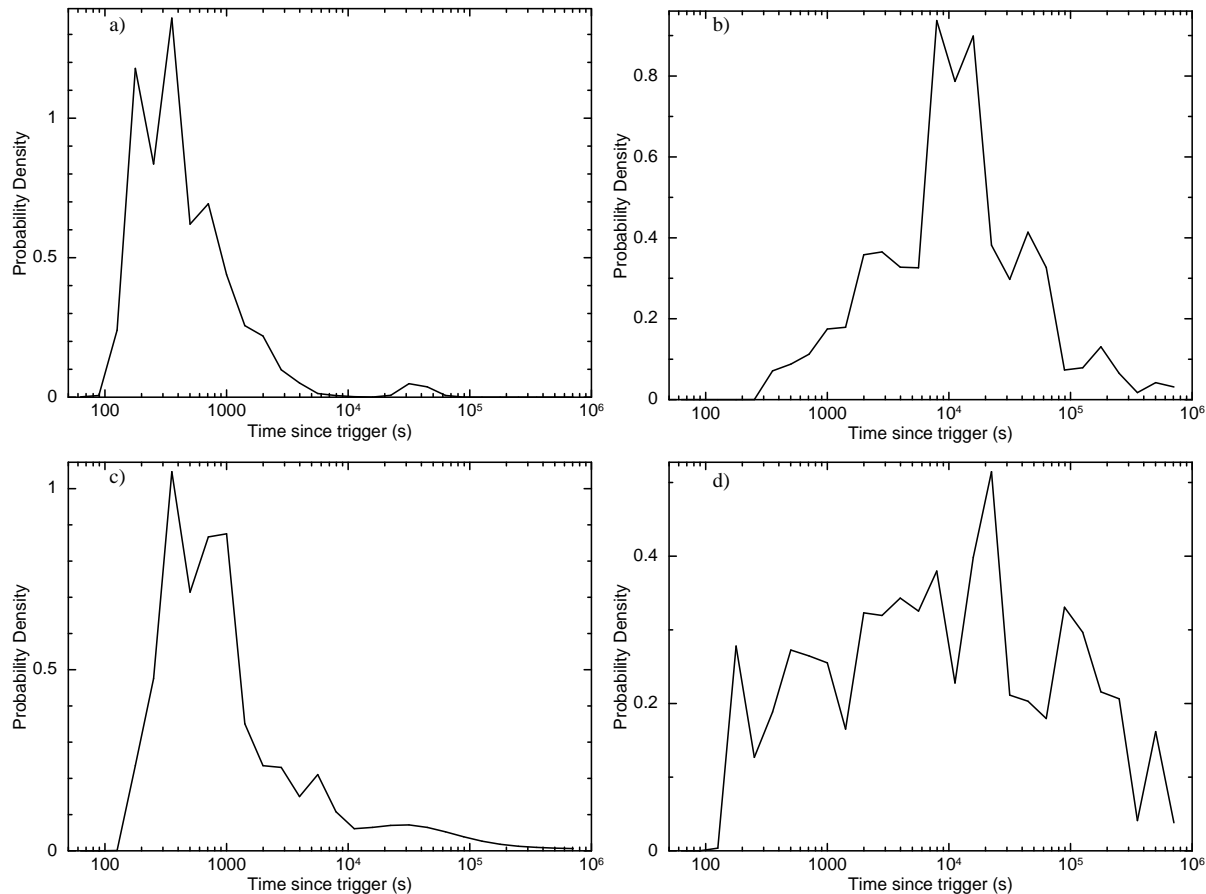


**Figure 14.** PDFs of the break times for the canonical light curve and curves with one break. Panels a) and b) give the start and end times respectively of the plateau phase of canonical light curve. Panel c) shows the break times for light curves which show a single, flattening break (type b) and panel d) gives the break times for those which show a single, steepening break (type c).

that there is a ‘canonical’ X-ray GRB light curve, consisting of 4 power-law phases: a steep initial decay, a shallow plateau, and then a ‘normal’ decay which is steeper than the plateau, but not as steep as the first segment. There may also be a fourth segment, post-jet break decay. Panels c) and d) of Fig. 3 show light curves which conform to this behaviour. Nousek et al. noted that we do not see this exact behaviour in all GRB afterglows, and suggested that this is simply due to limited temporal coverage. O’Brien et al. (2006) meanwhile showed that, for GRBs observed by *Swift*, the prompt emission seen by the BAT transitions smoothly into the emission seen by the XRT.

Willingale et al. (2007) interpreted the observed X-ray emission as the combination of two components, each following a simple exponential-to-power-law form. A late-time break in the power-law may be added occasionally as well. Physically, the two exponential-to-power law components were identified with the prompt GRB emission from internal shocks in the ejecta, and afterglow emission from an external shock in the circumburst medium. Under this model, not all GRBs exhibit all segments of the ‘canonical’ curve. For example, the afterglow component can be sufficiently weak compared to the prompt component that it is never seen, alternatively it can dominate from an early time.

In this paper we have presented a sample of GRBs much

bigger than those used by Nousek et al. or Willingale et al. (who used 27 and 107 bursts respectively), and can thus consider the possibility of a unified afterglow model with more confidence.

We defined a subset of the bursts presented in this paper, comprising only those for which we can reasonably expect to have seen the three phases of the canonical light curve. By inspecting the break times (Table 7) of the canonical light curves (Table 11) we defined such bursts as having XRT data beginning at  $T \leq T_0 + 200$  s and extending to at  $T \geq T_0 + 50000$  s. We also specified that the light curve should contain at least 20 bins. This gave a sample of 162 GRBs, which are shown in bold type in Table 11 (Note that previous studies, e.g. O’Brien et al. (2006); Willingale et al. (2007), did not create such subsets; their samples are analogous to our complete sample, not this subset). Of these 162 bursts:

- 7 (4 %) have no breaks.
- 49 (30 %) have one break (25 type b, 24 type c).
- 68 (42 %) are canonical.
- 38 (24 %) are oddballs.

This immediately shows that the ‘canonical’ light curve, while the most common morphology actually occurs in less than half the GRBs in which it would be identifiable.

Whether or not the underlying afterglow behaviour follows a single behaviour is readily testable with our dataset and we discuss the different light curve morphologies in this context below. To aid this discussion, we show in Fig. 11 the  $\alpha$  and  $\beta$  PDFs for the various light curve phases, (the panels are as in Fig. 10) and in Fig. 14 PDFs of the break times for the different light curve morphologies. These figures were built using all 318 GRBs presented in this paper, not just the subset defined above. Immediately, we see from this that the  $\beta$  values are roughly the same in each light curve segment, although the steep-decay phase of the canonical curves and the steep portion of the one break, steep-to-shallow light curves have a wider range of values than the other phases (a similar conclusion was drawn by Butler & Kocevski 2007a). Note that we do not consider the ‘oddball’ bursts here since these need to be studied individually, whereas we are interested in the bulk properties of afterglows. Schematics of the morphologies discussed below were given in Fig. 9.

### 5.1 Light curves with no breaks

Although we have only seven GRBs with no breaks (Fig. 9, panel d) in our subsample, the distribution of  $\alpha$  values from these GRBs is inconsistent with the distribution from any phase of the canonical GRBs in Table 11 except for the normal decay phase. Even this consistency is low; the K-S test gives a 1.9% probability that the  $\alpha$  values of these 8 GRBs were drawn from the same sample as the normal decay phase of the canonical GRBs (note that the K-S test is not necessarily believable with such a low number of values). This suggests that the no-break GRBs are consistent with the Willingale et al. (2007) model provided we are seeing only the power-law phase of the afterglow component, however the lack of a steep decay phase means that either the prompt emission must decay very rapidly or the afterglow must be bright enough to dominate from a very early time. Further, the lack of a plateau phase implies that energy injection does not dominate at any time; the GRBs in this subset (panel g of Fig. 10) show reasonable agreement with standard afterglow theory, supporting this idea. The outlier in that panel with  $\alpha \sim 8$  is GRB 051221B, and is a candidate ‘naked’ GRB (Willingale et al. 2007).

### 5.2 Light curves with one break: type b (shallowing decays)

Under the Nousek/Willingale models, type b light curves should correspond to the first two segments of a ‘canonical’ light curve, with the plateau phase on-going when observations cease. In terms of Figs 10–11, this means that the black points (upper pane in Fig. 11) in panel e) should come from the same parent population as those in panel a), and those in panel f) from the same population as those in panel b). By eye, the first of these statements seems believable, and a K-S test gives a 17% probability that the  $\alpha$  values of the two samples came from the same parent population. However, the  $\alpha$  values of the shallow decay in these light curves and the plateau phase of the canonical ones are completely different. From Fig. 11 one can see that the distribution in the upper pane of panel f) ( $\bar{\alpha} = 0.085$ ) lies towards significantly higher  $\alpha$  than those in panel b) ( $\bar{\alpha} = 0.34$ ); a

K-S test gives a  $< 0.1\%$  chance that the two come from the same parent population. Further, although the distribution of plateau start times (Fig. 14, panel a) looks similar to that of the type b break times (Fig. 14, panel c), the latter are shifted towards later times; a K-S test gives a 0.3% chance that these share a common population.

It is still possible to reconcile the bursts with a single, steep to shallow break to the same behaviour as the canonical bursts, if the shallow phase is similar to the plateau phase, but the energy injection in these bursts is longer lived and at a lower rate than in the ‘canonical’ bursts. A rigorous investigation of this is beyond the scope of this paper, and will be tackled in a future publication. We do note however that if this is true, energy injection must continue at least to the end of the *Swift* observations, which in all but 3 of these cases, is more than a day (often many days) post-trigger. Producing such long lived energy injection at the necessary level, from the standard GRB progenitor models is difficult, however X-ray flares have been seen  $> 1$  day after the trigger (e.g. GRB 050502B, Falcone et al. 2006; GRB 080810, Page et al. in prep.; see Curran et al. 2008 for a discussion of late-time X-ray flares), implying that the central engine can still affect the afterglow on these timescales.

### 5.3 Light curves with one break: type c (steepening decays)

Compared to the canonical light curve, type c light curves in could correspond to the normal and post-jet break phases of a GRB light curve. From an  $(\alpha, \beta)$  point of view this is acceptable; K-S tests show  $> 1\%$  probability that the red points (lower pane) in panel e) of Figs. 10–11 come from the same population as those in panel c), and those in panel f) come from the same population as panel d). However, for this to be the case 7/25 (=28%) of the ‘jet breaks’ would have to occur within 1000 s of the GRB trigger, suggesting an extremely confined jet. Alternatively, the ‘jet breaks’ in the canonical light curves may not be jet breaks at all; this is suggested by panel d) of Fig. 10 and we discuss this further in Section 6.

Instead of the above, the two phases of these GRBs could be identified with the plateau and normal decay phases of the canonical light curve. The distribution of plateau end times (Fig. 14, panel b) is similar to the (poorly sampled) distribution of type-c break times (Fig. 14, panel d), and a K-S test gives a 40% probability that these represent the same population of times. However, a K-S test between the decay slopes of the shallow part of the type c light curves and the plateaux of canonical bursts gives a  $< 0.1\%$  probability that these come from the same population. This does not definitively rule out this interpretation: if the afterglow dominates the X-ray light curve before the prompt component decays, the effect of energy injection may be less than in a canonical GRB, giving a steeper shallow decay slope, as seen in our data. To investigate, we obtained the BAT fluence from the Swift data table<sup>16</sup> for all of the canonical GRBs in Table 11, and for the one break, shallow-to-steep GRBs from our subsample. If the latter bursts have systematically

<sup>16</sup> via <http://heasarc.gsfc.nasa.gov/docs/swift/results/>

lower fluence than the canonical GRBs, the above explanation holds. No such trend is seen however. strong enough to rule out and fitting flux-unit light curves the canonical GRBs, and will be done in a

## 6 UNDERSTANDING THE X-RAY AFTERGLOW

We have shown above that the different morphologies of GRB light curves are consistent with the two component model of Willingale et al. (2007); implying a consistent underlying behaviour (if not a canonical shape). We now consider what physical processes drive each of the phases obtainable from such a light curve. The large, homogeneously-generated data set in this paper is an ideal test bed for this. The usual explanation of the phases (e.g. Nousek et al. 2006; Zhang et al. 2006, O’Brien et al. 2006) is as follows:

- Steep decay – high latitude prompt emission (internal shocks).
- Plateau – emission from a collimated external forward shock (afterglow) which is undergoing energy injection. The edge of the jet is not visible to the observer.
- Normal decay – emission from a collimated external forward shock with no energy injection. The edge of the jet is not visible to the observer.
- Post jet-break – emission from a collimated external forward shock with no energy injection. The edge of the jet is visible to the observer.

To compare our data with theoretical predictions for the steep decay phase requires modelling of the BAT data, since  $\alpha$  in this regime is sensitive to  $T_0$ , which should be taken as the start time of the final pulse. This is beyond the scope of our XRT-data paper, however many other authors have confirmed that the steep decay phase is consistent with the expectation for high latitude emission (e.g. Tagliaferri et al. 2005; Barthelmy et al. 2005b; O’Brien et al. 2006; Goad et al. 2006; Liang et al. 2006; Willingale et al. 2007; Butler & Kocevski 2007b).

The plateau phase likewise is in good agreement with the above model. Zhang et al. (2006) give the closure relationships for the energy injection scenario, assuming the luminosity of the injecting source  $L \propto t^{-q}$ , where  $q \leq 1$ . The lower edge of the solid grey band plotted in Fig. 10 corresponds to the most tolerant  $q = 1$  limit from such relationships (as does the blue band in panel d for the post-jet break, energy injection relationships taken from Panaitescu et al. 2006). Points lying above this line are consistent with energy injection afterglow theory.

The normal decay phase is not in good agreement with the interpretation above. Panel c) of Fig. 10 shows many of the points to be inconsistent with afterglow theory without energy injection. This disagreement continues into the post jet-break phase (panel d), where the majority of points are consistent with the standard pre-jet break models, but very few are consistent with post jet-break theory. This suggests that the interpretation of the X-ray light curve as given above is incorrect unless energy injection continues for some time after the burst. (Note that we have not given an exhaustive study of jet breaks as we include only breaks which occur after the first three ‘canonical’ phases. For a targeted

study of potential jet breaks in any light curve morphology, see Racusin et al. 2009).

Other models have been proposed instead to explain the observed X-ray light curves. For example, Ghisellini et al. (2007) suggest that the long-term X-ray emission is actually ‘late prompt’ emission, from internal shocks with lower bulk Lorentz factors than in the initial case. They use this to model X-ray and optical light curves with some success (Ghisellini et al. 2008). However in such a model we may expect to see spectral evolution in the late-prompt emission analogous to that seen during the prompt emission; as Table 9, Fig. 11, and the hardness ratios on the XRT light curve repository (Evans et al. 2007) show, there is very little spectral evolution seen in XRT data after the first few hundred seconds post-trigger (O’Brien et al. in preparation). Note that the Ghisellini model implicitly assumes that the late-prompt component does not spectrally evolve, so does fit the observed hardness ratios, however why it does not evolve is not clear. The dust-scattering model of Shao & Dai (2007) suffers from the same problem (Shen et al. 2008). de Pasquale et al. (2008) recently suggested that the end of the X-ray plateau could signify a jet break, where energy injection is ongoing, subsequent ‘jet breaks’ would then signify the end of energy injection. However, this is not consistent with the points in panel d) of Fig. 10 – data taken after the end of the plateau and a subsequent break – which are generally inconsistent with post jet-break models with no energy injection.

The dataset presented in this paper represents the best diagnostic tool for afterglow models currently available, and can be used to place specific constraints on any given model for the X-ray emission. For example, considering the external forward shock model, Fig. 10 tells us that:

- 1) During the plateau phase, energy must be injected into the shock.
- 2) The so-called ‘post jet-break’ phase in the ‘canonical’ light curve is in fact better explained as occurring before the jet break but after the cessation of energy injection than by the standard interpretation of arising after the jet-break and cessation of energy injection.
- 3) Some mechanism must cause a steepening of the light curve, independent of energy injection. It must not invoke any spectral change.

The latter point arises because the break seen between the plateau and normal phases cannot always be caused by the cessation of energy injection: too many points in panel c) lie above the grey band hence must be undergoing energy injection.

There is a reasonable number of bursts whose normal decay phase is consistent with a standard forward shock with no energy injection (i.e. points in Fig. 10 panel c which lie within the grey band) as well as many which do require energy injection during this phase. Thus in the description above it must be possible for the unknown-origin break (in point 3 above) to occur before, or after the cessation of energy injection. Before this break while energy injection is ongoing, a GRB lies on panel b) of Fig. 10, after the break and once energy injection has ceased it lies on panel d). Whether the cessation of energy injection or the unknown-origin break occurs first would then determine whether the GRB lies in or above the grey band during its time on panel c).

There is a significant number of bursts lying above the grey band permitted by the closure relationships in Panel c) of Fig. 10, which do not show a subsequent break. Similarly, the black points in Panel f) represent the last observed state for many GRBs. This implies that for external, forward shock model of the afterglow, significant energy injection must last for days, if not weeks after the trigger. Ghisellini et al. (2008) suggest that this is possible, however it is not clear that their mechanism can produce sufficient levels of energy injection to sustain the shallow decay. Nonetheless, if energy injection from lasting central engine activity (or slow-moving shells ejected at the time of the burst) is responsible for the shallower-than-expected decay, we may expect bursts whose prompt emission is relatively faint compared to the afterglow emission to show little evidence of energy injection (unless the central engine gets brighter with time!). The red points in panels e)–f) of Fig. 10, and the points in panel g) are such bursts: their afterglows show no steep-decay phase, which (see Section 5) may mean that from an early time, the afterglow dominated any prompt emission. As can be seen, the majority of these are consistent with having no energy injection, supporting this model.

The discussion above does not tell us that the forward shock model for X-ray afterglows is the correct model for XRT afterglow emission, however it demonstrated that, with a little reorganising in light of the constraints placed by our dataset, it is still consistent with observations. Nonetheless, two difficulties remain: some mechanism must be found to produce a spectrally invariant temporal break with a wide range of  $\Delta\alpha$ ; and it must be possible to inject a significant amount of energy into the external shock for days to weeks after the explosion.

## 7 CONCLUSIONS

We have developed software to automatically produce light curves and hardness ratios, spectra and high-precision enhanced XRT positions of GRBs. Preliminary versions of these are available within minutes of a trigger, and the full versions available within a few hours. Users can interact with and customise these products as desired. We also provide general purpose versions of these tools to run for any object observed by XRT, available via a web interface.

These products are available online:

- Index: [http://www.swift.ac.uk/xrt\\_products](http://www.swift.ac.uk/xrt_products)
- Positions: [http://www.swift.ac.uk/xrt\\_positions](http://www.swift.ac.uk/xrt_positions)
- Light curves: [http://www.swift.ac.uk/xrt\\_curves](http://www.swift.ac.uk/xrt_curves)
- Spectra: [http://www.swift.ac.uk/xrt\\_spectra](http://www.swift.ac.uk/xrt_spectra)

Using this software we have performed a homogeneous analysis of all GRBs observed by the XRT to date, and presented positions and temporal and spectral indices, in various formats. Analysis of these data show that a variety of light curve morphologies exist, and the so-called ‘canonical’ curve, while the most common case, accounts for less than half of the light curves seen by *Swift*. Defining a subsample of 162 GRBs with sufficient coverage to detect the canonical shape, if it existed, we found:

- 8 (5 %) have no breaks.
- 49 (30 %) have one break (25 shallow, 24 steepen).

- 67 (41 %) are canonical.
- 38 (24 %) are oddballs.

We have, however, demonstrated that this range of morphologies can be explained by a single underlying behaviour; the two-component model suggested by Willingale et al. (2007), which involves a ‘prompt’ component and an ‘afterglow’ component. To achieve this we require a range of prompt-to-afterglow emission ratios, and a range of energy injection rates, both of which are easy to accept given the variations seen from burst to burst.

If the afterglow emission is due to the external forward shock model then in many cases this scenario can only explain the data if energy injection continues beyond the plateau phase, and lasts for days to weeks after the GRB. The data also require a mechanism which can cause a light curve break (i.e. the end of the plateau) without terminating energy injection, and without causing a change in the X-ray spectrum.

### 7.1 Usage policy

Anybody is welcome to use the products and tools details in this paper for their work. Although we have verified these tools as far as possible, we still strongly advise users to ‘sanity check’ their results, particularly with regards to light curve binning (Section 3.3).

If these products or tools are used in any publication, we ask that this paper be cited, and that users include the following statement in the acknowledgements:

“This work made use of data supplied by the UK Swift Science Data Centre at the University of Leicester.”

GRB	Times ignored from fit (s since trigger)	GRB	Times ignored from fit (s since trigger)
GRB 050406	115–430	GRB 070616	480–550, 714–995
GRB 050410	45000–100000	GRB 070621	135–220
GRB 050502B	298–1680, 24800–120000	GRB 070704	257–658
GRB 050607	223–428	GRB 070721B	124–141, 187–858
GRB 050712	179–960	GRB 070724A	90–150
GRB 050713A	96–152, 157–203	GRB 071021	148–300, 1000–9000
GRB 050714B	237–486	GRB 071031	109–700
GRB 050724	220–350, 15831–103776	GRB 071112C	523–726
GRB 050726	0–195, 200–320	GRB 071118	189–225, 321–900
GRB 050730	191–791, 72464–119752	GRB 071122	398–498
GRB 050801	160–700, 3000–6000	GRB 080210	165–379
GRB 050814	1161–1627, 1813–2718	GRB 080212	169–491
GRB 050820A	171–260	GRB 080229A	100–156
GRB 050822	115–193, 218–760	GRB 080310	130–980
GRB 050904	308–600, 1190–1378, 2900–55000	GRB 080319D	264–640
GRB 050908	298–477	GRB 080320	245–500, 650–1000
GRB 050915A	131–180	GRB 080325	158–400
GRB 050916	6501–29640	GRB 080506	364–1200
GRB 050922B	612–1517	GRB 080604	18000–100000
GRB 051117A	150–200, 300–700, 800–2000	GRB 080607	116–210, 3000–7000
GRB 051227	101–121		
GRB 060111A	79–515		
GRB 060115	292–564		
GRB 060124	250–1200,		
GRB 060202	154–163, 35137–52020, 110145–127545		
GRB 060204B	104–138, 246–413		
GRB 060206	1776–11829		
GRB 060210	103–612		
GRB 060218	159–3000		
GRB 060223A	800–2000		
GRB 060312	66–190, 475–817		
GRB 060319	198–474, 740–1861		
GRB 060413	490–950		
GRB 060418	107–215		
GRB 060510B	732–1007		
GRB 060512	147–380		
GRB 060526	208–647		
GRB 060602B	120–300		
GRB 060604	118–237		
GRB 060607A	90–400		
GRB 060707	180–400		
GRB 060712	250–400		
GRB 060714	107–190		
GRB 060719	170–400		
GRB 060729	165–188		
GRB 060814	118–294		
GRB 060904A	160–397, 572–1120		
GRB 060904B	91–726		
GRB 060926	290–1000		
GRB 060929	280–1100		
GRB 061121	66–80		
GRB 061202	126–200		
GRB 070107	250–547, 1245–1661, 64099–116566		
GRB 070110	30000–80000		
GRB 070129	218–1139		
GRB 070318	182–429		
GRB 070330	142–374		
GRB 070419B	87–118, 180–1000		
GRB 070517	700–2000		
GRB 070518	89–227		
GRB 070520B	120–380		

**Table 4** – *continued***Table 4.** Times identified as deviating from power-law decays, and excluded from the light curve fits, see Section 2.4.1 for details.

GRB	RA (J2000.0)	Dec (J2000.0)	Error <sup>1</sup>
GRB050124	12 51 30.55	+13 02 39.6	1.6
GRB050128	14 38 17.73	-34 45 55.2	1.7
GRB050219A	11 05 39.01	-40 41 03.1	2.1
GRB050219B	05 25 16.05	-57 45 29.3	1.5
GRB050223	18 05 32.38	-62 28 21.9	4.3
GRB050315	20 25 54.20	-42 36 01.5	1.5
GRB050318	03 18 50.99	-46 23 45.0	1.4
GRB050319	10 16 47.88	+43 32 55.3	1.4
GRB050326	00 27 48.50	-71 22 18.5	2.2
GRB050406	02 17 52.12	-50 11 16.4	1.9
GRB050408	12 02 17.27	+10 51 09.7	1.4
GRB050410	05 59 13.39	+79 36 11.8	2.0
GRB050416A	12 33 54.60	+21 03 27.2	1.4
GRB050421	20 29 02.79	+73 39 17.9	1.7
GRB050502B	09 30 10.08	+16 59 48.0	1.4
GRB050504	13 24 01.31	+40 42 15.0	2.8
GRB050505	09 27 03.31	+30 16 24.3	1.4
GRB050509A	20 42 20.00	+54 04 17.2	2.1
GRB050509B	12 36 13.75	+28 59 03.4	3.3
GRB050525A	18 32 32.68	+26 20 22.5	1.5
GRB050603	02 39 56.93	-25 10 54.7	1.4
GRB050701	15 09 01.55	-59 24 52.5	3.0
GRB050712	05 10 48.19	+64 54 48.2	1.5
GRB050713A	21 22 09.36	+77 04 28.9	1.4
GRB050713B	20 31 15.54	+60 56 43.8	1.4
GRB050714B	11 18 47.63	-15 32 48.9	1.5
GRB050716	22 34 20.79	+38 41 04.2	1.4
GRB050717	14 17 24.45	-50 32 00.4	1.5
GRB050721	16 53 44.54	-28 22 52.0	1.7
GRB050724	16 24 44.29	-27 32 26.9	1.5
GRB050726	13 20 11.91	-32 03 51.3	1.4
GRB050730	14 08 17.14	-03 46 18.4	1.4
GRB050802	14 37 05.81	+27 47 11.5	1.4
GRB050803	23 22 37.91	+05 47 09.1	1.4
GRB050813	16 07 56.97	+11 14 57.8	2.9
GRB050814	17 36 45.29	+46 20 22.2	1.4
GRB050815	19 34 22.94	+09 08 48.5	1.5
GRB050819	23 55 01.65	+24 51 38.8	1.5
GRB050820A	22 29 38.13	+19 33 37.5	1.4
GRB050822	03 24 27.24	-46 01 59.6	1.4
GRB050824	00 48 56.25	+22 36 33.3	1.5
GRB050826	05 51 01.62	-02 38 36.6	1.5
GRB050827	04 17 09.62	+18 12 01.1	1.5
GRB050904	00 54 50.88	+14 05 10.4	1.4
GRB050908	01 21 50.79	-12 57 18.5	1.5
GRB050915A	05 26 44.87	-28 00 58.8	1.4
GRB050915B	14 36 25.90	-67 24 33.4	1.6
GRB050916	09 03 57.26	-51 25 42.7	1.5
GRB050922B	00 23 13.40	-05 36 17.9	1.7
GRB050922C	21 09 33.02	-08 45 30.6	1.4
GRB051001	23 23 48.79	-31 31 21.9	1.7
GRB051006	07 23 14.12	+09 30 20.0	1.5
GRB051008	13 31 29.59	+42 05 53.0	1.4
GRB051016A	08 11 16.68	-18 17 53.1	1.5
GRB051016B	08 48 27.87	+13 39 19.7	1.4
GRB051021A	01 56 36.28	+09 04 01.6	1.5
GRB051021B	08 24 12.24	-45 32 28.5	1.6
GRB051022	23 56 04.06	+19 36 23.9	1.4
GRB051028	01 48 15.02	+47 45 11.4	1.7
GRB051109A	22 01 15.25	+40 49 22.6	1.4
GRB051109B	23 01 50.33	+38 40 46.5	1.5
GRB051111	23 12 33.08	+18 22 27.9	1.5
GRB051117A	15 13 34.09	+30 52 11.8	1.6

**Table 5.** All available enhanced XRT positions of GRBs observed by *Swift*. The positions are also available online at [http://www.swift.ac.uk/xrt\\_positions](http://www.swift.ac.uk/xrt_positions), which is updated auto-

GRB	RA (J2000.0)	Dec (J2000.0)	Error <sup>1</sup>
GRB051117B	05 40 43.39	-19 16 26.9	1.7
GRB051210	22 00 41.33	-57 36 49.4	1.7
GRB051211B	23 02 41.53	+55 04 50.7	1.6
GRB051221A	21 54 48.58	+16 53 26.0	1.4
GRB051221B	20 49 35.25	+53 02 10.7	2.1
GRB051227	08 20 58.31	+31 55 31.0	1.6
GRB060105	19 50 00.68	+46 20 55.4	1.4
GRB060108	09 48 02.13	+31 55 07.2	1.5
GRB060109	18 50 43.65	+31 59 26.5	1.4
GRB060111A	18 24 49.12	+37 36 14.0	1.5
GRB060111B	19 05 42.64	+70 22 33.0	1.4
GRB060115	03 36 08.29	+17 20 42.7	1.4
GRB060116	05 38 46.24	-05 26 13.9	1.5
GRB060121	09 09 52.09	+45 39 47.2	1.6
GRB060124	05 08 25.86	+69 44 26.5	1.4
GRB060202	02 23 22.97	+38 23 03.1	1.4
GRB060203	06 54 03.72	+71 48 38.9	1.4
GRB060204B	14 07 15.04	+27 40 37.0	1.4
GRB060206	13 31 43.44	+35 03 02.9	1.6
GRB060210	03 50 57.33	+27 01 33.7	1.4
GRB060211A	03 53 32.59	+21 29 19.1	1.5
GRB060211B	05 00 17.11	+14 56 57.3	1.6
GRB060218	03 21 39.65	+16 52 01.3	1.4
GRB060219	16 07 21.49	+32 18 57.1	1.5
GRB060223A	03 40 49.57	-17 07 49.9	1.5
GRB060306	02 44 22.83	-02 08 55.1	1.4
GRB060313	04 26 28.43	-10 50 41.5	1.4
GRB060319	11 45 33.05	+60 00 39.6	1.4
GRB060323	11 37 45.13	+49 59 08.3	1.6
GRB060403	18 49 21.60	+08 19 46.7	2.3
GRB060413	19 25 07.85	+13 45 29.9	1.4
GRB060418	15 45 42.66	-03 38 20.4	1.4
GRB060421	22 54 33.07	+62 43 51.4	1.7
GRB060427	08 17 04.03	+62 40 16.8	1.4
GRB060428A	08 14 10.81	-37 10 11.7	1.4
GRB060428B	15 41 25.70	+62 01 30.1	1.4
GRB060502A	16 03 42.50	+66 36 02.6	1.5
GRB060502B	18 35 45.25	+52 37 53.9	5.2
GRB060505	22 07 03.38	-27 48 52.9	1.9
GRB060507	05 59 50.67	+75 14 54.8	1.5
GRB060510B	15 56 29.25	+78 34 12.1	1.5
GRB060512	13 03 05.73	+41 11 26.6	1.5
GRB060515	08 29 09.61	+73 34 04.8	3.8
GRB060522	21 31 44.89	+02 53 10.3	1.5
GRB060526	15 31 18.34	+00 17 05.9	1.4
GRB060602B	17 49 31.83	-28 08 04.5	1.6
GRB060604	22 28 55.10	-10 54 55.7	1.4
GRB060605	21 28 37.35	-06 03 30.3	1.4
GRB060607A	21 58 50.41	-22 29 47.1	1.4
GRB060614	21 23 32.19	-53 01 36.5	1.4
GRB060707	23 48 19.11	-17 54 17.6	1.7
GRB060708	00 31 13.83	-33 45 32.2	1.4
GRB060712	12 16 16.16	+35 32 17.6	1.6
GRB060714	15 11 26.39	-06 33 59.0	1.4
GRB060717	11 23 21.61	+28 57 03.0	3.2
GRB060719	01 13 43.76	-48 22 50.1	1.4
GRB060729	06 21 31.84	-62 22 12.1	1.4
GRB060801	14 12 01.30	+16 58 54.0	1.5
GRB060804	07 28 49.32	-27 12 55.0	1.5
GRB060805A	14 43 43.45	+12 35 11.6	1.6
GRB060805B	18 10 05.41	+58 09 19.0	1.7
GRB060807	16 50 02.63	+31 35 30.2	1.4
GRB060813	07 27 35.38	-29 50 49.3	1.4

**Table 5 – continued** <sup>1</sup>arc seconds, 90% confidence radius. Also available online at [http://www.swift.ac.uk/xrt\\_positions](http://www.swift.ac.uk/xrt_positions), updated automatically with new GRBs.

GRB	RA (J2000.0)	Dec (J2000.0)	Error <sup>1</sup>
GRB060814	14 45 21.32	+20 35 09.2	1.4
GRB060825	01 12 29.43	+55 47 51.8	2.0
GRB060901	19 08 37.81	-06 38 05.7	2.9
GRB060904B	03 52 50.56	-00 43 30.1	1.4
GRB060906	02 43 00.90	+30 21 43.0	1.4
GRB060908	02 07 18.42	+00 20 32.4	1.4
GRB060912A	00 21 08.11	+20 58 19.2	1.4
GRB060919	18 27 41.74	-51 00 52.5	1.7
GRB060923A	16 58 28.10	+12 21 37.9	1.5
GRB060926	17 35 43.70	+13 02 16.6	1.6
GRB060927	21 58 12.02	+05 21 48.6	1.6
GRB060929	17 32 28.92	+29 50 06.2	1.5
GRB061002	14 41 23.51	+48 44 28.6	2.2
GRB061004	06 31 10.91	-45 54 24.3	1.4
GRB061006	07 24 07.83	-79 11 55.3	1.9
GRB061007	03 05 19.70	-50 30 02.8	1.4
GRB061019	06 06 31.01	+29 34 12.3	1.5
GRB061021	09 40 36.17	-21 57 05.1	1.4
GRB061025	20 03 36.87	-48 14 38.3	2.3
GRB061028	06 28 54.69	+46 17 57.5	1.6
GRB061110A	22 25 09.85	-02 15 31.1	1.6
GRB061110B	21 35 40.43	+06 52 31.9	1.7
GRB061121	09 48 54.61	-13 11 42.0	1.4
GRB061122	20 15 19.83	+15 31 00.8	1.4
GRB061126	05 46 24.55	+64 12 39.8	1.4
GRB061201	22 08 32.22	-74 34 48.2	1.4
GRB061202	07 02 06.20	-74 41 54.9	1.4
GRB061217	10 41 37.10	-21 07 33.8	3.4
GRB061222A	23 53 03.37	+46 31 57.5	1.4
GRB061222B	07 01 24.70	-25 51 35.3	1.7
GRB070103	23 30 13.75	+26 52 33.8	1.4
GRB070107	10 37 36.56	-53 12 47.6	1.4
GRB070110	00 03 39.27	-52 58 28.5	1.4
GRB070125	07 51 17.80	+31 09 04.8	1.5
GRB070129	02 28 00.93	+11 41 03.3	1.4
GRB070208	13 11 32.77	+61 57 54.9	1.5
GRB070219	17 20 46.19	+69 22 12.6	1.7
GRB070220	02 19 06.82	+68 48 16.5	1.4
GRB070223	10 13 48.37	+43 08 01.9	1.8
GRB070224	11 56 06.61	-13 19 49.8	1.6
GRB070227	08 02 19.33	-46 18 51.3	1.9
GRB070306	09 52 23.22	+10 28 55.3	1.4
GRB070309	17 34 39.86	-37 55 50.3	4.4
GRB070311	05 50 08.22	+03 22 29.4	1.5
GRB070318	03 13 56.72	-42 56 47.0	1.4
GRB070328	04 20 27.68	-34 04 00.6	1.4
GRB070330	17 58 10.24	-63 47 34.7	1.5
GRB070411	07 09 19.90	+01 03 52.4	1.5
GRB070412	12 06 10.03	+40 08 35.8	1.5
GRB070419A	12 10 58.83	+39 55 31.1	1.7
GRB070419B	21 02 49.84	-31 15 48.1	1.5
GRB070420	08 04 55.12	-45 33 21.2	1.4
GRB070429A	19 50 48.94	-32 24 17.4	2.1
GRB070429B	21 52 03.85	-38 49 40.8	2.3
GRB070506	23 08 52.30	+10 43 21.2	1.8
GRB070508	20 51 12.00	-78 23 04.7	1.4
GRB070509	15 51 50.40	-78 39 07.5	1.9
GRB070518	16 56 47.68	+55 17 42.6	1.6
GRB070520A	12 53 26.05	+74 59 23.3	3.4
GRB070520B	08 07 31.08	+57 36 30.0	1.8
GRB070521	16 10 38.60	+30 15 22.9	1.4
GRB070529	18 54 58.30	+20 39 34.3	1.4
GRB070531	00 26 58.58	+74 18 46.6	1.8

**Table 5** – *continued* <sup>1</sup>arc seconds, 90% confidence radius. Also available online at [http://www.swift.ac.uk/xrt\\_positions](http://www.swift.ac.uk/xrt_positions), updated automatically with new GRBs.

GRB	RA (J2000.0)	Dec (J2000.0)	Error <sup>1</sup>
GRB070611	00 07 58.15	-29 45 20.4	1.8
GRB070612B	17 26 54.46	-08 45 04.7	1.8
GRB070616	02 08 36.40	+56 56 45.0	1.4
GRB070621	21 35 10.17	-24 49 02.6	1.4
GRB070628	07 41 06.06	-20 16 45.3	1.4
GRB070704	23 38 47.31	+66 15 12.7	1.7
GRB070714A	02 51 43.36	+30 14 35.1	1.8
GRB070714B	03 51 22.30	+28 17 51.3	1.4
GRB070721A	00 12 39.20	-28 33 00.0	1.6
GRB070721B	02 12 32.98	-02 11 39.8	1.5
GRB070724A	01 51 14.08	-18 35 38.8	1.8
GRB070724B	01 09 56.68	+57 40 37.6	2.0
GRB070729	03 45 16.04	-39 19 19.9	2.5
GRB070802	02 27 35.91	-55 31 39.1	1.5
GRB070808	00 27 03.40	+01 10 35.4	1.5
GRB070810A	12 39 51.18	+10 45 02.8	1.4
GRB071025	23 40 17.02	+31 46 42.4	1.4
GRB071028A	07 59 16.66	+21 29 05.0	1.5
GRB071031	00 25 37.40	-58 03 33.9	1.5
GRB071104	19 42 26.78	+14 36 35.8	1.5
GRB071112C	02 36 50.89	+28 22 16.9	1.4
GRB071117	22 20 10.40	-63 26 36.6	1.5
GRB071118	19 58 51.77	+70 07 27.9	1.4
GRB071122	18 26 25.26	+47 04 29.5	1.8
GRB071227	03 52 31.09	-55 59 03.3	1.6
GRB080120	15 01 03.29	-10 52 30.5	1.8
GRB080123	22 35 46.16	-64 54 02.7	1.7
GRB080129	07 01 08.13	-07 50 47.8	1.4
GRB080130	17 26 27.27	-53 11 14.4	4.3
GRB080205	06 33 00.43	+62 47 31.2	1.5
GRB080207	13 50 03.02	+07 30 08.0	1.4
GRB080210	16 45 04.03	+13 49 36.3	1.5
GRB080212	15 24 35.44	-22 44 30.5	1.4
GRB080218B	11 51 49.66	-53 05 49.0	1.8
GRB080229A	15 12 52.31	-14 42 16.2	1.4
GRB080303	07 28 14.18	-70 14 03.2	1.5
GRB080307	09 06 30.73	+35 08 19.8	1.4
GRB080310	14 40 13.89	-00 10 30.4	1.4
GRB080319A	13 45 19.97	+44 04 49.1	1.7
GRB080319B	14 31 41.04	+36 18 09.2	1.4
GRB080319C	17 15 55.48	+55 23 31.7	1.7
GRB080319D	06 37 53.47	+23 56 33.7	1.5
GRB080320	11 50 56.37	+57 09 25.3	1.4
GRB080325	18 31 34.40	+36 31 26.1	1.7
GRB080328	05 21 55.81	+47 30 38.0	1.4
GRB080409	05 37 19.20	+05 05 05.1	1.6
GRB080411	02 31 54.82	-71 18 07.5	1.4
GRB080413A	19 09 11.73	-27 40 39.6	1.5
GRB080413B	21 44 34.62	-19 58 51.2	1.4
GRB080426	01 45 59.79	+69 28 06.0	1.5
GRB080430	11 01 14.63	+51 41 07.8	1.4
GRB080503	19 06 28.74	+68 47 35.8	1.6
GRB080506	21 57 41.79	+38 59 06.7	1.4
GRB080507	15 34 43.41	+56 26 08.4	2.3
GRB080514B	21 31 22.61	+00 42 30.3	1.7
GRB080516	08 02 34.16	-26 09 35.3	1.5
GRB080517	06 48 58.00	+50 44 06.3	1.6
GRB080520	18 40 46.50	-54 59 30.4	1.6
GRB080523	01 23 11.53	-64 01 50.9	1.5
GRB080602	01 16 42.18	-09 13 55.4	1.7
GRB080603A	18 37 37.95	+62 44 39.6	1.6
GRB080603B	11 46 07.46	+68 03 38.5	1.7
GRB080604	15 47 51.64	+20 33 28.5	1.5

**Table 5** – *continued* <sup>1</sup>arc seconds, 90% confidence radius. Also available online at [http://www.swift.ac.uk/xrt\\_positions](http://www.swift.ac.uk/xrt_positions), updated automatically with new GRBs.

GRB	RA (J2000.0)	Dec (J2000.0)	Error <sup>1</sup>
GRB080605	17 28 30.04	+04 00 56.9	1.5
GRB080607	12 59 47.14	+15 55 09.6	1.4
GRB080613A	14 13 04.98	+05 10 21.8	2.0
GRB080613B	11 35 11.51	-07 06 17.5	2.5
GRB080623	15 50 38.65	-62 02 57.3	1.5
GRB080625	19 53 37.09	+56 16 41.7	1.7
GRB080701	03 03 21.31	+75 28 29.3	1.7
GRB080702A	20 52 12.21	+72 18 46.7	1.8
GRB080702B	23 42 32.07	-05 31 51.7	2.2
GRB080703	06 47 12.43	-63 13 08.3	1.4
GRB080707	02 10 28.48	+33 06 35.1	1.5
GRB080710	00 33 05.68	+19 30 05.8	1.4
GRB080714	12 32 25.29	-60 16 40.2	1.5
GRB080721	14 57 55.76	-11 43 24.9	1.4
GRB080723A	18 17 57.70	-06 53 58.3	1.4
GRB080723B	11 47 19.77	-60 14 27.9	1.5

**Table 5** – *continued* <sup>1</sup>arc seconds, 90% confidence radius. Also available online at <http://www.swift.ac.uk/xrt-positions>, updated automatically with new GRBs.

GRB	Target ID	$T_{90}$	$F_{11}$	$\alpha_1$	$\alpha_2$	$\alpha_3$	$\alpha_4$	$\alpha_5$	$\alpha_6$
GRB 041223	00100585	109.1		$1.90^{+0.40}_{-0.39}$					
GRB 050124	00103647	4.0	1.12e-12	$1.50^{+0.15}_{-0.15}$					
GRB 050126	00103780	24.8	1.22e-13	$2.57^{+0.99}_{-0.46}$	$0.94^{+0.24}_{-0.31}$				
GRB 050128	00103906	19.2	2.25e-12	$0.955^{+0.038}_{-0.108}$	$1.361^{+0.075}_{-0.059}$				
GRB 050215B	00106107	8.1	3.10e-13	$0.92^{+0.15}_{-0.13}$					
GRB 050219A	00106415	23.7	8.73e-13	$2.91^{+0.25}_{-0.25}$	$0.754^{+0.089}_{-0.083}$				
GRB 050219B	00106442	30.7	3.53e-12	$1.254^{+0.038}_{-0.037}$					
GRB 050223	00106709	22.5	1.17e-13	$0.89^{+0.27}_{-0.22}$					
GRB 050315	00111063	95.6	4.24e-12	$3.51^{+0.24}_{-0.21}$	$0.257^{+0.034}_{-0.038}$	$1.216^{+0.064}_{-0.063}$			
GRB 050318	00111529	32	8.25e-13	$1.21^{+0.13}_{-0.17}$	$1.86^{+0.15}_{-0.13}$				
GRB 050319	00111622	152.5	3.26e-12	$4.77^{+0.24}_{-1.05}$	$0.493^{+0.048}_{-0.049}$	$0.96^{+0.20}_{-0.12}$	$3^{+26}_{-1}$		
GRB 050326	00112453	29.3	8.48e-13	$1.657^{+0.051}_{-0.049}$					
GRB 050401	00113120	33.3	3.52e-12	$0.569^{+0.022}_{-0.022}$	$1.428^{+0.095}_{-0.077}$				
GRB 050406	00113872	5.4	8.90e-14	$0.386^{+0.062}_{-0.266}$	$1^{+9}_{-2}$				
GRB 050408	00020004	N/A	1.40e-12	$0.960^{+0.026}_{-0.024}$					
GRB 050410	00114299	42.5	6.78e-13	$0.68^{+0.14}_{-0.10}$	$1.28^{+1.11}_{-0.28}$				
GRB 050412	00114485	26.5	4.44e-14	$1.39^{+0.25}_{-0.23}$					
GRB 050416A	00114753	2.5	8.27e-13	$1.64^{+1.18}_{-0.95}$	$0.29^{+0.26}_{-0.70}$	$0.859^{+0.023}_{-0.023}$			
GRB 050421	00115135	15.0	4.28e-18	$0.69^{+0.15}_{-1.10}$	$3.33^{+0.24}_{-0.21}$				
GRB 050422	00115214	59.3	5.48e-14	$4.84^{+1.35}_{-0.97}$	$0.91^{+0.13}_{-0.23}$				
GRB 050502B	00116116	17.7	3.99e-13	$0.743^{+0.049}_{-0.056}$	$1.74^{+2.77}_{-0.58}$				
GRB 050505	00117504	58.9	2.70e-12	$0.32^{+0.22}_{-0.10}$	$1.189^{+0.074}_{-0.069}$	$1.734^{+0.154}_{-0.096}$			
GRB 050509A	00118707	11.4	3.38e-13	$1.143^{+0.102}_{-0.092}$					
GRB 050520	00020010	N/A	4.35e-14	$1.73^{+0.47}_{-0.47}$					
GRB 050525A	00130088	8.8	1.18e-12	$0.646^{+0.724}_{-0.030}$	$1.586^{+0.040}_{-0.042}$				
GRB 050603	00131560	12.4	2.19e-12	$1.659^{+0.092}_{-0.087}$					
GRB 050607	00132247	26.4	1.98e-13	$-0.37^{+0.61}_{-0.91}$	$5^{+2}_{-1}$	$0.59^{+0.13}_{-0.17}$	$1.17^{+0.21}_{-0.13}$		
GRB 050701	00143708	21.8	3.10e-13	$1.22^{+0.19}_{-0.18}$					
GRB 050712	00145581	51.6	6.72e-13	$0.833^{+0.070}_{-0.082}$	$1.25^{+0.21}_{-0.17}$				
GRB 050713A	00145675	124.7	1.77e-12	$8.43^{+0.51}_{-2.78}$	$2.37^{+0.11}_{-0.19}$	$-0.22^{+0.12}_{-0.26}$	$1.157^{+0.029}_{-0.028}$		
GRB 050713B	00145754	54.2	5.47e-12	$3.08^{+0.13}_{-0.13}$	$-0.11^{+0.11}_{-0.13}$	$1.038^{+0.038}_{-0.038}$			
GRB 050714B	00145994	46.7	1.62e-13	$6.91^{+0.89}_{-0.86}$	$0.573^{+0.080}_{-0.079}$				
GRB 050716	00146227	69.1	5.34e-13	$0.21^{+0.22}_{-0.22}$	$2.116^{+0.071}_{-0.069}$	$0.974^{+0.060}_{-0.055}$			
GRB 050717	00146372	85.0	6.56e-14	$1.95^{+0.19}_{-0.10}$	$1.316^{+0.064}_{-0.054}$	$3^{+16}_{-1}$			
GRB 050721	00146970	98.4	5.18e-13	$1.592^{+0.094}_{-0.085}$	$0.91^{+0.16}_{-0.15}$				
GRB 050724	00147478	96.0	1.56e-13	$1.702^{+0.065}_{-0.069}$	$6.24^{+0.15}_{-0.32}$	$0.82^{+0.16}_{-0.12}$			
GRB 050726	00147788	49.9	3.52e-13	$0.982^{+0.041}_{-0.043}$	$1.83^{+0.19}_{-0.15}$				
GRB 050730	00148225	156.5	3.60e-12	$0.512^{+0.016}_{-0.016}$	$2.570^{+0.051}_{-0.050}$				
GRB 050801	00148522	19.4	1.57e-13	$1.022^{+0.086}_{-0.113}$	$1.27^{+1.36}_{-0.18}$				
GRB 050802	00148646	19.0	1.41e-12	$0.700^{+0.063}_{-0.061}$	$1.593^{+0.088}_{-0.049}$				
GRB 050803	00148833	87.9	2.35e-12	$5.35^{+0.65}_{-0.58}$	$0.515^{+0.044}_{-0.045}$	$1.677^{+0.080}_{-0.075}$			
GRB 050814	00150314	150.9	9.31e-13	$3.343^{+0.080}_{-0.069}$	$0.527^{+0.070}_{-0.069}$	$1.80^{+0.57}_{-0.26}$			
GRB 050815	00150532	2.9	7.34e-14	$0.15^{+0.12}_{-0.48}$	$1.92^{+0.34}_{-0.28}$				
GRB 050819	00151131	37.7	1.49e-13	$3.97^{+0.53}_{-0.40}$	$0.752^{+0.114}_{-0.100}$				
GRB 050820A	00151207	26	9.40e-12	$2.00^{+0.36}_{-0.32}$	$0.215^{+0.051}_{-0.243}$	$1.265^{+0.018}_{-0.017}$			
GRB 050822	00151486	103.4	1.65e-12	$3.00^{+0.34}_{-0.23}$	$0.206^{+0.076}_{-0.111}$	$1.052^{+0.042}_{-0.040}$			
GRB 050824	00151905	22.6	8.85e-13	$0.342^{+0.106}_{-0.079}$	$0.879^{+0.097}_{-0.070}$				
GRB 050826	00152113	35.5	3.06e-13	$1.30^{+0.19}_{-0.22}$	$0.75^{+0.17}_{-0.20}$	$1.60^{+2.18}_{-0.45}$			
GRB 050827	00152325	50.0		$1.56^{+0.15}_{-0.14}$					
GRB 050904	00153514	174.2	1.96e-13	$2.012^{+0.050}_{-0.048}$	$1.49^{+0.39}_{-1.06}$				
GRB 050908	00154112	19.4	6.28e-14	$1.293^{+0.069}_{-0.064}$					
GRB 050915A	00155242	52.0	2.94e-13	$0.911^{+0.032}_{-0.032}$					
GRB 050915B	00155284	40.9	2.61e-13	$5.32^{+0.32}_{-0.32}$	$0.690^{+0.041}_{-0.040}$				
GRB 050916	00155408	49.5	1.21e-13	$4.88^{+3.42}_{-0.98}$	$0.998^{+0.093}_{-0.081}$				
GRB 050922B	00156434	150.9	9.51e-13	$3.513^{+0.096}_{-0.091}$	$0.349^{+0.084}_{-0.075}$	$1.71^{+0.37}_{-0.32}$			
GRB 050922C	00156467	4.5	6.19e-13	$0.985^{+0.063}_{-0.063}$	$1.372^{+0.052}_{-0.049}$				
GRB 051001	00157870	189.1	2.33e-13	$0.84^{+0.90}_{-0.60}$	$3.235^{+0.111}_{-0.088}$	$0.752^{+0.075}_{-0.078}$			

**Table 6.** Power-law decay indices from light curve fits. A positive value of  $\alpha$  indicates a decay. The break times between indices are given in Table 7. For bursts where the light curve straddles  $T_0 + 11$  hrs, the model flux at 11 hours is given (in  $\text{erg cm}^{-2} \text{s}^{-1}$ ). The *Swift* target ID and BAT  $T_{90}$  (taken from the Swift Data Table) are given for reference.

GRB	Target ID	$T_{90}$	$F_{11}$	$\alpha_1$	$\alpha_2$	$\alpha_3$	$\alpha_4$	$\alpha_5$	$\alpha_6$
GRB 051006	00158593	34.8	2.91e-14	1.608 <sup>+0.073</sup> <sub>-0.063</sub>					
GRB 051008	00158855	>32	9.91e-13	0.966 <sup>+0.081</sup> <sub>-0.085</sub>	2.064 <sup>+0.110</sup> <sub>-0.097</sub>				
GRB 051016A	00159913	23.0	9.66e-14	3.86 <sup>+0.67</sup> <sub>-0.43</sub>	0.894 <sup>+0.049</sup> <sub>-0.047</sub>				
GRB 051016B	00159994	4.0	7.22e-13	7.10 <sup>+0.50</sup> <sub>-1.23</sub>	0.143 <sup>+0.076</sup> <sub>-0.086</sub>	1.009 <sup>+0.049</sup> <sub>-0.048</sub>			
GRB 051021A	00020018	N/A	8.62e-13	1.058 <sup>+0.072</sup> <sub>-0.063</sub>					
GRB 051021B	00160672	46.5	8.94e-14	1.933 <sup>+0.104</sup> <sub>-0.098</sub>	0.73 <sup>+0.45</sup> <sub>-0.56</sub>				
GRB 051022	00020019	N/A	8.65e-12	1.547 <sup>+0.075</sup> <sub>-0.072</sub>	2.27 <sup>+0.45</sup> <sub>-0.34</sub>				
GRB 051028	00020020	66.9	1.04e-12	1.15 <sup>+0.16</sup> <sub>-0.12</sub>					
GRB 051109A	00163136	37.2	2.82e-12	3.23 <sup>+0.53</sup> <sub>-0.42</sub>	0.513 <sup>+0.060</sup> <sub>-0.149</sub>	1.221 <sup>+0.025</sup> <sub>-0.023</sub>			
GRB 051109B	00163170	14.3	1.61e-13	3.66 <sup>+6.34</sup> <sub>-0.69</sub>	-0.09 <sup>+0.26</sup> <sub>-0.15</sub>	1.033 <sup>+0.077</sup> <sub>-0.067</sub>			
GRB 051111	00163438	46.1	3.12e-13	1.60 <sup>+0.11</sup> <sub>-0.10</sub>					
GRB 051117A	00164268	136.3	5.62e-13	1.055 <sup>+0.016</sup> <sub>-0.016</sub>	19 <sup>+107</sup> <sub>-14</sub>	0.917 <sup>+0.042</sup> <sub>-0.041</sub>			
GRB 051117B	00164279	9.0	2.84e-15	1.71 <sup>+0.33</sup> <sub>-0.31</sub>					
GRB 051210	00171931	1.3	9.42e-17	2.53 <sup>+0.13</sup> <sub>-0.12</sub>					
GRB 051211B	00020025	N/A	5.63e-13	0.982 <sup>+0.064</sup> <sub>-0.062</sub>					
GRB 051221A	00173780	1.4	7.50e-13	1.442 <sup>+0.061</sup> <sub>-0.059</sub>	0.07 <sup>+0.20</sup> <sub>-0.21</sub>	1.390 <sup>+0.079</sup> <sub>-0.070</sub>			
GRB 051221B	00173904	39.9	1.65e-28	8 <sup>+3</sup> <sub>-2</sub>					
GRB 051227	00174738	114.6	9.50e-14	2.54 <sup>+0.28</sup> <sub>-0.13</sub>	1.125 <sup>+0.067</sup> <sub>-0.082</sub>				
GRB 060105	00175942	54.4	1.87e-12	1.175 <sup>+0.162</sup> <sub>-0.099</sub>	0.798 <sup>+0.021</sup> <sub>-0.021</sub>	2.282 <sup>+0.073</sup> <sub>-0.073</sub>	0.26 <sup>+0.43</sup> <sub>-0.45</sub>	2.01 <sup>+0.22</sup> <sub>-0.15</sub>	
GRB 060108	00176453	14.3	5.35e-13	1.53 <sup>+0.55</sup> <sub>-0.34</sub>	0.32 <sup>+0.13</sup> <sub>-0.19</sub>	1.17 <sup>+0.17</sup> <sub>-0.11</sub>			
GRB 060109	00176620	115.4	4.77e-13	4.56 <sup>+0.35</sup> <sub>-0.29</sub>	0.108 <sup>+0.088</sup> <sub>-0.088</sub>	1.56 <sup>+0.11</sup> <sub>-0.10</sub>			
GRB 060110	00176702	26.0		1.86 <sup>+1.28</sup> <sub>-0.24</sub>					
GRB 060111A	00176818	13.2	4.89e-13	1.530 <sup>+0.043</sup> <sub>-0.039</sub>	0.830 <sup>+0.054</sup> <sub>-0.052</sub>				
GRB 060111B	00176918	58.8	2.45e-13	3.42 <sup>+0.44</sup> <sub>-0.44</sub>	0.967 <sup>+0.087</sup> <sub>-0.086</sub>	1.33 <sup>+0.18</sup> <sub>-0.13</sub>			
GRB 060115	00177408	139.6	3.87e-13	3.09 <sup>+0.20</sup> <sub>-0.22</sub>	0.838 <sup>+0.036</sup> <sub>-0.035</sub>				
GRB 060116	00177533	105.9	2.28e-13	1.049 <sup>+0.049</sup> <sub>-0.044</sub>					
GRB 060121	00020027	N/A	8.05e-13	1.204 <sup>+0.060</sup> <sub>-0.056</sub>					
GRB 060123	00020028	N/A		1.23 <sup>+0.13</sup> <sub>-0.13</sub>					
GRB 060124	00178750	75	1.04e-11	-0.31 <sup>+0.37</sup> <sub>-0.18</sub>	1.097 <sup>+0.066</sup> <sub>-0.074</sub>	1.465 <sup>+0.047</sup> <sub>-0.042</sub>			
GRB 060202	00179968	198.9	1.16e-12	2.733 <sup>+0.102</sup> <sub>-0.098</sub>	0.137 <sup>+0.062</sup> <sub>-0.064</sub>	5.68 <sup>+0.25</sup> <sub>-0.23</sub>	0.863 <sup>+0.031</sup> <sub>-0.029</sub>		
GRB 060203	00180151	68.2	4.21e-13	0.972 <sup>+0.060</sup> <sub>-0.057</sub>					
GRB 060204B	00180241	139.4	6.79e-13	3.86 <sup>+0.30</sup> <sub>-0.32</sub>	0.670 <sup>+0.085</sup> <sub>-0.097</sub>	1.492 <sup>+0.084</sup> <sub>-0.073</sub>			
GRB 060206	00180455	7.6	1.10e-12	-0.22 <sup>+0.53</sup> <sub>-0.58</sub>	0.944 <sup>+0.024</sup> <sub>-0.025</sub>				
GRB 060210	00180977	255.0	5.00e-12	0.942 <sup>+0.046</sup> <sub>-0.049</sub>	1.333 <sup>+0.103</sup> <sub>-0.051</sub>				
GRB 060211A	00181126	126.3	2.72e-13	4.02 <sup>+0.12</sup> <sub>-0.12</sub>	2.53 <sup>+0.30</sup> <sub>-0.47</sub>	0.509 <sup>+0.076</sup> <sub>-0.079</sub>			
GRB 060211B	00181156	27.7	3.80e-13	2.13 <sup>+0.22</sup> <sub>-0.18</sub>	-0.07 <sup>+0.53</sup> <sub>-0.87</sub>				
GRB 060218	00191157	21	3.86e-13	5.87 <sup>+0.41</sup> <sub>-0.56</sub>	1.129 <sup>+0.061</sup> <sub>-0.058</sub>				
GRB 060219	00191512	62.1	2.08e-13	10 <sup>+2</sup> <sub>-3</sub>	0.527 <sup>+0.085</sup> <sub>-0.100</sub>	1.31 <sup>+0.33</sup> <sub>-0.19</sub>			
GRB 060223A	00192059	11.3	2.97e-14	0.28 <sup>+0.11</sup> <sub>-0.73</sub>	1.34 <sup>+0.12</sup> <sub>-0.10</sub>				
GRB 060306	00200638	61.2	1.07e-12	3.81 <sup>+0.38</sup> <sub>-0.42</sub>	0.628 <sup>+0.050</sup> <sub>-0.063</sub>	1.069 <sup>+0.058</sup> <sub>-0.060</sub>			
GRB 060312	00201391	50.6	4.28e-13	2.515 <sup>+0.242</sup> <sub>-0.075</sub>	0.744 <sup>+0.045</sup> <sub>-0.041</sub>				
GRB 060313	00201487	0.74	3.54e-13	-0.36 <sup>+0.16</sup> <sub>-0.37</sub>	3 <sup>+4</sup> <sub>-1</sub>	0.743 <sup>+0.079</sup> <sub>-0.124</sub>	1.59 <sup>+0.13</sup> <sub>-0.14</sub>		
GRB 060319	00202035	10.6	8.23e-13	0.749 <sup>+0.055</sup> <sub>-0.077</sub>	1.168 <sup>+0.075</sup> <sub>-0.069</sub>				
GRB 060323	00202505	25.4	2.07e-13	1.027 <sup>+0.047</sup> <sub>-0.045</sub>					
GRB 060403	00203755	30.1	8.38e-14	1.501 <sup>+0.131</sup> <sub>-0.081</sub>	1.09 <sup>+0.31</sup> <sub>-1.56</sub>				
GRB 060413	00205096	147.7	5.26e-12	2.836 <sup>+0.073</sup> <sub>-0.072</sub>	0.209 <sup>+0.058</sup> <sub>-0.061</sub>	2.83 <sup>+0.17</sup> <sub>-0.14</sub>			
GRB 060418	00205851	103.1	5.27e-13	2.482 <sup>+0.066</sup> <sub>-0.070</sub>	1.03 <sup>+0.15</sup> <sub>-0.19</sub>	1.555 <sup>+0.091</sup> <sub>-0.075</sub>			
GRB 060421	00206257	12.2	2.42e-13	1.036 <sup>+0.054</sup> <sub>-0.053</sub>					
GRB 060427	00207281	64.0	1.15e-13	4.02 <sup>+0.33</sup> <sub>-0.31</sub>	1.290 <sup>+0.077</sup> <sub>-0.075</sub>				
GRB 060428A	00207364	39.5	5.00e-12	6.50 <sup>+0.71</sup> <sub>-1.30</sub>	0.519 <sup>+0.034</sup> <sub>-0.036</sub>	1.129 <sup>+0.074</sup> <sub>-0.068</sub>	2.23 <sup>+0.82</sup> <sub>-0.34</sub>		
GRB 060428B	00207399	57.9	2.69e-13	4.49 <sup>+0.14</sup> <sub>-0.14</sub>	0.971 <sup>+0.043</sup> <sub>-0.044</sub>				
GRB 060502A	00208169	28.4	2.19e-12	3.00 <sup>+0.24</sup> <sub>-0.23</sub>	0.575 <sup>+0.058</sup> <sub>-0.070</sub>	1.120 <sup>+0.064</sup> <sub>-0.063</sub>			
GRB 060505	00208654	4		1.04 <sup>+0.47</sup> <sub>-0.24</sub>					
GRB 060507	00208870	183.3	6.00e-13	0.08 <sup>+0.48</sup> <sub>-0.70</sub>	1.098 <sup>+0.075</sup> <sub>-0.070</sub>				
GRB 060510A	00209351	20.4	9.53e-12	2 <sup>+1</sup> <sub>-1</sub>	-0.002 <sup>+0.085</sup> <sub>-0.091</sub>	1.489 <sup>+0.044</sup> <sub>-0.042</sub>			
GRB 060510B	00209352	275.2	1.71e-13	0.225 <sup>+0.042</sup> <sub>-0.044</sub>	10.97 <sup>+0.53</sup> <sub>-0.60</sub>	0.88 <sup>+0.16</sup> <sub>-0.13</sub>			
GRB 060512	00209755	8.5	1.45e-13	3 <sup>+1</sup> <sub>-1</sub>	1.139 <sup>+0.058</sup> <sub>-0.060</sub>				

Table 6 – continued

GRB	Target ID	$T_{90}$	$F_{11}$	$\alpha_1$	$\alpha_2$	$\alpha_3$	$\alpha_4$	$\alpha_5$	$\alpha_6$
GRB 060515	00210084	52.0	2.70e-14	$1.79^{+0.52}_{-0.38}$					
GRB 060522	00211117	71.1	1.81e-13	$3.80^{+0.63}_{-0.49}$	$1.78^{+0.21}_{-0.21}$	$0.904^{+0.069}_{-0.054}$			
GRB 060526	00211957	298.2	8.15e-13	$1.222^{+0.073}_{-0.081}$	$0.36^{+0.15}_{-0.39}$	$0.947^{+0.161}_{-0.085}$	$2.91^{+2.19}_{-0.78}$		
GRB 060602A	00213180	75.0		$1.14^{+0.99}_{-0.32}$					
GRB 060602B	00213190	N/A	2.12e-13	$1.115^{+0.102}_{-0.086}$					
GRB 060604	00213486	95.0	9.56e-13	$2.99^{+0.41}_{-0.45}$	$0.53^{+0.12}_{-0.47}$	$1.238^{+0.080}_{-0.073}$			
GRB 060605	00213630	79.1	3.81e-13	$1.125^{+0.045}_{-0.199}$	$0.262^{+0.045}_{-0.279}$	$1.96^{+0.11}_{-0.10}$			
GRB 060607A	00213823	102.2	1.15e-12	$1.116^{+0.043}_{-0.047}$	$0.460^{+0.028}_{-0.039}$	$3.45^{+0.12}_{-0.12}$			
GRB 060614	00214805	108.7	6.28e-12	$1.91^{+0.14}_{-0.13}$	$3.573^{+0.075}_{-0.067}$	$0.077^{+0.082}_{-0.069}$	$1.863^{+0.070}_{-0.051}$		
GRB 060707	00217704	66.2	1.79e-12	$1.482^{+0.105}_{-0.099}$	$0.33^{+0.13}_{-0.60}$	$1.179^{+0.086}_{-0.089}$			
GRB 060708	00217805	10.2	6.62e-13	$4.21^{+0.22}_{-0.21}$	$0.675^{+0.046}_{-0.054}$	$1.308^{+0.076}_{-0.109}$			
GRB 060712	00218582	26.3	2.47e-13	$2.75^{+0.58}_{-0.66}$	$-0.199960^{+0.226000}_{-0.000036}$	$1.170^{+0.098}_{-0.089}$			
GRB 060714	00219101	115.0	8.33e-13	$9^{+1}_{-1}$	$0.47^{+0.18}_{-0.18}$	$1.236^{+0.052}_{-0.048}$			
GRB 060717	00219646	3.0	3.72e-14	$0.92^{+0.17}_{-0.20}$					
GRB 060719	00220020	66.9	4.94e-13	$6.46^{+0.45}_{-0.61}$	$0.21^{+0.11}_{-0.13}$	$1.225^{+0.079}_{-0.072}$			
GRB 060729	00221755	115.3	1.12e-11	$4.68^{+0.14}_{-0.20}$	$7.03^{+0.25}_{-0.24}$	$0.296^{+0.023}_{-0.023}$	$1.259^{+0.028}_{-0.029}$	$1.637^{+0.100}_{-0.078}$	
GRB 060801	00222154	0.49	1.63e-29	$-3.10^{+0.74}_{-6.89}$	$1.62^{+0.40}_{-0.34}$	$9^{+21}_{-4}$			
GRB 060804	00222546	17.8	8.34e-13	$-0.13^{+0.22}_{-0.10}$	$1.220^{+0.111}_{-0.073}$				
GRB 060805A	00222683	5.3	6.07e-14	$0.424^{+0.100}_{-0.105}$	$1.68^{+0.41}_{-0.44}$				
GRB 060805B	00020037	N/A		$0.86^{+0.37}_{-0.32}$					
GRB 060807	00223217	54.0	1.29e-12	$2.47^{+4.75}_{-0.49}$	$-0.035^{+0.080}_{-0.156}$	$1.105^{+0.087}_{-0.085}$	$2.02^{+0.30}_{-0.15}$		
GRB 060813	00224364	16.1	2.48e-12	$0.573^{+0.043}_{-0.043}$	$1.236^{+0.050}_{-0.053}$	$2.45^{+0.53}_{-0.38}$			
GRB 060814	00224552	145.3	2.30e-12	$3.42^{+0.21}_{-0.51}$	$2.162^{+0.088}_{-0.281}$	$3.27^{+0.56}_{-0.29}$	$0.624^{+0.053}_{-0.058}$	$1.388^{+0.042}_{-0.040}$	
GRB 060825	00226382	8.0	2.06e-13	$0.945^{+0.048}_{-0.048}$					
GRB 060901	00020039	N/A	8.05e-13	$1.37^{+0.41}_{-0.29}$					
GRB 060904A	00227996	80.1	1.83e-12	$3.98^{+0.12}_{-0.12}$	$0.58^{+0.13}_{-0.13}$	$1.155^{+0.144}_{-0.075}$			
GRB 060904B	00228006	171.5	4.54e-13	$0.762^{+0.057}_{-0.610}$	$1.354^{+0.063}_{-0.056}$				
GRB 060906	00228316	43.5	3.31e-13	$3.86^{+0.58}_{-1.30}$	$0.272^{+0.088}_{-0.094}$	$1.59^{+0.20}_{-0.16}$			
GRB 060908	00228581	19.3	1.87e-13	$0.578^{+0.052}_{-0.139}$	$1.58^{+0.12}_{-0.13}$				
GRB 060912A	00229185	5.0	2.64e-13	$0.75^{+0.17}_{-0.26}$	$1.126^{+0.056}_{-0.050}$				
GRB 060919	00230115	9.1	8.72e-14	$0.975^{+0.091}_{-0.083}$					
GRB 060923A	00230662	51.7	6.51e-13	$2.50^{+0.31}_{-0.26}$	$-0.18^{+0.29}_{-0.89}$	$1.213^{+0.053}_{-0.049}$			
GRB 060923B	00230702	8.6	1.17e-12	$0.622^{+0.077}_{-0.081}$					
GRB 060923C	00230711	75.8	5.86e-13	$3.16^{+0.23}_{-0.18}$	$0.591^{+0.060}_{-0.190}$	$2.00^{+0.90}_{-0.65}$			
GRB 060926	00231231	8.0	1.46e-13	$1.84^{+0.70}_{-0.89}$	$0.23^{+0.24}_{-0.83}$	$1.44^{+0.24}_{-0.19}$			
GRB 060927	00231362	22.5	7.65e-14	$0.730^{+0.070}_{-0.364}$	$1.76^{+0.83}_{-0.42}$				
GRB 060928	00020042	N/A		$0.72^{+1.70}_{-0.32}$					
GRB 060929	00231702	554.0	8.73e-14	$-0.04^{+0.71}_{-1.05}$	$1.01^{+0.13}_{-0.10}$				
GRB 061002	00231974	17.6	8.19e-14	$2.87^{+0.48}_{-0.37}$	$0.97^{+0.13}_{-0.16}$				
GRB 061004	00232339	6.2	2.68e-13	$1.72^{+0.19}_{-0.17}$	$0.39^{+0.15}_{-0.33}$	$1.18^{+0.12}_{-0.11}$			
GRB 061006	00232585	129.9	1.56e-13	$0.787^{+0.076}_{-0.071}$					
GRB 061007	00232683	75.3	1.07e-12	$1.945^{+0.053}_{-0.068}$	$1.643^{+0.022}_{-0.022}$	$2.52^{+0.93}_{-0.58}$	$1.497^{+0.051}_{-0.047}$		
GRB 061019	00234516	183.8	9.57e-13	$0.863^{+0.052}_{-0.078}$	$2.31^{+0.86}_{-0.69}$				
GRB 061021	00234905	46.2	3.03e-12	$2.001^{+0.111}_{-0.096}$	$0.541^{+0.074}_{-0.076}$	$1.075^{+0.017}_{-0.016}$			
GRB 061025	00020043	N/A	1.31e-13	$1.32^{+0.31}_{-0.31}$					
GRB 061028	00235715	106.2	3.67e-14	$4.68^{+0.21}_{-0.18}$	$0.68^{+0.26}_{-0.29}$				
GRB 061102	00236430	45.6	9.05e-14	$3.66^{+0.54}_{-0.51}$	$0.36^{+0.24}_{-0.23}$				
GRB 061110A	00238108	40.7	9.54e-14	$0.48^{+0.16}_{-0.13}$	$4.26^{+0.22}_{-0.14}$	$2.27^{+0.24}_{-0.29}$	$0.631^{+0.081}_{-0.084}$		
GRB 061110B	00238174	134.0	6.24e-14	$1.47^{+0.32}_{-0.28}$					
GRB 061121	00239899	81.3	7.36e-12	$2.80^{+0.29}_{-0.33}$	$8.07^{+0.59}_{-0.54}$	$3.90^{+0.56}_{-0.60}$	$0.265^{+0.044}_{-0.043}$	$1.010^{+0.071}_{-0.069}$	$1.553^{+0.046}_{-0.070}$
GRB 061122	00020044	N/A	1.65e-12	$1.276^{+0.070}_{-0.065}$					
GRB 061126	00240766	70.8	3.36e-12	$1.350^{+0.027}_{-0.023}$	$1.276^{+0.044}_{-0.052}$				
GRB 061201	00241840	0.76	1.76e-13	$0.54^{+0.13}_{-0.14}$	$1.86^{+0.18}_{-0.15}$				
GRB 061202	00241963	91.2	3.20e-12	$2.55^{+0.13}_{-0.13}$	$-0.27^{+0.13}_{-0.13}$	$1.741^{+0.059}_{-0.055}$			
GRB 061210	00243690	85.3		$1.58^{+1.44}_{-0.33}$					
GRB 061222A	00252588	71.4	8.33e-12	$4.18^{+0.12}_{-0.11}$	$0.296^{+0.076}_{-0.076}$	$0.976^{+0.103}_{-0.059}$	$1.708^{+0.054}_{-0.052}$		
GRB 061222B	00252593	40.0	6.48e-17	$2.97^{+0.17}_{-0.16}$					

Table 6 – *continued*

GRB	Target ID	$T_{90}$	$F_{11}$	$\alpha_1$	$\alpha_2$	$\alpha_3$	$\alpha_4$	$\alpha_5$	$\alpha_6$
GRB 070103	00254532	18.6	1.62e-13	$-0.64^{+0.22}_{-0.37}$	$0.86^{+0.18}_{-0.67}$	$1.43^{+0.12}_{-0.11}$			
GRB 070107	00255029	347.3	2.29e-12	$0.864^{+0.020}_{-0.021}$	$1.308^{+0.046}_{-0.040}$				
GRB 070110	00255445	88.4	6.83e-13	$2.558^{+0.051}_{-0.128}$	$0.612^{+0.586}_{-0.095}$	$0.132^{+0.037}_{-0.041}$	$9.65^{+0.35}_{-0.39}$	$0.892^{+0.045}_{-0.040}$	
GRB 070125	00020047	N/A		$0.65^{+0.36}_{-0.27}$	$2.01^{+0.18}_{-0.15}$				
GRB 070129	00258408	460.6	1.14e-12	$2.532^{+0.079}_{-0.070}$	$-0.093^{+0.230}_{-0.091}$	$1.034^{+0.051}_{-0.049}$	$2.41^{+1.38}_{-0.97}$		
GRB 070208	00259714	47.7	3.42e-13	$-0.98^{+0.20}_{-0.23}$	$0.99^{+0.13}_{-0.38}$	$1.58^{+0.59}_{-0.28}$			
GRB 070219	00261132	16.6	1.02e-13	$1.67^{+0.94}_{-0.55}$	$-0.27^{+0.75}_{-0.80}$	$0.99^{+0.20}_{-0.17}$			
GRB 070220	00261299	129.0	6.20e-13	$1.28^{+0.15}_{-0.17}$	$2.25^{+2.48}_{-0.27}$	$1.058^{+0.052}_{-0.040}$	$2.10^{+0.28}_{-0.14}$		
GRB 070223	00261664	88.5	2.58e-13	$0.666^{+0.053}_{-0.430}$	$2.48^{+0.44}_{-0.42}$	$0.916^{+0.087}_{-0.086}$			
GRB 070224	00261880	34.5	1.60e-13	$3.22^{+0.24}_{-0.21}$	$0.560^{+0.069}_{-0.089}$				
GRB 070227	00262347	7		$1.11^{+0.14}_{-0.13}$					
GRB 070306	00263361	209.5	8.85e-12	$-0.13^{+0.35}_{-0.58}$	$6.34^{+0.22}_{-0.20}$	$0.139^{+0.059}_{-0.057}$	$0.76^{+0.38}_{-0.25}$	$1.887^{+0.091}_{-0.085}$	
GRB 070311	00020052	N/A	6.71e-13	$1.26^{+0.20}_{-0.14}$	$-0.02^{+0.21}_{-10.00}$	$2.96^{+0.58}_{-0.47}$			
GRB 070318	00271019	74.6	1.33e-12	$1.083^{+0.011}_{-0.011}$					
GRB 070328	00272773	75.3	2.38e-12	$1.34^{+0.21}_{-0.13}$	$0.277^{+0.052}_{-0.052}$	$1.211^{+0.037}_{-0.111}$	$1.587^{+0.040}_{-0.034}$		
GRB 070330	00273180	9.0	3.18e-13	$0.881^{+0.046}_{-0.050}$					
GRB 070411	00275087	121.5	5.70e-13	$1.134^{+0.038}_{-0.037}$					
GRB 070412	00275119	33.8	3.13e-13	$3.25^{+0.49}_{-0.85}$	$0.881^{+0.053}_{-0.077}$	$1.48^{+6.21}_{-0.25}$			
GRB 070419A	00276205	115.6	3.56e-14	$1.92^{+0.16}_{-0.15}$	$3.71^{+0.47}_{-0.15}$	$0.53^{+0.47}_{-0.37}$			
GRB 070419B	00276212	236.4	1.07e-11	$1.1591^{+0.0093}_{-0.0089}$	$2.41^{+0.20}_{-0.16}$				
GRB 070420	00276321	76.5	3.01e-12	$4.50^{+0.19}_{-0.18}$	$0.351^{+0.085}_{-0.094}$	$2.78^{+0.48}_{-0.49}$	$0.87^{+0.16}_{-0.19}$	$1.87^{+0.21}_{-0.15}$	
GRB 070429A	00277571	163.3	5.61e-13	$7.01^{+0.28}_{-0.56}$	$4.13^{+0.35}_{-0.49}$	$0.466^{+0.057}_{-0.073}$	$3^{+7}_{-2}$		
GRB 070506	00278693	4.3	1.20e-12	$0.55^{+0.11}_{-0.11}$					
GRB 070508	00278854	20.9	3.00e-12	$0.476^{+0.035}_{-0.034}$	$1.149^{+0.045}_{-0.038}$	$1.654^{+0.087}_{-0.122}$			
GRB 070509	00278903	7.7	7.03e-14	$0.910^{+0.120}_{-0.099}$					
GRB 070517	00279494	7.6	1.85e-13	$0.408^{+0.061}_{-0.069}$	$2.33^{+7.67}_{-0.69}$				
GRB 070518	00279592	5.5	1.51e-13	$2.22^{+0.12}_{-0.11}$	$0.649^{+0.070}_{-0.079}$				
GRB 070520A	00279817	18.1	1.34e-13	$4.33^{+0.42}_{-0.42}$	$0.641^{+0.089}_{-0.090}$				
GRB 070520B	00279898	65.8	9.44e-14	$2.14^{+0.18}_{-0.16}$	$0.99^{+0.66}_{-0.57}$				
GRB 070521	00279935	37.9	9.45e-13	$-0.05^{+0.16}_{-0.21}$	$0.783^{+0.056}_{-0.060}$	$1.927^{+0.108}_{-0.098}$			
GRB 070529	00280706	109.2	3.45e-13	$9^{+2}_{-1}$	$0.799^{+0.152}_{-0.096}$	$1.306^{+0.086}_{-0.075}$			
GRB 070531	00280958	44.5		$1.46^{+0.14}_{-0.14}$					
GRB 070611	00282003	12.2	1.79e-13	$1.105^{+0.111}_{-0.097}$					
GRB 070612B	00282073	13.5	1.23e-13	$1.28^{+0.52}_{-0.47}$					
GRB 070616	00282445	402.4	4.63e-13	$-0.015^{+0.027}_{-0.036}$	$6.46^{+0.24}_{-0.21}$	$1.359^{+0.037}_{-0.043}$			
GRB 070621	00282808	33.3	2.90e-13	$3.645^{+0.036}_{-0.055}$	$1.37^{+0.19}_{-0.23}$	$0.958^{+0.043}_{-0.043}$			
GRB 070628	00283320	39.1	3.85e-12	$0.356^{+0.082}_{-0.084}$	$1.170^{+0.047}_{-0.047}$				
GRB 070704	00283791	38	6.61e-13	$2.75^{+0.62}_{-0.42}$	$0.839^{+0.080}_{-0.084}$				
GRB 070714A	00284850	2.0	3.83e-13	$0.635^{+0.055}_{-0.048}$					
GRB 070714B	00284856	64	5.97e-14	$1.28^{+0.19}_{-0.22}$	$2.29^{+0.22}_{-0.20}$	$0.36^{+0.46}_{-1.56}$	$1.565^{+0.088}_{-0.076}$		
GRB 070721A	00285653	3.4	1.38e-13	$2.82^{+0.57}_{-0.38}$	$0.798^{+0.057}_{-0.056}$				
GRB 070721B	00285654	34	3.63e-13	$5.43^{+0.84}_{-0.54}$	$0.780^{+0.041}_{-0.041}$	$2.34^{+0.27}_{-0.19}$			
GRB 070724A	00285948	0.4	1.37e-13	$2.50^{+0.20}_{-0.16}$	$0.70^{+0.21}_{-0.27}$				
GRB 070724B	00020055	N/A		$1.14^{+0.20}_{-0.17}$					
GRB 070802	00286809	16.4	3.41e-13	$2.36^{+0.58}_{-0.43}$	$0.157^{+0.086}_{-0.259}$	$1.18^{+0.15}_{-0.17}$			
GRB 070808	00287260	32	2.03e-13	$3.49^{+0.62}_{-0.47}$	$0.923^{+0.092}_{-0.079}$				
GRB 070809	00287344	1.3	5.06e-13	$0.511^{+0.055}_{-0.055}$					
GRB 070810A	00287364	11.0	2.86e-13	$0.49^{+0.31}_{-0.28}$	$1.29^{+0.12}_{-0.11}$				
GRB 070911	00290624	162		$1.516^{+0.075}_{-0.070}$					
GRB 070917	00291292	7.3		$0.87^{+0.58}_{-0.32}$					
GRB 070925	00020056	N/A	2.13e-13	$1.03^{+0.28}_{-0.21}$					
GRB 071001	00292826	58.5		$2.56^{+0.23}_{-0.19}$	$-0.07^{+0.17}_{-0.22}$				
GRB 071003	00292934	15	2.53e-12	$1.620^{+0.060}_{-0.056}$					
GRB 071010A	00293707	6	8.27e-13	$-0.34^{+0.55}_{-0.82}$	$1.79^{+0.30}_{-0.26}$				
GRB 071010B	00293795	>35.7	3.38e-12	$0.661^{+0.064}_{-0.064}$					
GRB 071011	00293924	61	2.98e-12	$0.927^{+0.046}_{-0.045}$	$2.45^{+2.09}_{-0.96}$				
GRB 071020	00294835	4.2	1.50e-12	$0.47^{+0.17}_{-0.22}$	$1.145^{+0.019}_{-0.017}$				

Table 6 – continued

GRB	Target ID	$T_{90}$	$F_{11}$	$\alpha_1$	$\alpha_2$	$\alpha_3$	$\alpha_4$	$\alpha_5$	$\alpha_6$
GRB 071021	00294974	225	3.10e-13	4.40 <sup>+0.43</sup> <sub>-0.26</sub>	0.813 <sup>+0.042</sup> <sub>-0.044</sub>				
GRB 071025	00295301	109	5.72e-13	3.59 <sup>+0.18</sup> <sub>-0.26</sub>	2.25 <sup>+0.14</sup> <sub>-0.20</sub>	1.322 <sup>+0.054</sup> <sub>-0.040</sub>	1.668 <sup>+0.064</sup> <sub>-0.063</sub>		
GRB 071028A	00295527	27.0	1.83e-13	3.18 <sup>+0.19</sup> <sub>-0.17</sub>	-0.06 <sup>+0.21</sup> <sub>-0.59</sub>	1.95 <sup>+1.20</sup> <sub>-0.85</sub>			
GRB 071031	00295670	18	2.51e-13	4.84 <sup>+0.48</sup> <sub>-0.31</sub>	0.95 <sup>+0.14</sup> <sub>-0.39</sub>	1.30 <sup>+8.70</sup> <sub>-0.35</sub>			
GRB 071101	00295779	9.0	6.64e-14	0.73 <sup>+0.13</sup> <sub>-0.15</sub>					
GRB 071104	00020058	N/A	8.88e-13	1.34 <sup>+0.26</sup> <sub>-0.26</sub>					
GRB 071112C	00296504	15	3.21e-13	1.424 <sup>+0.096</sup> <sub>-0.117</sub>	0.81 <sup>+0.13</sup> <sub>-0.18</sub>	1.535 <sup>+0.048</sup> <sub>-0.045</sub>			
GRB 071117	00296805	6.6	6.46e-13	0.979 <sup>+0.082</sup> <sub>-0.082</sub>					
GRB 071118	00296856	71	9.01e-13	2.24 <sup>+0.29</sup> <sub>-0.29</sub>	0.672 <sup>+0.069</sup> <sub>-0.071</sub>	2.05 <sup>+6.52</sup> <sub>-0.31</sub>			
GRB 071122	00297114	68.7		2.537 <sup>+0.108</sup> <sub>-0.097</sub>					
GRB 071227	00299787	1.8	2.32e-14	1.08 <sup>+0.22</sup> <sub>-0.24</sub>	5.48 <sup>+0.70</sup> <sub>-0.62</sub>	1.19 <sup>+0.16</sup> <sub>-0.13</sub>			
GRB 080120	00020060	N/A	9.14e-14	2.96 <sup>+0.66</sup> <sub>-0.53</sub>					
GRB 080123	00301578	115	2.93e-14	1.82 <sup>+0.13</sup> <sub>-0.20</sub>	8.12 <sup>+1.00</sup> <sub>-0.80</sub>	0.80 <sup>+0.30</sup> <sub>-0.25</sub>			
GRB 080129	00301981	48	7.99e-13	0.61 <sup>+0.16</sup> <sub>-0.12</sub>	1.30 <sup>+0.13</sup> <sub>-0.10</sub>				
GRB 080205	00302506	106.5	1.22e-13	3.29 <sup>+0.43</sup> <sub>-0.66</sub>	7.13 <sup>+0.86</sup> <sub>-1.41</sub>	0.52 <sup>+0.10</sup> <sub>-0.13</sub>	1.518 <sup>+0.059</sup> <sub>-0.056</sub>		
GRB 080207	00302728	34	6.49e-13	-0.27 <sup>+0.24</sup> <sub>-0.24</sub>	1.703 <sup>+0.063</sup> <sub>-0.060</sub>				
GRB 080210	00302888	45	4.81e-13	1.172 <sup>+0.046</sup> <sub>-0.048</sub>					
GRB 080212	00303105	123	8.79e-13	6.23 <sup>+0.32</sup> <sub>-0.31</sub>	0.43 <sup>+0.19</sup> <sub>-0.45</sub>	1.371 <sup>+0.074</sup> <sub>-0.070</sub>			
GRB 080218B	00303631	6.2	1.96e-13	0.988 <sup>+0.050</sup> <sub>-0.048</sub>					
GRB 080229A	00304379	64	1.66e-11	3.27 <sup>+0.17</sup> <sub>-0.18</sub>	-0.036 <sup>+0.067</sup> <sub>-0.085</sub>	0.897 <sup>+0.037</sup> <sub>-0.040</sub>	1.50 <sup>+0.65</sup> <sub>-0.20</sub>		
GRB 080229B	00020064	N/A		1.18 <sup>+0.18</sup> <sub>-0.17</sub>					
GRB 080303	00304549	67	2.25e-13	1.606 <sup>+0.075</sup> <sub>-0.071</sub>	0.788 <sup>+0.079</sup> <sub>-0.075</sub>				
GRB 080307	00305011	125.9	9.98e-14	-0.48 <sup>+0.14</sup> <sub>-0.13</sub>	1.945 <sup>+0.046</sup> <sub>-0.041</sub>	0.43 <sup>+0.14</sup> <sub>-0.17</sub>			
GRB 080310	00305288	365	9.77e-13	2.66 <sup>+0.69</sup> <sub>-0.67</sub>	0.32 <sup>+0.11</sup> <sub>-0.12</sub>	1.539 <sup>+0.095</sup> <sub>-0.084</sub>			
GRB 080319A	00306754	64	5.72e-13	0.907 <sup>+0.089</sup> <sub>-0.070</sub>					
GRB 080319B	00306757	>5	3.29e-12	1.352 <sup>+0.035</sup> <sub>-0.029</sub>	1.588 <sup>+0.016</sup> <sub>-0.015</sub>	2.89 <sup>+0.21</sup> <sub>-0.22</sub>	1.027 <sup>+0.061</sup> <sub>-0.066</sub>	2.35 <sup>+0.61</sup> <sub>-0.35</sub>	
GRB 080319C	00306778	34	2.18e-12	-2.17 <sup>+0.96</sup> <sub>-0.56</sub>	0.958 <sup>+0.078</sup> <sub>-0.078</sub>	1.66 <sup>+0.15</sup> <sub>-0.13</sub>			
GRB 080319D	00306793	24	1.92e-13	2.60 <sup>+0.23</sup> <sub>-0.19</sub>	0.82 <sup>+0.14</sup> <sub>-0.18</sub>				
GRB 080320	00306858	14	1.75e-12	1.88 <sup>+1.26</sup> <sub>-0.38</sub>	0.618 <sup>+0.057</sup> <sub>-0.052</sub>	1.190 <sup>+0.133</sup> <sub>-0.069</sub>			
GRB 080325	00307604	128.4	5.38e-13	4.57 <sup>+0.96</sup> <sub>-0.87</sub>	0.974 <sup>+0.073</sup> <sub>-0.074</sub>				
GRB 080328	00307931	90.6	2.73e-12	5.77 <sup>+0.48</sup> <sub>-0.43</sub>	0.706 <sup>+0.045</sup> <sub>-0.046</sub>	1.227 <sup>+0.059</sup> <sub>-0.056</sub>			
GRB 080330	00308041	61	1.07e-12	5.27 <sup>+0.42</sup> <sub>-0.41</sub>	0.18 <sup>+0.11</sup> <sub>-0.19</sub>	0.82 <sup>+8.12</sup> <sub>-0.27</sub>			
GRB 080405	00020065	N/A		0.15 <sup>+1.09</sup> <sub>-0.33</sub>					
GRB 080409	00308812	20.2	2.38e-13	-0.54 <sup>+0.32</sup> <sub>-0.84</sub>	0.900 <sup>+0.084</sup> <sub>-0.079</sub>				
GRB 080411	00309010	56	1.93e-11	0.925 <sup>+0.083</sup> <sub>-0.111</sub>	1.323 <sup>+0.023</sup> <sub>-0.023</sub>	1.73 <sup>+1.25</sup> <sub>-0.23</sub>			
GRB 080413A	00309096	46	2.25e-13	2.79 <sup>+0.20</sup> <sub>-0.19</sub>	1.175 <sup>+0.057</sup> <sub>-0.058</sub>				
GRB 080413B	00309111	8.0	2.34e-12	0.556 <sup>+0.067</sup> <sub>-0.099</sub>	0.976 <sup>+0.024</sup> <sub>-0.025</sub>	1.428 <sup>+0.115</sup> <sub>-0.099</sub>			
GRB 080426	00310219	1.7	1.15e-13	-0 <sup>+1</sup> <sub>-1</sub>	1.258 <sup>+0.067</sup> <sub>-0.060</sub>				
GRB 080430	00310613	16.2	2.28e-12	2.22 <sup>+0.17</sup> <sub>-0.15</sub>	0.491 <sup>+0.033</sup> <sub>-0.034</sub>	1.132 <sup>+0.043</sup> <sub>-0.042</sub>			
GRB 080503	00310785	17	2.69e-20	1.46 <sup>+0.16</sup> <sub>-0.13</sub>	2.51 <sup>+0.20</sup> <sub>-0.32</sub>	4.61 <sup>+0.28</sup> <sub>-0.32</sub>			
GRB 080506	00311159	15	5.24e-13	-0.49 <sup>+0.75</sup> <sub>-0.67</sub>	8.08 <sup>+0.73</sup> <sub>-0.82</sub>	1.81 <sup>+0.12</sup> <sub>-0.20</sub>	0.61 <sup>+0.20</sup> <sub>-0.21</sub>		
GRB 080507	00020068	N/A		1.89 <sup>+1.67</sup> <sub>-0.38</sub>					
GRB 080514B	00020069	N/A	2.62e-12	1.53 <sup>+0.27</sup> <sub>-0.20</sub>					
GRB 080515	00311658	21		0.77 <sup>+0.64</sup> <sub>-0.36</sub>					
GRB 080516	00311762	5.8	4.49e-13	0.34 <sup>+0.16</sup> <sub>-0.17</sub>	0.99 <sup>+0.13</sup> <sub>-0.13</sub>				
GRB 080517	00311874	64.6	9.60e-14	2.56 <sup>+0.23</sup> <sub>-0.21</sub>	0.65 <sup>+0.22</sup> <sub>-0.26</sub>				
GRB 080520	00312047	2.8	8.11e-14	0.99 <sup>+0.15</sup> <sub>-0.12</sub>					
GRB 080523	00312242	102	1.81e-13	1.58 <sup>+0.14</sup> <sub>-0.14</sub>	2.56 <sup>+0.17</sup> <sub>-0.14</sub>	0.75 <sup>+0.18</sup> <sub>-0.17</sub>			
GRB 080602	00312958	74		4.50 <sup>+0.81</sup> <sub>-0.86</sub>	-0.07 <sup>+0.16</sup> <sub>-0.23</sub>	0.70 <sup>+0.17</sup> <sub>-0.16</sub>			
GRB 080603A	00020074	N/A	1.11e-12	0.952 <sup>+0.094</sup> <sub>-0.075</sub>					
GRB 080603B	00313087	6		6 <sup>+2</sup> <sub>-2</sub>	3.14 <sup>+0.16</sup> <sub>-0.16</sub>	0.832 <sup>+0.040</sup> <sub>-0.035</sub>			
GRB 080604	00313116	82	5.34e-14	2.068 <sup>+0.053</sup> <sub>-0.049</sub>	0.18 <sup>+0.45</sup> <sub>-1.68</sub>				
GRB 080605	00313299	2	1.69e-12	0.520 <sup>+0.042</sup> <sub>-0.085</sub>	0.958 <sup>+0.142</sup> <sub>-0.051</sub>	1.708 <sup>+0.089</sup> <sub>-0.083</sub>			
GRB 080607	00313417	79	6.56e-13	8.00 <sup>+0.64</sup> <sub>-0.72</sub>	2.215 <sup>+0.083</sup> <sub>-0.087</sub>	1.418 <sup>+0.023</sup> <sub>-0.023</sub>	2.04 <sup>+7.96</sup> <sub>-0.48</sub>		
GRB 080613A	00020075	N/A	1.10e-12	1.29 <sup>+1.50</sup> <sub>-0.46</sub>					
GRB 080613B	00313954	105	4.32e-14	2.18 <sup>+0.11</sup> <sub>-0.11</sub>	50 <sup>+36</sup> <sub>-23</sub>	0.80 <sup>+0.14</sup> <sub>-0.11</sub>			
GRB 080623	00315080	15.2	5.97e-13	1.142 <sup>+0.051</sup> <sub>-0.046</sub>					

Table 6 – *continued*

GRB	Target ID	$T_{90}$	$F_{11}$	$\alpha_1$	$\alpha_2$	$\alpha_3$	$\alpha_4$	$\alpha_5$	$\alpha_6$
GRB 080625	00020076	N/A	1.88e-12	$1.409^{+0.085}_{-0.169}$	$2.39^{+1.29}_{-0.61}$				
GRB 080701	00315615	18	3.52e-13	$1.07^{+0.22}_{-0.15}$					
GRB 080702A	00315710	0.5	3.31e-14	$1.054^{+0.116}_{-0.095}$					
GRB 080703	00315819	3.4	8.08e-13	$0.559^{+0.036}_{-0.037}$	$2.30^{+0.29}_{-0.24}$				
GRB 080707	00316204	27.1	4.68e-13	$4.39^{+1.10}_{-0.57}$	$0.21^{+0.11}_{-0.12}$	$1.048^{+0.098}_{-0.092}$			
GRB 080710	00316534	12	8.31e-13	$1.050^{+0.081}_{-0.063}$	$1.80^{+0.23}_{-0.17}$				
GRB 080714	00316910	33	6.44e-13	$0.10^{+0.64}_{-0.92}$	$1.87^{+2.62}_{-0.49}$	$1.025^{+0.049}_{-0.047}$			
GRB 080721	00317508	16.2	7.26e-12	$0.710^{+0.046}_{-0.021}$	$-1.10^{+1.34}_{-0.40}$	$0.938^{+0.020}_{-0.020}$	$1.639^{+0.022}_{-0.022}$		
GRB 080723A	00317662	17.3	9.78e-13	$1.82^{+0.36}_{-0.31}$	$0.02^{+0.12}_{-0.25}$	$1.060^{+0.059}_{-0.054}$			
GRB 080723B	00020079	N/A	6.66e-12	$1.40^{+0.19}_{-0.20}$					

Table 6 – continued

GRB	Obs times*	$t_{\text{break}, 1}$	$t_{\text{break}, 2}$	$t_{\text{break}, 3}$	$t_{\text{break}, 4}$	$t_{\text{break}, 5}$
GRB 041223	16.7–28.6 ks					
GRB 050124	11.1–4967.5 ks					
GRB 050126	128 s–93.2 ks	$495^{+540}_{-260}$				
GRB 050128	105 s–99.6 ks	$6492^{+2247}_{-3355}$				
GRB 050215B	5.8–3011.3 ks					
GRB 050219A	112 s–3154.9 ks	$339^{+53}_{-37}$				
GRB 050219B	3.2–3205.2 ks					
GRB 050223	2.9–1047.2 ks					
GRB 050315	83 s–948.3 ks	$464^{+51}_{-47}$	$(5.87^{+0.62}_{+0.63}) \times 10^4$			
GRB 050318	3.3–832.7 ks	$(1.21^{+1.09}_{+0.41}) \times 10^4$				
GRB 050319	234 s–2436.1 ks	$396^{+38}_{-33}$	$(1.51^{+1.10}_{+0.49}) \times 10^4$	$(4^{+3}_{+1}) \times 10^5$		
GRB 050326	3.3–531.4 ks					
GRB 050401	133 s–1066.8 ks	$4554^{+621}_{-603}$				
GRB 050406	92 s–1407.0 ks	$(6^{+8}_{+6}) \times 10^5$				
GRB 050408	2.6–3310.6 ks					
GRB 050410	1.9–916.2 ks	$(4^{+12}_{+3}) \times 10^4$				
GRB 050412	104 s–545.7 ks					
GRB 050416A	84 s–6435.5 ks	$214^{+191}_{-79}$	$992^{+783}_{-308}$			
GRB 050421	116 s–486.2 ks	$157^{+43}_{-8}$				
GRB 050422	115 s–1522.3 ks	$280^{+186}_{-63}$				
GRB 050502B	68 s–916.3 ks	$(1.34^{+0.91}_{+0.39}) \times 10^5$				
GRB 050505	2.8–1207.9 ks	$7182^{+2571}_{-1345}$	$(4.37^{+1.56}_{+0.66}) \times 10^4$			
GRB 050509A	3.7–1285.2 ks					
GRB 050520	7.7–226.9 ks					
GRB 050525A	74 s–3021.5 ks	$6435^{+2293}_{-6170}$				
GRB 050603	33.8–1800.4 ks					
GRB 050607	96 s–2554.5 ks	$356^{+83}_{-74}$	$807^{+132}_{-122}$	$(1.16^{+1.12}_{+0.61}) \times 10^4$		
GRB 050701	5.8–886.2 ks					
GRB 050712	171 s–1833.9 ks	$(1.04^{+0.87}_{+0.49}) \times 10^5$				
GRB 050713A	77 s–1711.4 ks	$86^{+8}_{-2}$	$343^{+40}_{-17}$	$1100^{+1056}_{-489}$		
GRB 050713B	141 s–1424.1 ks	$729^{+76}_{-61}$	$(1.18^{+0.19}_{+0.15}) \times 10^4$			
GRB 050714B	157 s–955.1 ks	$362^{+51}_{-37}$				
GRB 050716	104 s–1765.2 ks	$180^{+8}_{-6}$	$1445^{+267}_{-228}$			
GRB 050717	91 s–601.9 ks	$311^{+81}_{-95}$	$(2^{+2}_{+2}) \times 10^4$			
GRB 050721	194 s–3385.4 ks	$4708^{+3710}_{-2387}$				
GRB 050724	79 s–731.3 ks	$201^{+3}_{-5}$	$505^{+38}_{-37}$			
GRB 050726	130 s–669.8 ks	$7101^{+1427}_{-1319}$				
GRB 050730	132 s–496.7 ks	$9090^{+267}_{-266}$				
GRB 050801	69 s–624.4 ks	$(1^{+47}_{+1}) \times 10^4$				
GRB 050802	311 s–1256.3 ks	$6520^{+1891}_{-1013}$				
GRB 050803	159 s–1371.3 ks	$264^{+17}_{-14}$	$(1.60^{+0.18}_{+0.17}) \times 10^4$			
GRB 050814	165 s–1077.3 ks	$974^{+62}_{-67}$	$(6^{+3}_{+2}) \times 10^4$			
GRB 050815	74 s–178.3 ks	$3844^{+1002}_{-3222}$				
GRB 050819	146 s–630.1 ks	$429^{+88}_{-71}$				
GRB 050820A	88 s–5029.3 ks	$163^{+93}_{-14}$	$6877^{+575}_{-506}$			
GRB 050822	111 s–4565.4 ks	$814^{+159}_{-152}$	$(1.68^{+0.28}_{+0.26}) \times 10^4$			
GRB 050824	6.1–2713.0 ks	$(6^{+10}_{+2}) \times 10^4$				
GRB 050826	112 s–284.2 ks	$2828^{+3765}_{-1592}$	$(4^{+5}_{+2}) \times 10^4$			
GRB 050827	64.1–881.0 ks					
GRB 050904	168 s–857.3 ks	$2107^{+309700}_{-659}$				
GRB 050908	112 s–578.5 ks					
GRB 050915A	92 s–475.0 ks					
GRB 050915B	149 s–955.6 ks	$419^{+33}_{-27}$				
GRB 050916	215 s–371.0 ks	$274^{+633}_{-54}$				
GRB 050922B	349 s–2361.8 ks	$2169^{+188}_{-165}$	$(2.26^{+0.85}_{+1.87}) \times 10^5$			
GRB 050922C	115 s–590.9 ks	$2001^{+1221}_{-676}$				
GRB 051001	193 s–550.4 ks	$249^{+35}_{-9}$	$1610^{+222}_{-183}$			

**Table 7.** Times of the breaks in the light curve fits. The power-law indices are given in Table 6.

\* Time range covered by the cleaned event lists. Zero is the BAT trigger time.

GRB	Obs times*	$t_{\text{break},1}$	$t_{\text{break},2}$	$t_{\text{break},3}$	$t_{\text{break},4}$	$t_{\text{break},5}$
GRB 051006	113 s–358.1 ks					
GRB 051008	3.0–542.4 ks	$(1.74^{+0.23}_{+0.20}) \times 10^4$				
GRB 051016A	120 s–931.0 ks	$291^{+39}_{-41}$				
GRB 051016B	83 s–1452.0 ks	$152^{+12}_{-9}$	$7103^{+1488}_{-1523}$			
GRB 051021A	11.2–1430.5 ks					
GRB 051021B	85 s–516.4 ks	$2584^{+2972}_{-1497}$				
GRB 051022	12.5–1263.3 ks	$(2.50^{+0.61}_{+0.55}) \times 10^5$				
GRB 051028	25.7–900.2 ks					
GRB 051109A	127 s–1549.5 ks	$200^{+38}_{-14}$	$5633^{+851}_{-1247}$			
GRB 051109B	91 s–24611.2 ks	$200^{+34}_{-76}$	$1408^{+572}_{-297}$			
GRB 051111	5.6–405.3 ks					
GRB 051117A	113 s–2054.3 ks	$(1.23^{+0.11}_{+0.51}) \times 10^4$	$(1.48^{+0.27}_{+0.50}) \times 10^4$			
GRB 051117B	140 s–383.6 ks					
GRB 051210	87 s–117.0 ks					
GRB 051211B	10.8–862.0 ks					
GRB 051221A	93 s–1199.9 ks	$3212^{+813}_{-735}$	$(2.42^{+0.45}_{+0.30}) \times 10^4$			
GRB 051221B	281 s–4640.1 ks					
GRB 051227	101 s–625.5 ks	$424^{+118}_{-69}$				
GRB 060105	95 s–579.7 ks	$191^{+32}_{-28}$	$2948^{+191}_{-194}$	$(2.67^{+0.24}_{+0.28}) \times 10^4$	$(5.21^{+0.77}_{+0.43}) \times 10^4$	
GRB 060108	96 s–463.1 ks	$541^{+421}_{-199}$	$(1.50^{+1.04}_{+0.40}) \times 10^4$			
GRB 060109	108 s–457.9 ks	$347^{+31}_{-30}$	$7616^{+942}_{-856}$			
GRB 060110	242.0–492.9 ks					
GRB 060111A	74 s–761.8 ks	$6227^{+1762}_{-1636}$				
GRB 060111B	87 s–444.8 ks	$172^{+15}_{-30}$	$(1.08^{+2.28}_{+0.52}) \times 10^4$			
GRB 060115	120 s–468.4 ks	$579^{+102}_{-66}$				
GRB 060116	159 s–745.6 ks					
GRB 060121	10.6–1042.1 ks					
GRB 060123	75.1–1042.6 ks					
GRB 060124	111 s–2619.5 ks	$2221^{+1044}_{-578}$	$(6.22^{+1.93}_{+0.99}) \times 10^4$			
GRB 060202	148 s–2735.6 ks	$308^{+7}_{-7}$	$744^{+6}_{-6}$	$1521^{+57}_{-53}$		
GRB 060203	3.0–605.1 ks					
GRB 060204B	102 s–810.5 ks	$261^{+29}_{-23}$	$7868^{+1377}_{-1176}$			
GRB 060206	63 s–3697.3 ks	$358^{+494}_{-100}$				
GRB 060210	102 s–1879.5 ks	$(3.16^{+2.18}_{+0.66}) \times 10^4$				
GRB 060211A	184 s–794.0 ks	$493^{+108}_{-58}$	$2571^{+986}_{-485}$			
GRB 060211B	88 s–186.9 ks	$1789^{+1980}_{-844}$				
GRB 060218	158 s–13673.0 ks	$9805^{+534}_{-436}$				
GRB 060219	125 s–694.6 ks	$178^{+27}_{-19}$	$(2.10^{+1.68}_{+0.94}) \times 10^4$			
GRB 060223A	91 s–128.5 ks	$386^{+160}_{-125}$				
GRB 060306	95 s–382.4 ks	$179^{+25}_{-13}$	$8422^{+7800}_{-2542}$			
GRB 060312	58 s–509.3 ks	$303^{+33}_{-53}$				
GRB 060313	84 s–428.8 ks	$190^{+27}_{-26}$	$324^{+200}_{-78}$	$7127^{+1602}_{-2444}$		
GRB 060319	139 s–3796.7 ks	$(3^{+2}_{+1}) \times 10^4$				
GRB 060323	286 s–375.1 ks					
GRB 060403	52 s–208.4 ks	$6353^{+101400}_{-5969}$				
GRB 060413	120 s–522.4 ks	$776^{+60}_{-55}$	$(2.415^{+0.089}_{+0.074}) \times 10^4$			
GRB 060418	83 s–920.4 ks	$343^{+27}_{-17}$	$1921^{+1460}_{-697}$			
GRB 060421	93 s–341.7 ks					
GRB 060427	138 s–98.0 ks	$302^{+37}_{-27}$				
GRB 060428A	76 s–3356.5 ks	$126^{+14}_{-11}$	$(6^{+2}_{+1}) \times 10^4$	$(8^{+4}_{+2}) \times 10^5$		
GRB 060428B	211 s–1487.1 ks	$663^{+43}_{-35}$				
GRB 060502A	84 s–1601.1 ks	$245^{+32}_{-17}$	$(2.59^{+1.14}_{+0.81}) \times 10^4$			
GRB 060505	51.7–1448.0 ks					
GRB 060507	2.8–893.5 ks	$6868^{+6428}_{-1570}$				
GRB 060510A	97 s–572.8 ks	$149^{+35}_{-18}$	$4650^{+724}_{-592}$			
GRB 060510B	126 s–1091.6 ks	$348^{+2}_{-3}$	$613^{+40}_{-36}$			
GRB 060512	109 s–346.2 ks	$195^{+288}_{-43}$				

Table 7 – continued \* Time range covered by the cleaned event lists. Zero is the BAT trigger time.

GRB	Obs times*	$t_{\text{break},1}$	$t_{\text{break},2}$	$t_{\text{break},3}$	$t_{\text{break},4}$	$t_{\text{break},5}$
GRB 060515	3.4–40.6 ks					
GRB 060522	147 s–509.1 ks	$226^{+37}_{-19}$	$927^{+236}_{-130}$			
GRB 060526	81 s–545.5 ks	$1433^{+1060}_{-295}$	$6592^{+9496}_{-4265}$	$(1.23^{+0.52}_{+0.33}) \times 10^5$		
GRB 060602A	152.6–870.0 ks					
GRB 060602B	88 s–653.7 ks					
GRB 060604	116 s–1920.6 ks	$635^{+172}_{-134}$	$(2.50^{+0.87}_{+1.26}) \times 10^4$			
GRB 060605	98 s–190.9 ks	$535^{+434}_{-161}$	$7465^{+597}_{-632}$			
GRB 060607A	73 s–325.5 ks	$548^{+85}_{-48}$	$(1.239^{+0.035}_{+0.041}) \times 10^4$			
GRB 060614	97 s–6464.1 ks	$179^{+8}_{-6}$	$1507^{+87}_{-95}$	$(4.45^{+0.44}_{+0.27}) \times 10^4$		
GRB 060707	126 s–2765.5 ks	$1263^{+949}_{-265}$	$(2.71^{+1.22}_{+0.95}) \times 10^4$			
GRB 060708	70 s–1336.7 ks	$184^{+14}_{-11}$	$(1.28^{+0.30}_{+0.58}) \times 10^4$			
GRB 060712	189 s–1047.1 ks	$787^{+213}_{-480}$	$7956^{+6926}_{-1350}$			
GRB 060714	106 s–1498.6 ks	$273^{+15}_{-11}$	$3593^{+2272}_{-1022}$			
GRB 060717	221 s–39.6 ks					
GRB 060719	84 s–1094.3 ks	$191^{+20}_{-16}$	$8130^{+1720}_{-1332}$			
GRB 060729	130 s–13063.0 ks	$206^{+5}_{-6}$	$405^{+10}_{-10}$	$(7.60^{+0.42}_{+0.40}) \times 10^4$	$(1.00^{+0.35}_{+0.19}) \times 10^6$	
GRB 060801	70 s–312.9 ks	$109^{+51}_{-20}$	$437^{+59}_{-130}$			
GRB 060804	127 s–312.6 ks	$914^{+326}_{-240}$				
GRB 060805A	98 s–328.3 ks	$8730^{+3041}_{-6633}$				
GRB 060805B	126.5–377.4 ks					
GRB 060807	112 s–532.3 ks	$195^{+41}_{-51}$	$4613^{+422}_{-923}$	$(2.93^{+1.28}_{+0.62}) \times 10^4$		
GRB 060813	84 s–260.3 ks	$1133^{+255}_{-233}$	$(5.16^{+1.23}_{+0.91}) \times 10^4$			
GRB 060814	77 s–1383.7 ks	$89^{+4}_{-6}$	$325^{+60}_{-112}$	$750^{+81}_{-45}$	$(1.58^{+0.61}_{+0.17}) \times 10^4$	
GRB 060825	71 s–589.4 ks					
GRB 060901	13.8–115.9 ks					
GRB 060904A	71 s–1292.2 ks	$286^{+20}_{-18}$	$2820^{+4728}_{-1179}$			
GRB 060904B	76 s–675.0 ks	$4804^{+1185}_{-4625}$				
GRB 060906	153 s–365.5 ks	$285^{+79}_{-52}$	$(1.12^{+0.18}_{+0.18}) \times 10^4$			
GRB 060908	79 s–1087.5 ks	$848^{+210}_{-301}$				
GRB 060912A	114 s–868.4 ks	$741^{+1112}_{-316}$				
GRB 060919	92 s–313.4 ks					
GRB 060923A	86 s–1190.5 ks	$350^{+74}_{-73}$	$2523^{+1236}_{-1019}$			
GRB 060923B	124 s–732.9 ks					
GRB 060923C	211 s–1382.1 ks	$836^{+98}_{-95}$	$(2.43^{+0.69}_{+1.41}) \times 10^5$			
GRB 060926	65 s–284.0 ks	$154^{+795}_{-81}$	$2367^{+4739}_{-1854}$			
GRB 060927	70 s–208.3 ks	$4344^{+1406}_{-2874}$				
GRB 060928	477.0–866.9 ks					
GRB 060929	98 s–619.5 ks	$438^{+2994}_{-188}$				
GRB 061002	137 s–46.8 ks	$427^{+164}_{-105}$				
GRB 061004	68 s–533.4 ks	$416^{+145}_{-87}$	$3072^{+1843}_{-1071}$			
GRB 061006	148 s–370.9 ks					
GRB 061007	86 s–1603.8 ks	$357^{+140}_{-52}$	$4840^{+830}_{-339}$	$6881^{+2959}_{-964}$		
GRB 061019	2.8–762.0 ks	$(1.56^{+0.68}_{+0.83}) \times 10^5$				
GRB 061021	78 s–4384.1 ks	$330^{+56}_{-51}$	$7357^{+1469}_{-1014}$			
GRB 061025	5.6–190.3 ks					
GRB 061028	204 s–157.2 ks	$1061^{+368}_{-202}$				
GRB 061102	106 s–130.9 ks	$1032^{+560}_{-304}$				
GRB 061110A	75 s–907.9 ks	$143^{+5}_{-3}$	$359^{+59}_{-37}$	$3005^{+1133}_{-699}$		
GRB 061110B	3.0–75.1 ks					
GRB 061121	61 s–2199.4 ks	$116^{+3}_{-3}$	$150^{+4}_{-4}$	$212^{+11}_{-8}$	$2425^{+437}_{-397}$	$(2.22^{+0.47}_{+0.34}) \times 10^4$
GRB 061122	24.5–1267.4 ks					
GRB 061126	1.6–2819.5 ks	$(4^{+7}_{+3}) \times 10^4$				
GRB 061201	84 s–160.5 ks	$2233^{+808}_{-594}$				
GRB 061202	125 s–635.6 ks	$1109^{+133}_{-121}$	$(1.537^{+0.094}_{+0.083}) \times 10^4$			
GRB 061210	209.2–989.9 ks					
GRB 061222A	104 s–1538.8 ks	$219^{+6}_{-6}$	$2084^{+188}_{-518}$	$(5.80^{+1.78}_{+0.68}) \times 10^4$		
GRB 061222B	151 s–416.6 ks					

**Table 7** – *continued* \* Time range covered by the cleaned event lists. Zero is the BAT trigger time.

GRB	Obs times*	$t_{\text{break},1}$	$t_{\text{break},2}$	$t_{\text{break},3}$	$t_{\text{break},4}$	$t_{\text{break},5}$
GRB 070103	72 s–179.9 ks	$616^{+55}_{-180}$	$4628^{+1985}_{-2918}$			
GRB 070107	182 s–817.1 ks	$(1.76^{+0.39}_{+0.28}) \times 10^4$				
GRB 070110	99 s–2306.2 ks	$317^{+45}_{-42}$	$4043^{+440}_{-2940}$	$(2.068^{+0.021}_{+0.021}) \times 10^4$	$(2.716^{+0.082}_{+0.041}) \times 10^4$	
GRB 070125	46.7–1614.9 ks	$(10^{+4}_{+2}) \times 10^4$				
GRB 070129	139 s–1637.1 ks	$1786^{+284}_{-179}$	$(1.21^{+0.17}_{+0.22}) \times 10^4$	$(8^{+5}_{+4}) \times 10^5$		
GRB 070208	119 s–480.4 ks	$923^{+351}_{-277}$	$(1.43^{+1.32}_{+0.59}) \times 10^4$			
GRB 070219	86 s–255.0 ks	$627^{+1167}_{-232}$	$3315^{+53930}_{-1827}$			
GRB 070220	85 s–237.9 ks	$167^{+10}_{-21}$	$291^{+34}_{-32}$	$(1.147^{+0.312}_{+0.092}) \times 10^4$		
GRB 070223	116 s–1081.6 ks	$166^{+8}_{-14}$	$1458^{+408}_{-496}$			
GRB 070224	149 s–1388.5 ks	$826^{+218}_{-131}$				
GRB 070227	55.8–1301.0 ks					
GRB 070306	157 s–1146.0 ks	$185^{+3}_{-3}$	$424^{+15}_{-16}$	$(1.89^{+0.41}_{+0.25}) \times 10^4$	$(3.99^{+1.10}_{+0.59}) \times 10^4$	
GRB 070311	7.0–765.9 ks	$(3.43^{+1.85}_{+0.68}) \times 10^4$	$(1.75^{+0.17}_{+0.66}) \times 10^5$			
GRB 070318	69 s–1006.2 ks					
GRB 070328	94 s–1088.9 ks	$184^{+11}_{-17}$	$602^{+29}_{-24}$	$4990^{+1117}_{-1839}$		
GRB 070330	71 s–416.5 ks					
GRB 070411	463 s–727.6 ks					
GRB 070412	67 s–682.8 ks	$105^{+15}_{-18}$	$(1.45^{+1.89}_{+0.91}) \times 10^4$			
GRB 070419A	119 s–828.0 ks	$216^{+11}_{-8}$	$2336^{+1614}_{-1014}$			
GRB 070419B	87 s–561.0 ks	$(5.02^{+0.60}_{+0.55}) \times 10^4$				
GRB 070420	105 s–752.6 ks	$215^{+10}_{-8}$	$4669^{+423}_{-497}$	$8125^{+984}_{-599}$	$(3.78^{+1.04}_{+0.74}) \times 10^4$	
GRB 070429A	159 s–1347.7 ks	$215^{+26}_{-10}$	$808^{+121}_{-103}$	$(5^{+4}_{+2}) \times 10^5$		
GRB 070506	413 s–436.1 ks					
GRB 070508	82 s–758.9 ks	$574^{+55}_{-42}$	$(1.02^{+0.38}_{+0.62}) \times 10^4$			
GRB 070509	71 s–161.5 ks					
GRB 070517	108 s–389.2 ks	$(1.81^{+1.02}_{+0.29}) \times 10^4$				
GRB 070518	76 s–1672.8 ks	$1029^{+303}_{-198}$				
GRB 070520A	164 s–1939.5 ks	$735^{+162}_{-113}$				
GRB 070520B	104 s–362.9 ks	$1884^{+1522}_{-1475}$				
GRB 070521	80 s–487.4 ks	$333^{+111}_{-81}$	$9002^{+1015}_{-940}$			
GRB 070529	137 s–729.9 ks	$162^{+16}_{-14}$	$2533^{+3265}_{-1053}$			
GRB 070531	138 s–1.1 ks					
GRB 070611	3.3–456.8 ks					
GRB 070612B	3.3–409.1 ks					
GRB 070616	137 s–371.1 ks	$547^{+3}_{-3}$	$1107^{+33}_{-36}$			
GRB 070621	116 s–856.2 ks	$349^{+31}_{-42}$	$1211^{+369}_{-242}$			
GRB 070628	114 s–83.3 ks	$6613^{+824}_{-638}$				
GRB 070704	159 s–417.0 ks	$590^{+239}_{-156}$				
GRB 070714A	66 s–175.2 ks					
GRB 070714B	67 s–134.5 ks	$140^{+17}_{-19}$	$434^{+124}_{-30}$	$731^{+326}_{-125}$		
GRB 070721A	87 s–654.7 ks	$295^{+85}_{-66}$				
GRB 070721B	98 s–259.5 ks	$147^{+7}_{-8}$	$8981^{+803}_{-841}$			
GRB 070724A	73 s–565.6 ks	$797^{+502}_{-309}$				
GRB 070724B	68.9–718.7 ks					
GRB 070802	141 s–404.5 ks	$507^{+127}_{-103}$	$7282^{+3621}_{-1821}$			
GRB 070808	118 s–180.0 ks	$289^{+55}_{-45}$				
GRB 070809	80 s–71.4 ks					
GRB 070810A	91 s–39.7 ks	$1552^{+6800}_{-718}$				
GRB 070911	52.2–1960.6 ks					
GRB 070917	237.4–1355.0 ks					
GRB 070925	12.3–371.8 ks					
GRB 071001	88 s–4.8 ks	$557^{+132}_{-87}$				
GRB 071003	22.3–909.7 ks					
GRB 071010A	34.0–555.6 ks	$(8^{+2}_{+2}) \times 10^4$				
GRB 071010B	6.2–156.1 ks					
GRB 071011	3.0–1596.0 ks	$(5^{+1}_{+1}) \times 10^5$				
GRB 071020	67 s–1480.6 ks	$168^{+46}_{-27}$				

Table 7 – continued \* Time range covered by the cleaned event lists. Zero is the BAT trigger time.

GRB	Obs times*	$t_{\text{break}, 1}$	$t_{\text{break}, 2}$	$t_{\text{break}, 3}$	$t_{\text{break}, 4}$	$t_{\text{break}, 5}$
GRB 071021	136 s–1000.7 ks	$447^{+51}_{-60}$				
GRB 071025	149 s–497.6 ks	$183^{+15}_{-10}$	$318^{+305}_{-18}$	$3557^{+1494}_{-3061}$		
GRB 071028A	124 s–87.5 ks	$1228^{+529}_{-277}$	$(2.52^{+0.80}_{+1.03}) \times 10^4$			
GRB 071031	109 s–596.7 ks	$1608^{+230}_{-450}$	$(6^{+53}_{+6}) \times 10^4$			
GRB 071101	72 s–92.7 ks					
GRB 071104	20.6–67.1 ks					
GRB 071112C	89 s–624.4 ks	$243^{+71}_{-35}$	$881^{+176}_{-159}$			
GRB 071117	2.9–62.8 ks					
GRB 071118	129 s–121.8 ks	$401^{+68}_{-71}$	$(1.28^{+0.41}_{+0.10}) \times 10^4$			
GRB 071122	146 s–1.5 ks					
GRB 071227	85 s–358.1 ks	$185^{+21}_{-7}$	$373^{+62}_{-39}$			
GRB 080120	8.5–84.5 ks					
GRB 080123	108 s–58.9 ks	$216^{+6}_{-6}$	$433^{+54}_{-40}$			
GRB 080129	3.2–837.6 ks	$(1.19^{+0.49}_{+0.19}) \times 10^4$				
GRB 080205	107 s–221.4 ks	$152^{+7}_{-10}$	$189^{+10}_{-7}$	$411^{+82}_{-74}$		
GRB 080207	130 s–324.6 ks	$279^{+42}_{-34}$				
GRB 080210	160 s–403.8 ks					
GRB 080212	112 s–195.6 ks	$247^{+62}_{-40}$	$7682^{+8097}_{-1244}$			
GRB 080218B	930 s–574.3 ks					
GRB 080229A	96 s–540.2 ks	$209^{+7}_{-7}$	$1233^{+74}_{-130}$	$(3^{+8}_{+2}) \times 10^4$		
GRB 080229B	74.9–919.8 ks					
GRB 080303	78 s–983.5 ks	$2424^{+1094}_{-739}$				
GRB 080307	105 s–6349.2 ks	$283^{+11}_{-9}$	$(2.59^{+1.22}_{+0.70}) \times 10^4$			
GRB 080310	95 s–832.5 ks	$443^{+340}_{-127}$	$(1.07^{+0.16}_{+0.13}) \times 10^4$			
GRB 080319A	565 s–117.0 ks					
GRB 080319B	64 s–2823.7 ks	$474^{+135}_{-71}$	$(1.58^{+0.16}_{+0.14}) \times 10^4$	$(4.11^{+0.44}_{+0.35}) \times 10^4$	$(8^{+3}_{+1}) \times 10^5$	
GRB 080319C	230 s–713.8 ks	$353^{+38}_{-31}$	$5768^{+3361}_{-2584}$			
GRB 080319D	159 s–456.9 ks	$988^{+434}_{-212}$				
GRB 080320	174 s–2290.9 ks	$559^{+218}_{-227}$	$(6^{+3}_{+1}) \times 10^4$			
GRB 080325	158 s–474.4 ks	$775^{+320}_{-123}$				
GRB 080328	105 s–42.6 ks	$158^{+5}_{-5}$	$2308^{+647}_{-508}$			
GRB 080330	76 s–585.9 ks	$166^{+9}_{-11}$	$1011^{+65440}_{-253}$			
GRB 080405	155.2–283.1 ks					
GRB 080409	87 s–126.6 ks	$501^{+196}_{-129}$				
GRB 080411	4.3–5539.0 ks	$(1.38^{+0.69}_{+0.29}) \times 10^4$	$(1.25^{+1.10}_{+0.40}) \times 10^6$			
GRB 080413A	67 s–148.7 ks	$164^{+22}_{-17}$				
GRB 080413B	134 s–662.2 ks	$624^{+201}_{-130}$	$(6^{+13}_{+1}) \times 10^4$			
GRB 080426	226 s–94.7 ks	$412^{+641}_{-92}$				
GRB 080430	55 s–3469.8 ks	$328^{+49}_{-45}$	$(3.32^{+0.55}_{+0.58}) \times 10^4$			
GRB 080503	81 s–278.4 ks	$140^{+10}_{-8}$	$249^{+53}_{-28}$			
GRB 080506	146 s–174.1 ks	$183^{+4}_{-3}$	$244^{+11}_{-9}$	$3947^{+1697}_{-1193}$		
GRB 080507	109.3–214.7 ks					
GRB 080514B	37.0–228.3 ks					
GRB 080515	132.8–579.8 ks					
GRB 080516	86 s–47.7 ks	$2555^{+2345}_{-1106}$				
GRB 080517	129 s–69.9 ks	$1002^{+555}_{-317}$				
GRB 080520	106 s–167.5 ks					
GRB 080523	92 s–202.9 ks	$192^{+20}_{-12}$	$2076^{+658}_{-505}$			
GRB 080602	117 s–1.4 ks	$146^{+11}_{-9}$	$453^{+132}_{-110}$			
GRB 080603A	10.4–606.4 ks					
GRB 080603B	68 s–12.3 ks	$76^{+10}_{-3}$	$160^{+7}_{-10}$			
GRB 080604	125 s–441.2 ks	$(1.35^{+4.44}_{+0.65}) \times 10^4$				
GRB 080605	96 s–949.1 ks	$274^{+112}_{-37}$	$4180^{+1267}_{-1015}$			
GRB 080607	85 s–376.5 ks	$102^{+2}_{-2}$	$334^{+27}_{-19}$	$(10^{+16}_{+5}) \times 10^4$		
GRB 080613A	24.2–146.8 ks					
GRB 080613B	75 s–214.1 ks	$217^{+4}_{-3}$	$237^{+14}_{-8}$			
GRB 080623	1.6–610.6 ks					

**Table 7** – *continued* \* Time range covered by the cleaned event lists. Zero is the BAT trigger time.

GRB	Obs times*	$t_{\text{break}, 1}$	$t_{\text{break}, 2}$	$t_{\text{break}, 3}$	$t_{\text{break}, 4}$	$t_{\text{break}, 5}$
GRB 080625	17.9–818.1 ks	$(1.67_{-1.09}^{+0.88}) \times 10^5$				
GRB 080701	2.9–131.2 ks					
GRB 080702A	74 s–121.6 ks					
GRB 080703	103 s–180.9 ks	$(2.14_{-0.23}^{+0.23}) \times 10^4$				
GRB 080707	74 s–416.6 ks	$184_{-26}^{+18}$	$7703_{-6696}^{+2997}$			
GRB 080710	3.1–646.9 ks	$(2.21_{-0.52}^{+0.55}) \times 10^4$				
GRB 080714	86 s–450.2 ks	$126_{-27}^{+71}$	$287_{-72}^{+158}$			
GRB 080721	113 s–1405.7 ks	$290_{-27}^{+9}$	$306_{-9}^{+12}$	$3990_{-323}^{+346}$		
GRB 080723A	96 s–573.3 ks	$380_{-71}^{+92}$	$2880_{-613}^{+1151}$			
GRB 080723B	13.4–40.6 ks					

**Table 7** – *continued* \* Time range covered by the cleaned event lists. Zero is the BAT trigger time.

GRB	Galactic $N_{\text{H}}$	redshift	WT Mode		PC Mode	
			intrinsic $N_{\text{H}}$	Spectral index ( $\beta$ )	intrinsic $N_{\text{H}}$	Spectral index ( $\beta$ )
GRB 041218	27.4		$21.6^{+133.6}_{-21.6}$	$2.3^{+5.4}_{-2.0}$	$< 50.27$	$0.55^{+1.23}_{-0.69}$
GRB 041223	10.1				$3.1^{+4.5}_{-3.1}$	$1.13^{+0.19}_{-0.16}$
GRB 050124	2.66		$0.96^{+8.00}_{-0.96}$	$0.54^{+0.35}_{-0.24}$	$2.1^{+2.6}_{-2.0}$	$0.94^{+0.21}_{-0.20}$
GRB 050126	4.62	1.29			$< 11.50$	$1.14^{+0.22}_{-0.15}$
GRB 050128	5.19		$< 125.82$	$0.41^{+1.80}_{-0.45}$	$4.9^{+2.0}_{-1.9}$	$0.968^{+0.087}_{-0.044}$
GRB 050215B	1.85				$< 8.82$	$0.65^{+0.59}_{-0.28}$
GRB 050219A	9.50		$17.4^{+4.7}_{-4.4}$	$1.16^{+0.16}_{-0.15}$	$4.8^{+11.8}_{-4.8}$	$0.66^{+0.37}_{-0.32}$
GRB 050219B	2.98		$21.9^{+5.0}_{-4.6}$	$1.09^{+0.18}_{-0.17}$	$12.3^{+4.2}_{-4.9}$	$1.07^{+0.19}_{-0.20}$
GRB 050223	7.08	0.5915			$< 16.31$	$0.87^{+0.50}_{-0.39}$
GRB 050315	3.69	1.949	$117.8^{+87.2}_{-64.0}$	$1.11^{+0.35}_{-0.29}$	$76.2^{+18.0}_{-17.0}$	$1.021^{+0.042}_{-0.070}$
GRB 050318	1.86	1.44	$15.3^{+137.9}_{-15.3}$	$1.48^{+3.13}_{-0.71}$	$11.0^{+8.3}_{-6.1}$	$0.992^{+0.080}_{-0.087}$
GRB 050319	1.26	3.24			$10.2^{+22.9}_{-10.2}$	$0.998^{+0.066}_{-0.048}$
GRB 050326	4.16		$6.6^{+6.9}_{-6.0}$	$1.05^{+0.33}_{-0.30}$	$13.5^{+7.2}_{-2.4}$	$1.01^{+0.14}_{-0.14}$
GRB 050401	4.40	2.9	$155.6^{+19.2}_{-18.3}$	$0.895^{+0.041}_{-0.040}$	$139.3^{+64.9}_{-59.3}$	$0.79^{+0.11}_{-0.11}$
GRB 050406	1.86		$< 3.43$	$1.27^{+0.30}_{-0.16}$	$7.2^{+30.7}_{-7.2}$	$0.96^{+0.69}_{-0.81}$
GRB 050408	1.73	1.236			$125.2^{+24.0}_{-19.9}$	$1.19^{+0.13}_{-0.12}$
GRB 050410	6.95		$8.8^{+17.4}_{-8.8}$	$1.21^{+0.69}_{-0.55}$	$3.3^{+35.7}_{-3.3}$	$0.71^{+0.41}_{-0.31}$
GRB 050412	1.92		$26.8^{+47.1}_{-23.3}$	$0.72^{+0.87}_{-0.18}$	$1.5^{+9.8}_{-1.5}$	$0.62^{+0.36}_{-0.29}$
GRB 050416A	2.45	0.6535	$53.8^{+56.4}_{-43.6}$	$2.4^{+1.6}_{-1.4}$	$54.1^{+5.8}_{-7.8}$	$1.053^{+0.071}_{-0.052}$
GRB 050421	15.3		$70.8^{+29.3}_{-23.4}$	$0.40^{+0.29}_{-0.27}$	$53.5^{+28.0}_{-20.7}$	$1.39^{+0.52}_{-0.40}$
GRB 050422	91.1		$10.0^{+52.3}_{-10.0}$	$2.07^{+1.01}_{-0.49}$	$< 22.79$	$1.39^{+0.46}_{-0.41}$
GRB 050502B	3.59		$7.05^{+0.67}_{-0.66}$	$1.245^{+0.034}_{-0.034}$	$0.82^{+2.06}_{-0.82}$	$0.945^{+0.077}_{-0.100}$
GRB 050504	1.11				$23.4^{+35.0}_{-23.4}$	$1.5^{+1.6}_{-1.3}$
GRB 050505	1.71	4.27			$175.1^{+41.0}_{-31.4}$	$1.020^{+0.034}_{-0.053}$
GRB 050509A	30.3				$23.0^{+45.4}_{-19.8}$	$1.06^{+0.79}_{-0.65}$
GRB 050509B	1.55	0.225			$8.0^{+8.1}_{-8.0}$	$0.92^{+1.09}_{-0.60}$
GRB 050520	1.26				$150.4^{+222.2}_{-75.2}$	$-0.4^{+1.0}_{-1.0}$
GRB 050525A	9.07	0.606			$14.6^{+8.5}_{-6.8}$	$1.04^{+0.14}_{-0.12}$
GRB 050603	2.23	2.821			$44.9^{+22.3}_{-29.0}$	$1.06^{+0.10}_{-0.11}$
GRB 050607	12.6				$9.3^{+2.1}_{-4.6}$	$1.302^{+0.085}_{-0.175}$
GRB 050701	150.0				$276.2^{+161.7}_{-132.9}$	$1.45^{+0.77}_{-0.35}$
GRB 050712	12.3		$8.4^{+3.2}_{-3.0}$	$1.28^{+0.14}_{-0.13}$	$6.6^{+4.0}_{-1.9}$	$1.15^{+0.14}_{-0.16}$
GRB 050713A	10.7		$23.7^{+2.2}_{-2.1}$	$1.173^{+0.066}_{-0.064}$	$26.0^{+5.2}_{-4.3}$	$1.14^{+0.14}_{-0.13}$
GRB 050713B	19.5		$12.8^{+4.1}_{-3.9}$	$0.652^{+0.093}_{-0.097}$	$24.6^{+4.9}_{-5.5}$	$1.08^{+0.14}_{-0.13}$
GRB 050714	32.9				$170.3^{+173.5}_{-145.2}$	$1.5^{+1.5}_{-1.3}$
GRB 050714B	4.63		$77.9^{+12.6}_{-11.1}$	$5.21^{+0.69}_{-0.61}$	$28.9^{+6.5}_{-7.2}$	$2.64^{+0.38}_{-0.37}$
GRB 050716	8.42		$2.2^{+1.8}_{-1.7}$	$0.306^{+0.057}_{-0.057}$	$8.1^{+1.8}_{-4.0}$	$1.08^{+0.12}_{-0.16}$
GRB 050717	20.2		$19.8^{+5.4}_{-5.0}$	$0.480^{+0.097}_{-0.095}$	$16.7^{+9.6}_{-8.9}$	$0.76^{+0.16}_{-0.20}$
GRB 050721	14.5		$11.2^{+5.2}_{-4.8}$	$0.61^{+0.14}_{-0.13}$	$14.8^{+7.2}_{-3.4}$	$0.86^{+0.18}_{-0.16}$
GRB 050724	14.0	0.257	$43.4^{+3.7}_{-3.6}$	$0.663^{+0.042}_{-0.042}$	$17.0^{+8.2}_{-8.2}$	$0.81^{+0.14}_{-0.17}$
GRB 050726	4.95		$4.8^{+2.6}_{-2.5}$	$1.20^{+0.14}_{-0.14}$	$1.4^{+2.2}_{-1.4}$	$1.024^{+0.112}_{-0.061}$
GRB 050730	3.01	3.97	$52.2^{+22.6}_{-21.8}$	$0.598^{+0.033}_{-0.032}$	$20.5^{+25.1}_{-20.5}$	$0.615^{+0.035}_{-0.035}$
GRB 050801	6.34				$< 1.96$	$0.89^{+0.18}_{-0.12}$
GRB 050802	1.85		$3.9^{+3.4}_{-3.1}$	$0.99^{+0.19}_{-0.18}$	$3.57^{+1.07}_{-0.62}$	$0.918^{+0.036}_{-0.062}$
GRB 050803	5.04		$13.5^{+4.5}_{-4.2}$	$0.81^{+0.17}_{-0.15}$	$14.6^{+2.4}_{-2.4}$	$1.058^{+0.091}_{-0.089}$
GRB 050813	4.45				$6.3^{+41.0}_{-6.3}$	$1.5^{+0.0}_{-1.6}$
GRB 050814	2.28	5.3	$78.8^{+62.2}_{-59.3}$	$1.103^{+0.069}_{-0.067}$	$< 55.21$	$0.922^{+0.074}_{-0.062}$
GRB 050815	23.3				$4.1^{+10.8}_{-4.1}$	$0.61^{+0.14}_{-0.22}$
GRB 050819	4.61		$< 5.08$	$1.35^{+0.34}_{-0.17}$	$1.8^{+3.0}_{-1.8}$	$1.11^{+0.20}_{-0.22}$
GRB 050820A	4.41	2.612	$< 5.96$	$0.033^{+0.042}_{-0.027}$	$35.9^{+15.2}_{-14.4}$	$0.966^{+0.051}_{-0.050}$
GRB 050820B	8.52	2.612			$50.5^{+371.6}_{-50.5}$	$0.65^{+0.51}_{-0.38}$
GRB 050822	1.41		$13.0^{+1.4}_{-1.3}$	$1.583^{+0.074}_{-0.070}$	$6.6^{+2.1}_{-1.1}$	$1.139^{+0.076}_{-0.104}$
GRB 050824	3.70	0.83			$3.7^{+8.2}_{-3.7}$	$0.93^{+0.14}_{-0.14}$
GRB 050826	19.0	0.3			$86.4^{+17.1}_{-28.0}$	$1.26^{+0.18}_{-0.29}$
GRB 050827	16.2				$22.3^{+5.1}_{-9.5}$	$0.873^{+0.095}_{-0.234}$
GRB 050904	4.53	6.29	$375.5^{+95.2}_{-91.7}$	$0.351^{+0.034}_{-0.034}$	$261.9^{+96.9}_{-94.1}$	$0.908^{+0.049}_{-0.047}$

**Table 8.** Best-fit results for time-averaged spectra. Column densities are in units of  $10^{20}$  cm $^{-2}$ . WT and PC mode were fitted independently.

GRB	WT Mode			PC Mode		
	Galactic $N_{\text{H}}$	redshift	intrinsic $N_{\text{H}}$	Spectral index ( $\beta$ )	intrinsic $N_{\text{H}}$	Spectral index ( $\beta$ )
GRB 050908	2.38	3.35			$0.65^{+44.49}_{-0.65}$	$1.91^{+0.24}_{-0.13}$
GRB 050915A	1.97		$11.5^{+5.7}_{-5.2}$	$1.18^{+0.27}_{-0.25}$	$9.2^{+3.5}_{-4.5}$	$1.29^{+0.16}_{-0.22}$
GRB 050915B	22.2		$9.7^{+4.9}_{-4.5}$	$1.68^{+0.20}_{-0.19}$	$18.4^{+7.8}_{-10.3}$	$1.36^{+0.19}_{-0.27}$
GRB 050916	81.0				$13.5^{+19.4}_{-12.2}$	$0.64^{+0.16}_{-0.23}$
GRB 050922B	3.14		$13.3^{+1.6}_{-1.5}$	$1.700^{+0.086}_{-0.083}$	$13.4^{+2.7}_{-2.5}$	$1.58^{+0.13}_{-0.12}$
GRB 050922C	5.37	2.198	$17.3^{+14.4}_{-13.7}$	$1.028^{+0.073}_{-0.072}$	$43.7^{+18.3}_{-10.6}$	$1.287^{+0.084}_{-0.077}$
GRB 051001	1.15		$12.4^{+1.9}_{-1.8}$	$0.443^{+0.061}_{-0.060}$	$15.4^{+2.8}_{-6.3}$	$1.26^{+0.25}_{-0.27}$
GRB 051006	8.10		$46.4^{+21.6}_{-17.5}$	$0.47^{+0.31}_{-0.29}$	$73.2^{+26.6}_{-21.8}$	$1.64^{+0.40}_{-0.40}$
GRB 051008	0.959				$31.5^{+3.1}_{-3.5}$	$0.930^{+0.047}_{-0.088}$
GRB 051012	10.0				$1.6^{+38.5}_{-1.6}$	$0.58^{+2.11}_{-0.74}$
GRB 051016A	12.2		$27.4^{+21.7}_{-17.9}$	$2.00^{+0.85}_{-0.72}$	$36.6^{+7.6}_{-12.7}$	$2.35^{+0.46}_{-0.46}$
GRB 051016B	3.20	0.9364	$85.2^{+33.4}_{-28.3}$	$4.01^{+0.98}_{-0.80}$	$55.4^{+6.1}_{-14.0}$	$0.937^{+0.055}_{-0.133}$
GRB 051021A	4.61				$5.3^{+3.6}_{-5.3}$	$1.09^{+0.24}_{-0.26}$
GRB 051021B	71.0		< 31.14	$0.30^{+0.41}_{-0.27}$	$12.0^{+33.0}_{-12.0}$	$0.68^{+0.33}_{-0.31}$
GRB 051022	3.76	0.8			$315.1^{+35.9}_{-33.8}$	$1.04^{+0.12}_{-0.11}$
GRB 051028	11.5				$13.8^{+4.4}_{-8.6}$	$1.22^{+0.17}_{-0.31}$
GRB 051109A	16.1	2.346	$21.5^{+48.7}_{-21.5}$	$1.13^{+0.16}_{-0.15}$	$49.6^{+29.5}_{-27.2}$	$1.062^{+0.079}_{-0.077}$
GRB 051109B	11.5				$13.3^{+3.6}_{-6.8}$	$1.17^{+0.23}_{-0.23}$
GRB 051111	5.26	1.55			$60.0^{+19.1}_{-23.6}$	$1.25^{+0.10}_{-0.15}$
GRB 051117A	1.78		$11.52^{+0.42}_{-0.41}$	$1.075^{+0.018}_{-0.018}$	$9.2^{+2.8}_{-2.6}$	$1.277^{+0.136}_{-0.072}$
GRB 051117B	4.67				$21.7^{+16.6}_{-15.6}$	$0.68^{+0.46}_{-0.34}$
GRB 051210	1.91		$2.5^{+5.4}_{-2.5}$	$0.28^{+0.21}_{-0.18}$	$44.6^{+16.0}_{-29.4}$	$2.26^{+0.63}_{-0.92}$
GRB 051211B	32.0				$6.8^{+6.3}_{-6.8}$	$1.04^{+0.11}_{-0.25}$
GRB 051221A	5.66	0.5465			$15.9^{+3.8}_{-3.1}$	$1.059^{+0.087}_{-0.065}$
GRB 051221B	46.1		$33.7^{+904.9}_{-33.7}$	$-0.02^{+4.05}_{-0.73}$	$87.0^{+135.0}_{-49.1}$	$1.06^{+1.17}_{-0.80}$
GRB 051227	3.35		$18.0^{+8.8}_{-7.7}$	$0.40^{+0.22}_{-0.21}$	$4.6^{+6.6}_{-4.6}$	$0.99^{+0.33}_{-0.31}$
GRB 060105	14.8		$18.34^{+0.99}_{-0.98}$	$0.946^{+0.027}_{-0.027}$	$20.4^{+2.5}_{-2.3}$	$1.085^{+0.079}_{-0.076}$
GRB 060108	1.79	2.03	< 143.21	$0.53^{+1.42}_{-0.96}$	$39.4^{+25.3}_{-27.6}$	$0.96^{+0.10}_{-0.13}$
GRB 060109	10.4		$17.2^{+4.8}_{-4.5}$	$1.21^{+0.17}_{-0.16}$	$22.8^{+2.2}_{-5.0}$	$1.33^{+0.11}_{-0.15}$
GRB 060110	21.8				$4.1^{+30.9}_{-4.1}$	$0.80^{+0.84}_{-0.58}$
GRB 060111A	2.93		$18.63^{+0.97}_{-0.95}$	$1.267^{+0.039}_{-0.038}$	$13.2^{+4.7}_{-4.8}$	$1.21^{+0.20}_{-0.19}$
GRB 060111B	7.66		$11.9^{+4.9}_{-4.5}$	$1.20^{+0.21}_{-0.19}$	$21.9^{+4.8}_{-5.7}$	$1.30^{+0.16}_{-0.18}$
GRB 060115	9.48	3.53	$135.7^{+59.1}_{-53.6}$	$0.852^{+0.088}_{-0.084}$	< 42.08	$1.124^{+0.099}_{-0.083}$
GRB 060116	17.6		$49.7^{+273.6}_{-49.7}$	$0.7^{+2.5}_{-2.1}$	$51.2^{+7.8}_{-16.2}$	$0.89^{+0.14}_{-0.26}$
GRB 060121	1.38				$8.3^{+4.5}_{-4.8}$	$1.28^{+0.24}_{-0.24}$
GRB 060123	1.27				$10.5^{+8.4}_{-6.9}$	$0.75^{+0.31}_{-0.25}$
GRB 060124	8.98	2.297	$37.2^{+7.3}_{-7.1}$	$0.423^{+0.019}_{-0.019}$	$64.3^{+16.4}_{-15.5}$	$1.021^{+0.054}_{-0.052}$
GRB 060202	4.40		$39.7^{+1.2}_{-1.2}$	$1.159^{+0.031}_{-0.030}$	$41.6^{+2.3}_{-4.4}$	$1.747^{+0.061}_{-0.139}$
GRB 060203	6.35				$7.1^{+2.3}_{-4.1}$	$1.20^{+0.18}_{-0.18}$
GRB 060204B	1.66		$19.5^{+1.9}_{-1.8}$	$0.993^{+0.067}_{-0.066}$	$12.2^{+1.8}_{-1.6}$	$1.281^{+0.065}_{-0.099}$
GRB 060206	9.33e-01	4.05	< 271.78	$1.46^{+1.47}_{-0.84}$	$117.3^{+145.0}_{-117.3}$	$1.21^{+0.27}_{-0.24}$
GRB 060210	6.08	3.91	$227.3^{+24.6}_{-24.0}$	$0.934^{+0.031}_{-0.031}$	$179.8^{+36.4}_{-34.5}$	$1.079^{+0.049}_{-0.048}$
GRB 060211A	11.3		$7.4^{+1.9}_{-1.8}$	$0.942^{+0.072}_{-0.069}$	$6.7^{+5.7}_{-5.8}$	$0.96^{+0.12}_{-0.22}$
GRB 060211B	17.0		$2.6^{+16.8}_{-2.6}$	$1.25^{+0.80}_{-0.39}$	$5.5^{+5.6}_{-5.5}$	$0.75^{+0.15}_{-0.28}$
GRB 060218	9.37	0.0331	$26.35^{+0.45}_{-0.43}$	$0.7478^{+0.0102}_{-0.0099}$	$34.6^{+3.1}_{-4.9}$	$2.56^{+0.16}_{-0.18}$
GRB 060219	2.34				$35.1^{+9.5}_{-8.8}$	$2.19^{+0.38}_{-0.33}$
GRB 060223A	6.91	4.41			$273.9^{+146.4}_{-190.5}$	$1.06^{+0.17}_{-0.19}$
GRB 060306	3.44		$37.9^{+10.9}_{-9.8}$	$1.15^{+0.29}_{-0.27}$	$36.8^{+2.2}_{-4.4}$	$1.275^{+0.053}_{-0.120}$
GRB 060312	11.6		$10.2^{+2.5}_{-2.4}$	$1.172^{+0.097}_{-0.094}$	< 2.17	$0.848^{+0.119}_{-0.086}$
GRB 060313	4.93		< 7.85	$0.74^{+0.40}_{-0.19}$	< 0.92	$0.949^{+0.075}_{-0.074}$
GRB 060319	1.46				$43.6^{+5.1}_{-5.2}$	$1.254^{+0.074}_{-0.131}$
GRB 060322	10.7				$17.6^{+15.1}_{-17.6}$	$2.35^{+2.47}_{-0.96}$
GRB 060323	1.48		$3.8^{+9.8}_{-3.8}$	$1.02^{+0.45}_{-0.31}$	$2.0^{+2.9}_{-2.0}$	$0.99^{+0.30}_{-0.24}$
GRB 060403	44.0		$18.6^{+15.5}_{-13.8}$	$0.37^{+0.19}_{-0.18}$	$15.6^{+30.1}_{-15.6}$	$1.32^{+0.56}_{-0.68}$
GRB 060413	108.0		$127.0^{+16.0}_{-15.6}$	$0.89^{+0.10}_{-0.10}$	$80.3^{+18.9}_{-18.2}$	$0.38^{+0.12}_{-0.11}$
GRB 060418	8.81	1.49	$57.4^{+6.2}_{-5.9}$	$1.129^{+0.041}_{-0.040}$	$37.5^{+25.4}_{-22.6}$	$0.96^{+0.15}_{-0.14}$
GRB 060421	90.0				$34.2^{+42.2}_{-34.2}$	$0.58^{+0.14}_{-0.46}$

GRB	Galactic $N_{\text{H}}$	redshift	WT Mode		PC Mode	
			intrinsic $N_{\text{H}}$	Spectral index ( $\beta$ )	intrinsic $N_{\text{H}}$	Spectral index ( $\beta$ )
GRB 060427	3.85		$10.3^{+3.0}_{-2.8}$	$1.78^{+0.18}_{-0.17}$	$12.0^{+4.7}_{-4.9}$	$1.42^{+0.21}_{-0.22}$
GRB 060428A	76.7		< 16.19	$2.30^{+0.53}_{-0.26}$	$18.6^{+12.6}_{-11.7}$	$1.03^{+0.15}_{-0.15}$
GRB 060428B	1.33		$6.5^{+1.5}_{-1.4}$	$1.86^{+0.11}_{-0.10}$	< 1.28	$1.040^{+0.115}_{-0.090}$
GRB 060501	22.8				$30.0^{+99.4}_{-30.0}$	$1.62^{+2.21}_{-0.57}$
GRB 060502A	3.45	1.51	$53.8^{+16.8}_{-15.3}$	$2.48^{+0.27}_{-0.25}$	$24.1^{+13.5}_{-12.8}$	$1.034^{+0.115}_{-0.058}$
GRB 060502B	4.24				$7.6^{+22.3}_{-7.6}$	$1.10^{+2.77}_{-0.81}$
GRB 060505	1.72				$8.1^{+19.1}_{-8.1}$	$0.65^{+0.69}_{-0.55}$
GRB 060507	8.84				$4.8^{+2.1}_{-3.9}$	$1.08^{+0.14}_{-0.16}$
GRB 060510A	36.1		< 5.19	$2.35^{+0.38}_{-0.32}$	< 3.00	$0.932^{+0.079}_{-0.043}$
GRB 060510B	4.07	4.9	$321.2^{+40.3}_{-39.8}$	$0.239^{+0.021}_{-0.022}$	$145.5^{+120.7}_{-72.8}$	$1.19^{+0.17}_{-0.16}$
GRB 060512	1.53	0.4428	$30.3^{+17.5}_{-15.1}$	$4.54^{+1.13}_{-0.96}$	< 2.31	$1.80^{+0.11}_{-0.11}$
GRB 060515	2.44				< 6.77	$0.81^{+0.52}_{-0.33}$
GRB 060522	4.10	5.11	$143.3^{+333.8}_{-143.3}$	$0.56^{+0.23}_{-0.20}$	$210.7^{+192.9}_{-138.5}$	$1.14^{+0.13}_{-0.11}$
GRB 060526	5.02	3.21	$55.0^{+15.4}_{-14.8}$	$0.892^{+0.035}_{-0.035}$	< 28.22	$0.931^{+0.086}_{-0.084}$
GRB 060602A	2.48				$59.3^{+39.3}_{-31.8}$	$4.2^{+0.0}_{-2.4}$
GRB 060602B	121.0				$396.6^{+138.7}_{-103.2}$	$2.29^{+0.67}_{-0.56}$
GRB 060604	4.09	2.68	$159.3^{+18.0}_{-17.1}$	$1.172^{+0.050}_{-0.050}$	$71.1^{+38.6}_{-33.6}$	$1.17^{+0.13}_{-0.12}$
GRB 060605	3.95	3.8	$0.053^{+150.957}_{-0.053}$	$0.63^{+0.41}_{-0.30}$	$31.5^{+37.6}_{-31.5}$	$1.000^{+0.054}_{-0.043}$
GRB 060607A	2.42	3.082	$27.4^{+12.1}_{-11.7}$	$0.702^{+0.031}_{-0.031}$	$49.2^{+25.7}_{-24.7}$	$0.654^{+0.056}_{-0.054}$
GRB 060614	1.87		$1.72^{+0.64}_{-0.62}$	$0.897^{+0.035}_{-0.035}$	$1.45^{+1.15}_{-0.61}$	$0.890^{+0.064}_{-0.043}$
GRB 060707	1.44	3.43	< 56.85	$0.89^{+0.23}_{-0.22}$	$3.1^{+51.6}_{-3.1}$	$1.071^{+0.132}_{-0.094}$
GRB 060708	2.10		$11.9^{+2.8}_{-2.6}$	$2.27^{+0.19}_{-0.18}$	$3.0^{+1.1}_{-1.8}$	$1.218^{+0.079}_{-0.101}$
GRB 060712	1.66				$15.3^{+2.3}_{-4.8}$	$1.81^{+0.13}_{-0.23}$
GRB 060714	6.05	2.71	$138.8^{+19.8}_{-18.8}$	$0.810^{+0.043}_{-0.043}$	$93.0^{+37.5}_{-35.5}$	$1.024^{+0.101}_{-0.096}$
GRB 060717	1.24				$24.6^{+29.7}_{-17.1}$	$2.36^{+1.65}_{-0.56}$
GRB 060719	2.03		$26.3^{+6.8}_{-5.9}$	$2.22^{+0.38}_{-0.32}$	$38.7^{+5.7}_{-5.9}$	$1.78^{+0.19}_{-0.19}$
GRB 060729	4.49	0.54	$20.6^{+2.0}_{-2.0}$	$2.206^{+0.075}_{-0.072}$	$13.2^{+1.7}_{-1.7}$	$1.067^{+0.038}_{-0.037}$
GRB 060801	1.35	1.13			$62.0^{+1.7}_{-18.9}$	$0.94^{+0.27}_{-0.26}$
GRB 060804	45.1				< 6.46	$1.09^{+0.15}_{-0.12}$
GRB 060805A	1.55				$8.0^{+7.8}_{-6.7}$	$1.29^{+0.41}_{-0.36}$
GRB 060805B	3.16				$0.18^{+6.16}_{-0.18}$	$0.73^{+0.24}_{-0.21}$
GRB 060807	2.45				$12.1^{+2.4}_{-2.2}$	$1.087^{+0.098}_{-0.096}$
GRB 060813	30.5		$8.4^{+3.4}_{-3.2}$	$0.877^{+0.078}_{-0.077}$	$6.0^{+3.6}_{-3.3}$	$0.904^{+0.086}_{-0.076}$
GRB 060814	2.33		$23.7^{+1.3}_{-1.3}$	$0.787^{+0.038}_{-0.038}$	$30.5^{+2.6}_{-2.5}$	$1.296^{+0.084}_{-0.082}$
GRB 060825	29.2		$6.7^{+33.6}_{-6.7}$	$0.93^{+0.69}_{-0.47}$	$5.2^{+16.9}_{-5.2}$	$0.53^{+0.27}_{-0.28}$
GRB 060901	21.3				$25.7^{+27.9}_{-18.8}$	$0.91^{+0.50}_{-0.44}$
GRB 060904A	1.33		$14.0^{+1.2}_{-1.1}$	$1.100^{+0.051}_{-0.049}$	< 22.76	$-0.00^{+0.91}_{-0.69}$
GRB 060904B	11.3	0.7	$46.9^{+3.9}_{-3.7}$	$1.095^{+0.043}_{-0.041}$	$38.9^{+9.5}_{-6.3}$	$1.188^{+0.096}_{-0.142}$
GRB 060906	9.81	3.69	$347.2^{+454.5}_{-281.2}$	$1.56^{+0.46}_{-0.40}$	$245.0^{+138.6}_{-130.5}$	$1.14^{+0.13}_{-0.16}$
GRB 060908	2.34	2.43	$43.7^{+39.9}_{-36.9}$	$1.24^{+0.20}_{-0.19}$	$95.1^{+51.1}_{-45.7}$	$1.13^{+0.18}_{-0.12}$
GRB 060912A	3.85	0.94	$17.1^{+54.2}_{-17.1}$	$0.78^{+0.85}_{-0.67}$	$18.6^{+7.8}_{-8.6}$	$0.88^{+0.11}_{-0.11}$
GRB 060919	5.90				$92.2^{+38.9}_{-36.7}$	$1.08^{+0.42}_{-0.51}$
GRB 060923A	4.52		$8.9^{+8.1}_{-6.4}$	$0.95^{+0.32}_{-0.28}$	$9.5^{+3.1}_{-6.1}$	$0.92^{+0.13}_{-0.23}$
GRB 060923B	8.44				$29.8^{+12.9}_{-10.9}$	$1.16^{+0.33}_{-0.30}$
GRB 060923C	5.14		$0.81^{+4.49}_{-0.81}$	$0.87^{+0.23}_{-0.12}$	$7.9^{+4.8}_{-3.7}$	$1.04^{+0.16}_{-0.18}$
GRB 060926	7.58	3.2	$205.1^{+175.3}_{-129.3}$	$1.01^{+0.23}_{-0.22}$	$341.2^{+234.4}_{-195.1}$	$1.04^{+0.21}_{-0.28}$
GRB 060927	4.61	5.6			$122.1^{+251.0}_{-122.1}$	$0.89^{+0.16}_{-0.16}$
GRB 060928	94.3				$613.0^{+399.6}_{-523.5}$	$2.7^{+1.6}_{-1.1}$
GRB 060929	3.61		$11.9^{+1.4}_{-1.3}$	$0.773^{+0.049}_{-0.049}$	$10.2^{+4.6}_{-5.9}$	$1.22^{+0.25}_{-0.25}$
GRB 061002	3.71		$15.3^{+8.0}_{-7.0}$	$1.30^{+0.35}_{-0.30}$	$20.6^{+13.9}_{-15.3}$	$1.51^{+0.67}_{-0.67}$
GRB 061004	4.69		< 10.84	$0.70^{+0.52}_{-0.25}$	$3.3^{+1.6}_{-3.3}$	$0.976^{+0.092}_{-0.167}$
GRB 061006	14.1	0.4377			$17.9^{+16.8}_{-17.9}$	$0.98^{+0.25}_{-0.32}$
GRB 061007	1.77	1.26	$44.7^{+2.6}_{-2.5}$	$0.884^{+0.023}_{-0.023}$	$52.7^{+10.4}_{-9.7}$	$1.018^{+0.087}_{-0.083}$
GRB 061019	37.8				$68.8^{+14.5}_{-11.4}$	$1.07^{+0.14}_{-0.22}$
GRB 061021	4.52		< 0.20	$0.963^{+0.050}_{-0.050}$	$4.63^{+1.22}_{-0.72}$	$1.029^{+0.055}_{-0.051}$
GRB 061025	4.06				$2.6^{+13.0}_{-2.6}$	$0.72^{+0.63}_{-0.37}$
GRB 061028	13.1		$9.7^{+6.3}_{-5.7}$	$0.39^{+0.15}_{-0.15}$	$10.7^{+10.4}_{-10.7}$	$1.46^{+0.36}_{-0.43}$

GRB	Galactic $N_{\text{H}}$	redshift	WT Mode		PC Mode	
			intrinsic $N_{\text{H}}$	Spectral index ( $\beta$ )	intrinsic $N_{\text{H}}$	Spectral index ( $\beta$ )
GRB 061102	4.57		$8.5^{+5.4}_{-4.7}$	$2.20^{+0.40}_{-0.35}$	$3.0^{+34.6}_{-3.0}$	$0.36^{+0.92}_{-0.70}$
GRB 061110A	4.26		$10.3^{+1.2}_{-1.1}$	$1.989^{+0.074}_{-0.068}$	< 0.70	$0.86^{+0.15}_{-0.10}$
GRB 061110B	3.37	3.44			$342.2^{+250.0}_{-257.8}$	$1.24^{+0.31}_{-0.27}$
GRB 061121	3.99	1.314	$42.9^{+6.1}_{-5.8}$	$0.617^{+0.042}_{-0.041}$	$53.5^{+8.5}_{-8.0}$	$0.914^{+0.061}_{-0.059}$
GRB 061122	12.5				$5.1^{+4.7}_{-4.7}$	$1.04^{+0.17}_{-0.18}$
GRB 061126	10.2		$9.5^{+4.6}_{-4.2}$	$0.86^{+0.16}_{-0.15}$	$14.1^{+2.1}_{-2.0}$	$0.936^{+0.065}_{-0.064}$
GRB 061201	5.31		< 19.12	$-0.03^{+0.62}_{-0.26}$	$7.9^{+4.3}_{-5.1}$	$0.68^{+0.17}_{-0.18}$
GRB 061202	11.8		$45.4^{+4.8}_{-4.5}$	$0.917^{+0.085}_{-0.082}$	$51.8^{+5.5}_{-5.2}$	$1.208^{+0.103}_{-0.100}$
GRB 061210	3.20				$62.8^{+92.0}_{-55.5}$	$1.9^{+1.7}_{-1.3}$
GRB 061217	3.41				$58.7^{+200.7}_{-49.0}$	$0.40^{+1.13}_{-0.86}$
GRB 061222A	9.01		$32.4^{+2.9}_{-2.8}$	$1.196^{+0.078}_{-0.076}$	$27.1^{+2.7}_{-2.6}$	$1.071^{+0.071}_{-0.069}$
GRB 061222B	26.5	3.36	$395.7^{+143.6}_{-125.0}$	$1.60^{+0.15}_{-0.14}$	$448.1^{+338.5}_{-329.4}$	$0.97^{+0.18}_{-0.23}$
GRB 070103	4.43				$27.1^{+3.1}_{-6.3}$	$1.35^{+0.18}_{-0.21}$
GRB 070107	29.9		$3.4^{+2.3}_{-2.2}$	$0.903^{+0.060}_{-0.059}$	$7.0^{+2.9}_{-2.7}$	$1.102^{+0.077}_{-0.073}$
GRB 070110	1.61	2.352	$10.3^{+17.4}_{-10.3}$	$0.904^{+0.092}_{-0.085}$	$10.1^{+11.7}_{-10.1}$	$1.107^{+0.063}_{-0.061}$
GRB 070125	4.28				$7.1^{+2.9}_{-5.1}$	$1.11^{+0.21}_{-0.23}$
GRB 070129	6.96		$11.59^{+0.77}_{-0.75}$	$0.846^{+0.027}_{-0.026}$	$7.6^{+5.2}_{-1.8}$	$1.270^{+0.062}_{-0.103}$
GRB 070208	1.75	1.17			$71.2^{+15.3}_{-20.8}$	$1.18^{+0.14}_{-0.18}$
GRB 070219	3.95		$22.7^{+175.7}_{-22.7}$	$1.1^{+4.8}_{-2.0}$	$31.9^{+19.3}_{-9.8}$	$1.53^{+0.21}_{-0.20}$
GRB 070220	34.8		$10.4^{+4.6}_{-4.4}$	$0.435^{+0.077}_{-0.076}$	$18.2^{+7.2}_{-6.7}$	$0.61^{+0.11}_{-0.11}$
GRB 070223	1.39		$52.5^{+5.7}_{-5.4}$	$0.748^{+0.098}_{-0.096}$	$47.6^{+15.8}_{-14.5}$	$1.23^{+0.33}_{-0.36}$
GRB 070224	3.76		< 4.78	$1.58^{+0.40}_{-0.19}$	< 4.11	$1.20^{+0.24}_{-0.22}$
GRB 070227	23.9				$10.0^{+17.0}_{-10.0}$	$1.25^{+0.48}_{-0.42}$
GRB 070306	2.85		$39.2^{+2.4}_{-2.3}$	$1.248^{+0.065}_{-0.062}$	$33.2^{+3.2}_{-3.1}$	$1.115^{+0.087}_{-0.083}$
GRB 070309	52.9				$0.48^{+19.90}_{-0.48}$	$5.4^{+0.0}_{-1.2}$
GRB 070311	23.6				$23.7^{+8.9}_{-10.2}$	$1.13^{+0.21}_{-0.23}$
GRB 070318	1.44	0.84	$44.8^{+5.4}_{-5.2}$	$0.621^{+0.054}_{-0.053}$	$65.1^{+6.1}_{-5.1}$	$1.004^{+0.077}_{-0.073}$
GRB 070328	2.61		$20.37^{+1.01}_{-0.98}$	$1.237^{+0.033}_{-0.037}$	$20.4^{+2.0}_{-2.4}$	$1.171^{+0.087}_{-0.085}$
GRB 070330	5.45				$8.8^{+7.0}_{-5.3}$	$0.976^{+0.084}_{-0.144}$
GRB 070411	26.3	2.95			$155.3^{+164.1}_{-130.2}$	$1.29^{+0.21}_{-0.18}$
GRB 070412	2.68		$19.6^{+10.9}_{-9.2}$	$1.23^{+0.43}_{-0.36}$	$12.4^{+5.2}_{-5.8}$	$1.08^{+0.13}_{-0.23}$
GRB 070419A	2.42	0.97	$52.6^{+5.8}_{-5.5}$	$1.249^{+0.070}_{-0.067}$	$35.6^{+16.4}_{-19.2}$	$1.15^{+0.25}_{-0.26}$
GRB 070419B	6.72		$13.75^{+0.94}_{-0.92}$	$0.822^{+0.031}_{-0.030}$	$6.4^{+2.2}_{-2.1}$	$0.601^{+0.073}_{-0.073}$
GRB 070420	33.1		$5.7^{+3.6}_{-3.4}$	$1.52^{+0.12}_{-0.11}$	$7.4^{+4.3}_{-4.0}$	$1.017^{+0.092}_{-0.092}$
GRB 070429A	8.39		$37.2^{+4.5}_{-4.1}$	$2.62^{+0.21}_{-0.19}$	$5.2^{+10.4}_{-5.2}$	$0.75^{+0.36}_{-0.29}$
GRB 070429B	1.80				$60.7^{+44.9}_{-30.3}$	$2.1^{+1.0}_{-1.4}$
GRB 070506	3.79	2.31			$29.6^{+48.1}_{-27.9}$	$1.02^{+0.23}_{-0.22}$
GRB 070508	7.84		$27.0^{+1.5}_{-1.5}$	$0.907^{+0.038}_{-0.038}$	$22.1^{+4.7}_{-2.1}$	$0.92^{+0.12}_{-0.11}$
GRB 070509	7.89				$41.8^{+21.7}_{-12.9}$	$1.19^{+0.36}_{-0.55}$
GRB 070517	8.30				$3.9^{+5.1}_{-3.9}$	$1.11^{+0.23}_{-0.22}$
GRB 070518	1.49		$8.9^{+2.2}_{-2.1}$	$1.62^{+0.13}_{-0.13}$	$1.6^{+4.0}_{-1.6}$	$1.21^{+0.29}_{-0.24}$
GRB 070520A	2.15		$22.2^{+3.8}_{-3.5}$	$2.19^{+0.20}_{-0.19}$	$23.5^{+7.9}_{-17.6}$	$2.12^{+0.31}_{-0.37}$
GRB 070520B	3.76		$19.4^{+1.5}_{-1.4}$	$1.517^{+0.065}_{-0.062}$	$17.0^{+12.4}_{-11.0}$	$1.43^{+0.32}_{-0.47}$
GRB 070521	2.92		$56.8^{+79.4}_{-39.7}$	$1.18^{+1.03}_{-0.83}$	$58.6^{+6.9}_{-6.0}$	$1.05^{+0.12}_{-0.12}$
GRB 070529	17.9	2.5	$534.1^{+543.1}_{-352.4}$	$1.94^{+0.83}_{-0.64}$	$247.6^{+82.3}_{-125.5}$	$1.02^{+0.13}_{-0.17}$
GRB 070531	21.2				$2.2^{+13.2}_{-2.2}$	$0.07^{+0.25}_{-0.18}$
GRB 070611	1.38	2.04			$17.9^{+38.3}_{-17.9}$	$0.92^{+0.24}_{-0.23}$
GRB 070612B	15.7				$58.7^{+25.8}_{-29.4}$	$1.46^{+0.46}_{-0.80}$
GRB 070615	4.93				$5.3^{+41.8}_{-5.3}$	$0.5^{+3.4}_{-4.2}$
GRB 070616	34.0		$5.5^{+1.2}_{-1.2}$	$0.214^{+0.019}_{-0.019}$	$9.0^{+4.1}_{-6.0}$	$1.40^{+0.11}_{-0.18}$
GRB 070621	3.81		$37.7^{+3.2}_{-3.0}$	$1.428^{+0.055}_{-0.092}$	$37.6^{+6.5}_{-5.7}$	$1.68^{+0.19}_{-0.20}$
GRB 070628	57.8		$39.8^{+74.5}_{-39.8}$	$3.2^{+2.2}_{-1.2}$	$10.1^{+5.2}_{-5.0}$	$1.025^{+0.082}_{-0.079}$
GRB 070704	71.0		$33.8^{+5.9}_{-5.7}$	$0.734^{+0.061}_{-0.061}$	$49.8^{+37.3}_{-20.8}$	$0.98^{+0.18}_{-0.33}$
GRB 070707	6.15				$0.64^{+16.62}_{-0.64}$	$1.94^{+2.03}_{-0.61}$
GRB 070714A	9.22				$46.9^{+20.6}_{-17.5}$	$1.04^{+0.36}_{-0.33}$
GRB 070714B	6.43	0.92	$30.8^{+12.8}_{-10.9}$	$0.266^{+0.086}_{-0.084}$	$48.6^{+14.3}_{-15.1}$	$1.065^{+0.081}_{-0.103}$
GRB 070721A	1.61		$7.1^{+14.4}_{-7.1}$	$2.48^{+1.16}_{-0.45}$	$4.4^{+6.5}_{-2.7}$	$1.38^{+0.35}_{-0.20}$

GRB	Galactic $N_{\text{H}}$	redshift	WT Mode		PC Mode	
			intrinsic $N_{\text{H}}$	Spectral index ( $\beta$ )	intrinsic $N_{\text{H}}$	Spectral index ( $\beta$ )
GRB 070721B	2.33		$1.6^{+2.1}_{-1.6}$	$0.421^{+0.091}_{-0.085}$	$0.76^{+2.32}_{-0.76}$	$0.501^{+0.098}_{-0.050}$
GRB 070724A	1.17		$21.0^{+6.5}_{-6.0}$	$0.60^{+0.18}_{-0.18}$	$11.6^{+10.4}_{-11.6}$	$0.69^{+0.28}_{-0.29}$
GRB 070724B	30.7				$27.5^{+15.8}_{-17.4}$	$1.17^{+0.49}_{-0.40}$
GRB 070729	2.58				$0.024^{+9.135}_{-0.024}$	$0.62^{+0.86}_{-0.43}$
GRB 070802	2.90	2.45			$122.7^{+80.0}_{-100.7}$	$1.08^{+0.17}_{-0.18}$
GRB 070805	19.2				$0.057^{+39.184}_{-0.057}$	$1.2^{+4.0}_{-1.3}$
GRB 070808	2.83		$79.6^{+53.2}_{-39.6}$	$0.60^{+0.66}_{-0.56}$	$85.3^{+18.8}_{-20.0}$	$1.04^{+0.26}_{-0.27}$
GRB 070809	6.40				$< 3.87$	$0.39^{+0.18}_{-0.13}$
GRB 070810A	1.75	2.17			$68.1^{+27.7}_{-15.2}$	$1.141^{+0.128}_{-0.094}$
GRB 070911	2.39				$7.3^{+4.6}_{-5.3}$	$1.10^{+0.24}_{-0.24}$
GRB 070913	8.10				$11.9^{+3.2}_{-11.9}$	$1.4^{+1.2}_{-1.2}$
GRB 070917	17.3				$1.4^{+56.3}_{-1.4}$	$0.69^{+1.25}_{-0.61}$
GRB 070925	12.9				$1.7^{+30.3}_{-1.7}$	$0.96^{+1.13}_{-0.54}$
GRB 071001	76.2		$< 5.08$	$1.95^{+0.23}_{-0.23}$	$< 3.00$	$1.46^{+0.12}_{-0.18}$
GRB 071003	10.7				$4.8^{+3.5}_{-3.7}$	$1.04^{+0.13}_{-0.12}$
GRB 071008	8.78e-01				$< 25.70$	$1.82^{+1.56}_{-0.90}$
GRB 071010A	6.54				$40.1^{+10.3}_{-12.2}$	$1.67^{+0.27}_{-0.33}$
GRB 071010B	1.01	0.947			$24.0^{+21.9}_{-18.3}$	$1.10^{+0.33}_{-0.17}$
GRB 071011	51.8				$34.3^{+32.9}_{-17.5}$	$1.35^{+0.45}_{-0.41}$
GRB 071017	119.0				$489.6^{+353.4}_{-288.2}$	$1.05^{+0.99}_{-0.85}$
GRB 071020	5.12		$4.7^{+1.9}_{-1.8}$	$0.906^{+0.078}_{-0.074}$	$3.7^{+3.9}_{-3.6}$	$0.70^{+0.15}_{-0.15}$
GRB 071021	4.80		$15.1^{+2.4}_{-2.3}$	$1.097^{+0.091}_{-0.089}$	$13.7^{+1.9}_{-3.2}$	$1.205^{+0.082}_{-0.125}$
GRB 071025	5.13		$5.7^{+1.3}_{-1.3}$	$0.409^{+0.043}_{-0.043}$	$8.7^{+2.2}_{-1.8}$	$1.273^{+0.092}_{-0.098}$
GRB 071028A	5.09		$5.5^{+5.5}_{-4.7}$	$1.14^{+0.26}_{-0.24}$	$1.7^{+3.5}_{-1.7}$	$1.05^{+0.14}_{-0.19}$
GRB 071028B	1.22				$1.2^{+15.3}_{-1.2}$	$1.01^{+1.13}_{-0.78}$
GRB 071031	1.22	2.69	$88.1^{+8.9}_{-8.7}$	$0.848^{+0.026}_{-0.026}$	$17.0^{+34.4}_{-17.0}$	$0.86^{+0.14}_{-0.15}$
GRB 071101	56.3				$124.7^{+314.6}_{-124.7}$	$1.7^{+2.3}_{-1.1}$
GRB 071104	27.5				$2.0^{+5.8}_{-2.0}$	$0.85^{+0.19}_{-0.19}$
GRB 071109	24.9				$< 29.04$	$0.41^{+1.36}_{-0.67}$
GRB 071112C	7.44	0.82	$5.9^{+4.8}_{-4.6}$	$0.733^{+0.072}_{-0.070}$	$7.1^{+8.4}_{-4.4}$	$0.740^{+0.080}_{-0.112}$
GRB 071117	2.33	1.33			$117.9^{+19.8}_{-30.4}$	$1.15^{+0.16}_{-0.10}$
GRB 071118	9.70		$19.5^{+5.5}_{-5.2}$	$0.69^{+0.15}_{-0.14}$	$18.9^{+3.9}_{-3.7}$	$0.714^{+0.099}_{-0.096}$
GRB 071122	4.75	1.14	$20.2^{+12.0}_{-11.1}$	$1.07^{+0.15}_{-0.14}$	$< 11.07$	$0.64^{+0.19}_{-0.13}$
GRB 071227	1.25		$15.0^{+4.3}_{-4.0}$	$0.68^{+0.14}_{-0.14}$	$2.3^{+11.3}_{-2.3}$	$0.78^{+0.53}_{-0.34}$
GRB 080120	7.70				$4.9^{+5.7}_{-3.1}$	$1.33^{+0.26}_{-0.27}$
GRB 080121	1.23				$< 6.81$	$1.01^{+0.71}_{-0.41}$
GRB 080123	2.30		$9.2^{+2.7}_{-2.6}$	$0.74^{+0.11}_{-0.10}$	$14.0^{+10.7}_{-9.3}$	$1.62^{+0.47}_{-0.33}$
GRB 080129	64.2				$11.1^{+11.3}_{-11.1}$	$1.053^{+0.100}_{-0.181}$
GRB 080130	12.4				$< 28.39$	$0.30^{+0.99}_{-0.59}$
GRB 080205	7.14		$12.0^{+3.5}_{-3.3}$	$1.11^{+0.14}_{-0.14}$	$16.4^{+3.0}_{-5.7}$	$0.94^{+0.15}_{-0.19}$
GRB 080207	1.95		$94.8^{+10.0}_{-9.5}$	$0.333^{+0.093}_{-0.093}$	$69.0^{+7.9}_{-8.0}$	$1.51^{+0.13}_{-0.15}$
GRB 080210	5.47	2.64	$215.3^{+61.8}_{-53.7}$	$1.71^{+0.19}_{-0.18}$	$148.7^{+72.5}_{-66.8}$	$1.22^{+0.12}_{-0.10}$
GRB 080212	7.26		$21.6^{+1.1}_{-1.1}$	$1.907^{+0.050}_{-0.049}$	$12.8^{+2.3}_{-2.1}$	$1.290^{+0.059}_{-0.060}$
GRB 080218B	13.7				$32.9^{+12.1}_{-16.1}$	$1.54^{+0.30}_{-0.45}$
GRB 080229A	8.97		$24.9^{+2.2}_{-2.2}$	$1.991^{+0.098}_{-0.093}$	$17.4^{+2.5}_{-2.4}$	$0.865^{+0.070}_{-0.068}$
GRB 080229B	87.8				$49.3^{+37.6}_{-13.7}$	$1.73^{+0.34}_{-0.17}$
GRB 080303	12.6		$3.6^{+5.9}_{-3.6}$	$1.01^{+0.22}_{-0.20}$	$1.3^{+3.0}_{-1.3}$	$0.99^{+0.15}_{-0.16}$
GRB 080307	2.37		$2.5^{+1.4}_{-1.4}$	$0.445^{+0.057}_{-0.056}$	$8.7^{+4.4}_{-5.0}$	$0.888^{+0.094}_{-0.208}$
GRB 080310	3.28	2.43	$50.0^{+5.4}_{-5.3}$	$0.677^{+0.017}_{-0.017}$	$< 9.25$	$0.996^{+0.064}_{-0.065}$
GRB 080319A	1.45				$10.0^{+4.6}_{-4.4}$	$1.16^{+0.20}_{-0.18}$
GRB 080319B	1.12	0.94	$11.89^{+0.92}_{-0.92}$	$0.770^{+0.014}_{-0.014}$	$9.5^{+4.1}_{-3.9}$	$0.803^{+0.064}_{-0.063}$
GRB 080319C	2.21	1.95			$71.7^{+19.9}_{-18.7}$	$0.690^{+0.081}_{-0.079}$
GRB 080319D	21.7		$< 143.82$	$0.42^{+3.12}_{-0.80}$	$8.0^{+7.5}_{-6.7}$	$1.02^{+0.21}_{-0.20}$
GRB 080320	1.35				$5.1^{+2.1}_{-1.8}$	$1.060^{+0.103}_{-0.099}$
GRB 080325	3.81		$28.0^{+1.3}_{-1.3}$	$1.360^{+0.043}_{-0.042}$	$23.6^{+9.1}_{-8.3}$	$1.46^{+0.27}_{-0.30}$
GRB 080328	33.8		$10.2^{+3.8}_{-3.6}$	$1.139^{+0.094}_{-0.092}$	$10.2^{+3.4}_{-3.3}$	$1.029^{+0.077}_{-0.075}$
GRB 080330	1.22	1.51	$16.7^{+15.3}_{-14.1}$	$1.14^{+0.16}_{-0.15}$	$12.0^{+13.8}_{-12.0}$	$0.89^{+0.13}_{-0.12}$

GRB	Galactic $N_{\text{H}}$	redshift	WT Mode		PC Mode	
			intrinsic $N_{\text{H}}$	Spectral index ( $\beta$ )	intrinsic $N_{\text{H}}$	Spectral index ( $\beta$ )
GRB 080405	3.31				< 12.47	$0.89^{+0.52}_{-0.36}$
GRB 080409	23.4				$37.3^{+14.2}_{-19.1}$	$1.28^{+0.30}_{-0.22}$
GRB 080411	5.77	1.03			$44.4^{+4.8}_{-4.5}$	$1.024^{+0.044}_{-0.044}$
GRB 080413A	8.71	2.43	$187.2^{+42.1}_{-37.9}$	$2.17^{+0.17}_{-0.16}$	$53.4^{+75.8}_{-53.4}$	$1.13^{+0.21}_{-0.24}$
GRB 080413B	3.06	1.1	$27.5^{+9.2}_{-8.5}$	$1.032^{+0.103}_{-0.100}$	$26.0^{+5.4}_{-5.4}$	$0.989^{+0.065}_{-0.040}$
GRB 080426	36.5				$16.5^{+5.1}_{-11.5}$	$1.10^{+0.12}_{-0.25}$
GRB 080430	9.59e-01	0.767	$15.4^{+7.7}_{-7.1}$	$1.44^{+0.21}_{-0.19}$	$34.8^{+4.3}_{-3.5}$	$1.102^{+0.074}_{-0.066}$
GRB 080503	5.57		$5.1^{+1.6}_{-1.6}$	$0.346^{+0.051}_{-0.051}$	< 2.22	$1.53^{+0.35}_{-0.20}$
GRB 080506	16.6		$0.10^{+1.73}_{-0.10}$	$0.623^{+0.055}_{-0.030}$	< 2.50	$0.990^{+0.122}_{-0.077}$
GRB 080507	1.31				$18.6^{+22.3}_{-16.2}$	$1.69^{+1.05}_{-0.83}$
GRB 080514B	3.75				$5.5^{+3.7}_{-5.5}$	$1.00^{+0.24}_{-0.26}$
GRB 080515	4.65				$1.3^{+19.5}_{-1.3}$	$0.84^{+0.81}_{-0.39}$
GRB 080516	32.2				$58.3^{+21.9}_{-15.9}$	$1.26^{+0.18}_{-0.24}$
GRB 080517	8.12		$16.3^{+28.3}_{-16.3}$	$1.21^{+1.03}_{-0.80}$	$18.4^{+8.4}_{-8.2}$	$0.95^{+0.24}_{-0.27}$
GRB 080520	6.84	1.55			$138.2^{+39.8}_{-59.3}$	$1.30^{+0.22}_{-0.28}$
GRB 080523	2.10		$6.0^{+1.6}_{-1.5}$	$1.461^{+0.092}_{-0.088}$	< 2.39	$0.83^{+0.18}_{-0.12}$
GRB 080602	3.51		$12.7^{+6.3}_{-5.7}$	$0.90^{+0.25}_{-0.24}$	$13.5^{+3.4}_{-3.3}$	$1.01^{+0.13}_{-0.12}$
GRB 080603A	4.69	1.69			$68.1^{+27.4}_{-25.2}$	$1.43^{+0.20}_{-0.19}$
GRB 080603B	1.23	2.69	$93.2^{+22.4}_{-21.5}$	$0.678^{+0.060}_{-0.060}$	$79.8^{+75.7}_{-62.5}$	$0.99^{+0.23}_{-0.21}$
GRB 080604	3.81	1.42	< 3.44	$1.066^{+0.069}_{-0.066}$	$5.9^{+12.1}_{-5.9}$	$0.65^{+0.13}_{-0.13}$
GRB 080605	6.67	1.64	$71.3^{+8.1}_{-7.9}$	$0.755^{+0.036}_{-0.035}$	$70.3^{+30.0}_{-25.1}$	$0.829^{+0.121}_{-0.073}$
GRB 080607	1.69	3.04	$377.4^{+23.1}_{-21.9}$	$1.044^{+0.036}_{-0.035}$	$260.5^{+51.1}_{-29.9}$	$1.101^{+0.098}_{-0.092}$
GRB 080613A	2.03				< 4.56	$0.25^{+0.37}_{-0.20}$
GRB 080613B	3.17		$2.9^{+2.4}_{-2.3}$	$0.173^{+0.079}_{-0.079}$	$8.0^{+12.0}_{-8.0}$	$1.26^{+0.66}_{-0.53}$
GRB 080623	25.9				$14.2^{+6.4}_{-7.0}$	$1.14^{+0.16}_{-0.19}$
GRB 080625	14.5				$8.8^{+6.4}_{-5.9}$	$1.28^{+0.23}_{-0.22}$
GRB 080701	17.8				$57.9^{+21.8}_{-18.3}$	$1.87^{+0.44}_{-0.40}$
GRB 080702A	15.3				$61.6^{+44.0}_{-50.0}$	$1.08^{+0.55}_{-0.79}$
GRB 080702B	2.94				$3.9^{+37.3}_{-3.9}$	$1.01^{+1.87}_{-0.84}$
GRB 080703	5.13				$2.3^{+1.6}_{-1.3}$	$0.585^{+0.053}_{-0.056}$
GRB 080707	6.99	1.23	$20.8^{+55.5}_{-20.8}$	$1.44^{+0.83}_{-0.52}$	$38.1^{+18.8}_{-19.2}$	$1.11^{+0.17}_{-0.18}$
GRB 080710	4.10	0.85			$12.5^{+4.9}_{-4.4}$	$1.050^{+0.068}_{-0.093}$
GRB 080714	54.4		< 4.95	$0.52^{+0.13}_{-0.13}$	$5.1^{+22.2}_{-5.1}$	$0.67^{+0.37}_{-0.20}$
GRB 080721	6.94	2.6	$70.9^{+6.0}_{-5.9}$	$0.833^{+0.016}_{-0.016}$	$86.4^{+21.5}_{-20.4}$	$0.991^{+0.059}_{-0.057}$
GRB 080723A	39.4				$62.1^{+16.3}_{-14.7}$	$1.19^{+0.20}_{-0.10}$
GRB 080723B	74.3				$10.5^{+16.8}_{-10.5}$	$0.87^{+0.21}_{-0.18}$

GRB	Mode	$\beta_1$	$\beta_2$	$\beta_3$	$\beta_4$	$\beta_5$	$\beta_6$
GRB 050126	PC	$1.29^{+0.20}_{-0.20}$	$1.04^{+0.52}_{-0.36}$				
GRB 050128	WT		$0.35^{+1.74}_{-0.63}$				
	PC	$0.98^{+0.13}_{-0.12}$	$0.966^{+0.088}_{-0.092}$				
GRB 050219A	WT	$1.08^{+0.18}_{-0.17}$	$1.09^{+0.29}_{-0.13}$				
	PC		$1.16^{+0.48}_{-0.53}$				
GRB 050315	WT		$1.09^{+0.34}_{-0.29}$				
	PC	$1.07^{+0.11}_{-0.10}$	$0.979^{+0.085}_{-0.059}$	$1.088^{+0.060}_{-0.104}$			
GRB 050318	WT	$1.51^{+3.51}_{-0.73}$					
	PC	$0.99^{+0.10}_{-0.10}$	$0.99^{+0.12}_{-0.12}$				
GRB 050319	WT			$1.19^{+0.53}_{-0.28}$			
	PC	$1.49^{+0.17}_{-0.16}$	$0.908^{+0.075}_{-0.069}$	$1.09^{+0.11}_{-0.14}$	$14.0^{+8.0}_{-4.7}$		
GRB 050401	WT	$0.895^{+0.041}_{-0.040}$	$1.05^{+0.26}_{-0.25}$				
	PC	$0.70^{+0.16}_{-0.15}$	$0.94^{+0.12}_{-0.14}$				
GRB 050406	WT	$1.28^{+0.28}_{-0.17}$					
	PC	$1.13^{+1.55}_{-0.44}$	$-0.962^{+unconstr.}_{-unconstr.}$				
GRB 050410	WT	$1.28^{+0.69}_{-0.32}$					
	PC	$0.89^{+0.44}_{-0.44}$	$1.2^{+unconstr.}_{-unconstr.}$				
GRB 050416A	PC	$0.80^{+0.26}_{-0.25}$	$1.08^{+0.21}_{-0.20}$	$1.356^{+0.094}_{-0.069}$			
GRB 050421	WT	$0.44^{+0.32}_{-0.30}$	$0.12^{+0.70}_{-0.58}$				
	PC		$1.21^{+0.14}_{-0.28}$				
GRB 050422	PC	$1.69^{+0.31}_{-0.27}$	$1.02^{+0.80}_{-0.31}$				
GRB 050502B	WT	$1.246^{+0.034}_{-0.034}$					
	PC	$0.942^{+0.058}_{-0.091}$	$1.22^{+0.51}_{-0.33}$				
GRB 050505	PC	$0.93^{+0.16}_{-0.15}$	$1.032^{+0.070}_{-0.063}$	$1.106^{+0.126}_{-0.088}$			
GRB 050525A	PC	$0.94^{+0.30}_{-0.28}$	$2.25^{+0.31}_{-0.32}$				
GRB 050607	PC	$1.20^{+0.14}_{-0.14}$	$1.208^{+0.096}_{-0.105}$	$0.90^{+0.23}_{-0.22}$	$1.47^{+0.46}_{-0.27}$		
GRB 050712	WT	$1.27^{+0.14}_{-0.13}$					
	PC	$1.13^{+0.10}_{-0.12}$	$1.32^{+0.19}_{-0.42}$				
GRB 050713A	WT	$1.66^{+0.25}_{-0.23}$	$1.111^{+0.065}_{-0.064}$	$1.10^{+0.61}_{-0.55}$	$1.58^{+0.86}_{-0.68}$		
	PC				$1.216^{+0.080}_{-0.139}$		
GRB 050713B	PC	$0.63^{+0.21}_{-0.20}$	$1.12^{+0.18}_{-0.17}$	$0.988^{+0.060}_{-0.111}$			
GRB 050714B	WT	$5.21^{+0.69}_{-0.61}$					
	PC	$4.1^{+1.6}_{-1.1}$	$2.60^{+0.46}_{-0.36}$				
GRB 050716	WT	$0.126^{+0.094}_{-0.093}$	$0.536^{+0.080}_{-0.078}$				
	PC		$0.86^{+0.26}_{-0.25}$	$1.18^{+0.11}_{-0.10}$			
GRB 050717	WT	$0.478^{+0.097}_{-0.095}$	$0.07^{+1.00}_{-0.96}$				
	PC		$0.65^{+0.13}_{-0.11}$	$0.19^{+0.64}_{-0.77}$			
GRB 050721	WT	$0.61^{+0.14}_{-0.13}$					
	PC	$0.577^{+0.102}_{-0.098}$	$1.45^{+0.36}_{-0.24}$				
GRB 050724	WT	$0.590^{+0.049}_{-0.048}$	$1.54^{+0.13}_{-0.12}$				
	PC			$0.78^{+0.11}_{-0.16}$			
GRB 050726	WT	$1.19^{+0.14}_{-0.13}$					
	PC	$0.851^{+0.100}_{-0.067}$	$1.36^{+0.16}_{-0.14}$				
GRB 050730	WT	$0.597^{+0.033}_{-0.032}$	$1.06^{+0.98}_{-0.67}$				
	PC	$0.480^{+0.063}_{-0.041}$	$0.691^{+0.035}_{-0.022}$				
GRB 050801	PC	$0.946^{+0.121}_{-0.083}$	$0.85^{+0.40}_{-0.28}$				
GRB 050802	WT	$0.99^{+0.19}_{-0.18}$					
	PC	$0.86^{+0.12}_{-0.11}$	$1.021^{+0.043}_{-0.085}$				
GRB 050803	WT	$0.81^{+0.17}_{-0.15}$	$2.16^{+1.26}_{-0.88}$				
	PC	$0.39^{+0.39}_{-0.18}$	$0.850^{+0.083}_{-0.081}$	$2.01^{+0.18}_{-0.32}$			
GRB 050814	WT	$1.092^{+0.068}_{-0.066}$	$1.6^{+1.6}_{-1.2}$				
	PC	$1.097^{+0.100}_{-0.094}$	$1.036^{+0.092}_{-0.065}$	$0.81^{+0.21}_{-0.19}$			
GRB 050815	PC	$0.65^{+0.36}_{-0.28}$	$0.62^{+0.23}_{-0.33}$				

**Table 9.** Spectral indices for the time-resolved spectra.  $\beta_1$  corresponds to the time during which the decay followed  $\alpha_1$  in Table 6. Column densities for these spectra are given in Table 10.

GRB	Mode	$\beta_1$	$\beta_2$	$\beta_3$	$\beta_4$	$\beta_5$	$\beta_6$
GRB 050819	WT	$1.29^{+0.27}_{-0.15}$					
	PC	$1.33^{+0.32}_{-0.22}$	$1.40^{+0.50}_{-0.47}$				
GRB 050820A	WT	$1.04^{+0.20}_{-0.18}$	$-0.197^{+0.050}_{-0.038}$				
	PC		$0.853^{+0.080}_{-0.077}$	$1.084^{+0.035}_{-0.034}$			
GRB 050822	WT	$1.583^{+0.074}_{-0.070}$	$3.42^{+2.18}_{-0.91}$	$0.40^{+1.25}_{-0.54}$			
	PC	$1.86^{+0.70}_{-0.44}$	$1.00^{+0.17}_{-0.15}$	$1.54^{+0.17}_{-0.14}$			
GRB 050824	PC	$0.90^{+0.15}_{-0.15}$	$1.76^{+0.25}_{-0.41}$				
GRB 050826	PC	$0.96^{+0.34}_{-0.32}$	$1.23^{+0.43}_{-0.33}$	$1.24^{+0.55}_{-0.48}$			
GRB 050904	WT	$0.365^{+0.034}_{-0.034}$					
	PC	$0.652^{+0.086}_{-0.082}$	$0.890^{+0.046}_{-0.038}$				
GRB050915B	WT	$1.66^{+0.20}_{-0.19}$	$-1.76^{+3.47}_{-0.76}$				
	PC	$1.08^{+0.65}_{-0.48}$	$1.424^{+0.073}_{-0.192}$				
GRB050916	PC	$1.47^{+1.56}_{-0.61}$	$0.72^{+0.26}_{-0.23}$				
GRB 050922B	WT	$1.706^{+0.087}_{-0.084}$					
	PC	$1.314^{+0.070}_{-0.067}$	$1.37^{+0.36}_{-0.35}$	$1.92^{+0.46}_{-0.69}$			
GRB 050922C	WT	$1.032^{+0.073}_{-0.072}$					
	PC	$0.969^{+0.122}_{-0.075}$	$1.319^{+0.087}_{-0.087}$				
GRB 051001	WT	$0.103^{+0.096}_{-0.093}$	$0.716^{+0.082}_{-0.081}$				
	PC		$1.05^{+0.42}_{-0.39}$	$1.62^{+0.40}_{-0.39}$			
GRB 051008	PC	$0.90^{+0.11}_{-0.11}$	$1.25^{+0.12}_{-0.33}$				
GRB 051016A	WT	$2.00^{+0.85}_{-0.72}$					
	PC	$3.7^{+1.8}_{-1.4}$	$2.12^{+0.27}_{-0.20}$				
GRB 051016B	WT	$4.00^{+0.96}_{-0.79}$					
	PC	$1.14^{+1.18}_{-0.54}$	$1.03^{+0.21}_{-0.21}$	$1.047^{+0.098}_{-0.080}$			
GRB 051021B	WT	$0.29^{+0.42}_{-0.26}$					
	PC	$0.51^{+0.40}_{-0.24}$	$1.51^{+0.85}_{-0.72}$				
GRB 051022	PC	$1.04^{+0.11}_{-0.11}$	$1.10^{+0.37}_{-0.30}$				
GRB 051109A	WT	$1.10^{+0.17}_{-0.14}$	$1.45^{+1.13}_{-0.48}$				
	PC		$1.15^{+0.15}_{-0.14}$	$1.088^{+0.030}_{-0.058}$			
GRB 051109B	PC	$1.25^{+0.28}_{-0.29}$	$1.75^{+0.52}_{-0.46}$	$1.24^{+0.35}_{-0.16}$			
GRB 051117A	WT	$1.064^{+0.018}_{-0.018}$	$2.2^{+2.6}_{-1.4}$				
	PC	$1.24^{+0.13}_{-0.13}$		$1.32^{+0.17}_{-0.10}$			
GRB 051221A	PC	$1.01^{+0.18}_{-0.17}$	$0.92^{+0.18}_{-0.23}$	$1.19^{+0.13}_{-0.21}$			
GRB 051227	WT	$0.46^{+0.21}_{-0.21}$					
	PC	$0.78^{+0.27}_{-0.25}$	$1.27^{+0.56}_{-0.59}$				
GRB 060105	WT	$1.098^{+0.057}_{-0.055}$	$0.900^{+0.031}_{-0.030}$				
	PC			$0.878^{+0.065}_{-0.063}$	$1.22^{+0.17}_{-0.21}$	$1.49^{+0.15}_{-0.24}$	
GRB 060108	WT		$0.38^{+0.52}_{-0.26}$				
	PC	$0.98^{+0.20}_{-0.18}$	$0.96^{+0.24}_{-0.30}$	$1.17^{+0.21}_{-0.24}$			
GRB 060109	WT	$1.23^{+0.18}_{-0.17}$					
	PC	$0.94^{+0.45}_{-0.25}$	$1.22^{+0.22}_{-0.21}$	$1.55^{+0.16}_{-0.11}$			
GRB 060111A	WT	$1.268^{+0.039}_{-0.038}$					
	PC	$1.29^{+0.34}_{-0.31}$	$1.22^{+0.10}_{-0.11}$				
GRB 060111B	WT	$1.17^{+0.24}_{-0.22}$	$1.55^{+0.62}_{-0.54}$				
	PC		$1.22^{+0.21}_{-0.18}$	$1.29^{+0.16}_{-0.47}$			
GRB 060115	WT	$0.852^{+0.088}_{-0.084}$					
	PC	$1.002^{+0.085}_{-0.082}$	$1.21^{+0.13}_{-0.11}$				
GRB 060124	PC	$1.01^{+0.82}_{-0.69}$	$1.030^{+0.061}_{-0.058}$	$1.072^{+0.050}_{-0.067}$			
GRB 060202	WT	$1.372^{+0.051}_{-0.050}$	$1.052^{+0.043}_{-0.043}$	$0.992^{+0.087}_{-0.085}$			
	PC			$0.72^{+0.15}_{-0.14}$	$2.26^{+0.10}_{-0.18}$		
GRB 060204B	WT	$0.863^{+0.075}_{-0.074}$	$1.70^{+0.18}_{-0.17}$				
	PC	$0.76^{+0.28}_{-0.27}$	$1.03^{+0.15}_{-0.14}$	$1.81^{+0.13}_{-0.15}$			
GRB 060206	WT	$1.44^{+1.51}_{-0.91}$					
	PC	$0.95^{+0.21}_{-0.14}$	$0.98^{+0.17}_{-0.17}$				
GRB 060210	WT	$0.934^{+0.031}_{-0.031}$	$1.33^{+2.66}_{-0.66}$				
	PC	$1.103^{+0.058}_{-0.056}$	$1.047^{+0.070}_{-0.080}$				
GRB 060211A	WT	$0.942^{+0.072}_{-0.069}$					
	PC	$1.10^{+0.52}_{-0.23}$	$0.64^{+0.22}_{-0.13}$	$1.44^{+0.34}_{-0.16}$			

GRB	Mode	$\beta_1$	$\beta_2$	$\beta_3$	$\beta_4$	$\beta_5$	$\beta_6$
GRB 060211B	WT	$1.23^{+0.84}_{-0.38}$					
	PC	$0.70^{+0.21}_{-0.25}$	$0.88^{+0.83}_{-0.61}$				
GRB 060218	WT	$0.7474^{+0.0102}_{-0.0099}$					
	PC	$1.91^{+0.22}_{-0.21}$	$4.13^{+0.78}_{-0.17}$				
GRB 060219	PC	$2.09^{+1.10}_{-0.87}$	$2.14^{+0.26}_{-0.43}$	$2.33^{+0.81}_{-0.59}$			
GRB 060223A	WT		$0.88^{+0.42}_{-0.36}$				
	PC	$0.86^{+0.32}_{-0.14}$	$1.12^{+0.18}_{-0.24}$				
GRB 060306	WT	$1.17^{+0.29}_{-0.27}$	$0.91^{+2.10}_{-1.00}$				
	PC	$0.66^{+0.82}_{-0.37}$	$1.21^{+0.18}_{-0.17}$	$1.301^{+0.075}_{-0.174}$			
GRB 060312	WT	$1.168^{+0.097}_{-0.093}$					
GRB 060313	WT	$1.19^{+0.34}_{-0.29}$	$0.89^{+0.20}_{-0.18}$				
	PC	$0.74^{+0.40}_{-0.19}$	$1.5^{+2.5}_{-1.2}$				
GRB 060319	WT	$0.59^{+0.38}_{-0.17}$	$0.71^{+0.16}_{-0.24}$	$0.832^{+0.116}_{-0.067}$	$1.38^{+0.28}_{-0.14}$		
	PC	$1.11^{+0.11}_{-0.11}$	$1.70^{+0.16}_{-0.24}$				
GRB 060403	WT	$0.39^{+0.19}_{-0.18}$					
	PC	$0.78^{+0.69}_{-0.48}$	$1.17^{+0.77}_{-1.16}$				
GRB 060413	WT	$0.88^{+0.10}_{-0.10}$					
	PC	$0.54^{+0.18}_{-0.17}$	$0.41^{+0.13}_{-0.12}$	$0.73^{+0.32}_{-0.21}$			
GRB 060418	WT	$1.143^{+0.043}_{-0.041}$	$1.04^{+0.11}_{-0.11}$	$1.03^{+0.41}_{-0.29}$			
	PC		$0.88^{+0.11}_{-0.11}$	$1.31^{+0.23}_{-0.24}$			
GRB 060427	WT	$1.78^{+0.18}_{-0.17}$					
	PC	$1.17^{+0.31}_{-0.27}$	$1.36^{+0.13}_{-0.16}$				
GRB 060428A	WT	$2.30^{+0.50}_{-0.25}$					
	PC	$1.7^{+1.8}_{-1.1}$	$1.02^{+0.14}_{-0.14}$	$0.87^{+0.11}_{-0.11}$	$1.42^{+0.31}_{-0.51}$		
GRB 060428B	WT	$1.86^{+0.11}_{-0.10}$					
	PC	$1.13^{+0.40}_{-0.21}$	$1.15^{+0.21}_{-0.20}$				
GRB 060502A	WT	$2.48^{+0.27}_{-0.25}$					
	PC	$1.34^{+0.17}_{-0.15}$	$1.02^{+0.13}_{-0.12}$	$0.95^{+0.15}_{-0.17}$			
GRB 060507	WT		$1.6^{+2.8}_{-5.4}$				
	PC	$0.83^{+0.27}_{-0.16}$	$1.16^{+0.12}_{-0.19}$				
GRB 060510A	WT	$2.30^{+0.20}_{-0.28}$					
	PC		$0.871^{+0.044}_{-0.043}$	$0.975^{+0.040}_{-0.085}$			
GRB 060510B	WT	$0.190^{+0.023}_{-0.023}$	$0.814^{+0.073}_{-0.073}$				
	PC		$0.92^{+0.21}_{-0.19}$	$1.243^{+0.131}_{-0.099}$			
GRB 060512	WT	$4.53^{+1.13}_{-0.96}$					
	PC	$1.85^{+0.42}_{-0.23}$	$1.80^{+0.12}_{-0.12}$				
GRB 060522	WT	$0.51^{+0.21}_{-0.19}$					
	PC	$0.65^{+0.28}_{-0.23}$	$1.17^{+0.21}_{-0.14}$	$1.29^{+0.37}_{-0.29}$			
GRB 060526	WT	$0.892^{+0.035}_{-0.035}$					
	PC	$0.77^{+0.13}_{-0.13}$	$1.09^{+0.20}_{-0.14}$	$1.15^{+0.21}_{-0.25}$	$1.04^{+0.63}_{-0.36}$		
GRB 060604	WT	$1.173^{+0.050}_{-0.050}$					
	PC		$1.14^{+0.18}_{-0.18}$	$1.24^{+0.14}_{-0.16}$			
GRB 060605	WT	$0.63^{+0.37}_{-0.32}$					
	PC	$0.57^{+0.13}_{-0.12}$	$1.12^{+0.14}_{-0.13}$	$1.23^{+0.12}_{-0.10}$			
GRB 060607A	WT	$0.705^{+0.032}_{-0.032}$	$0.71^{+0.25}_{-0.16}$	$0.60^{+0.84}_{-0.61}$			
	PC		$0.483^{+0.036}_{-0.031}$	$0.613^{+0.035}_{-0.050}$			
GRB 060614	WT	$0.254^{+0.052}_{-0.051}$	$1.332^{+0.041}_{-0.040}$	$1.07^{+0.35}_{-0.21}$			
	PC			$0.822^{+0.093}_{-0.057}$	$0.98^{+0.13}_{-0.14}$		
GRB 060707	WT	$0.89^{+0.23}_{-0.22}$					
	PC	$1.01^{+0.14}_{-0.11}$	$1.31^{+0.22}_{-0.22}$	$0.99^{+0.22}_{-0.21}$			
GRB 060708	WT	$2.26^{+0.19}_{-0.18}$					
GRB 060712	WT		$1.22^{+0.16}_{-0.14}$	$1.19^{+0.11}_{-0.11}$			
	PC	$1.90^{+0.51}_{-0.44}$	$1.67^{+0.62}_{-0.55}$	$1.72^{+0.17}_{-0.18}$			
GRB 060714	WT	$0.816^{+0.044}_{-0.043}$					
	PC	$1.38^{+0.42}_{-0.30}$	$0.93^{+0.13}_{-0.13}$	$1.32^{+0.16}_{-0.17}$			
GRB 060719	WT	$2.20^{+0.37}_{-0.32}$					
	PC	$1.19^{+0.74}_{-0.61}$	$2.08^{+0.27}_{-0.25}$	$1.85^{+0.13}_{-0.19}$			

GRB	Mode	$\beta_1$	$\beta_2$	$\beta_3$	$\beta_4$	$\beta_5$	$\beta_6$
GRB 060729	WT	$2.06^{+0.10}_{-0.10}$	$2.96^{+0.18}_{-0.16}$				
	PC		$1.96^{+0.28}_{-0.28}$	$1.060^{+0.045}_{-0.044}$	$1.088^{+0.030}_{-0.041}$	$0.867^{+0.087}_{-0.120}$	
GRB 060801	PC	$0.59^{+0.30}_{-0.29}$	$0.70^{+0.26}_{-0.23}$	$5.3^{+2.4}_{-2.6}$			
GRB 060804	PC	$1.09^{+0.21}_{-0.19}$	$1.27^{+0.18}_{-0.34}$				
GRB 060805A	PC	$1.28^{+0.45}_{-0.39}$	$1.17^{+0.36}_{-0.59}$				
GRB 060807	PC	$0.95^{+0.56}_{-0.34}$	$0.91^{+0.21}_{-0.20}$	$1.17^{+0.12}_{-0.11}$	$1.80^{+0.27}_{-0.35}$		
GRB 060813	WT	$0.884^{+0.078}_{-0.078}$					
	PC		$0.882^{+0.085}_{-0.081}$	$1.11^{+0.27}_{-0.40}$			
GRB 060814	WT	$0.36^{+0.14}_{-0.14}$	$0.784^{+0.039}_{-0.038}$	$1.16^{+0.13}_{-0.13}$			
	PC			$0.95^{+0.21}_{-0.20}$	$1.200^{+0.092}_{-0.090}$	$1.404^{+0.067}_{-0.137}$	
GRB 060904A	WT	$0.962^{+0.058}_{-0.056}$	$2.04^{+0.14}_{-0.13}$				
	PC			$1.63^{+0.47}_{-0.25}$			
GRB 060904B	WT	$1.095^{+0.043}_{-0.041}$					
	PC	$1.00^{+0.25}_{-0.22}$	$1.33^{+0.13}_{-0.14}$				
GRB 060906	WT	$1.36^{+0.64}_{-0.50}$	$1.57^{+0.68}_{-0.38}$				
	PC		$1.20^{+0.22}_{-0.22}$	$1.04^{+0.17}_{-0.14}$			
GRB 060908	WT	$1.24^{+0.20}_{-0.19}$	$1.87^{+1.21}_{-0.87}$				
	PC	$1.14^{+0.27}_{-0.26}$	$0.95^{+0.20}_{-0.19}$				
GRB 060912A	PC	$0.87^{+0.15}_{-0.15}$	$1.13^{+0.15}_{-0.10}$				
GRB 060923A	WT	$0.91^{+0.34}_{-0.32}$	$1.20^{+1.37}_{-0.59}$	$1.20^{+0.31}_{-0.25}$			
	PC	$0.55^{+0.40}_{-0.35}$	$0.62^{+0.52}_{-0.22}$	$1.42^{+0.26}_{-0.16}$			
GRB 060923C	WT	$0.87^{+0.22}_{-0.12}$					
	PC	$0.752^{+0.101}_{-0.089}$	$1.93^{+0.28}_{-0.32}$	$1.32^{+0.70}_{-0.28}$			
GRB 060926	WT	$0.78^{+0.78}_{-0.42}$	$1.03^{+0.26}_{-0.25}$				
	PC			$1.18^{+0.27}_{-0.30}$			
GRB 060927	PC	$0.81^{+0.22}_{-0.17}$	$1.04^{+0.38}_{-0.31}$				
GRB 060929	WT		$0.777^{+0.050}_{-0.049}$				
	PC	$1.48^{+0.69}_{-0.59}$	$1.00^{+0.17}_{-0.33}$				
GRB 061002	WT	$1.35^{+0.39}_{-0.36}$	$1.25^{+0.91}_{-0.39}$				
	PC		$1.48^{+0.71}_{-0.64}$				
GRB 061004	WT	$0.70^{+0.54}_{-0.25}$					
	PC	$0.37^{+0.29}_{-0.14}$	$1.35^{+0.26}_{-0.31}$	$1.23^{+0.24}_{-0.23}$			
GRB 061007	WT	$0.832^{+0.064}_{-0.062}$	$0.893^{+0.025}_{-0.025}$				
	PC		$0.99^{+0.33}_{-0.29}$	$0.97^{+0.15}_{-0.15}$	$1.30^{+0.13}_{-0.12}$		
GRB 061019	PC	$1.035^{+0.064}_{-0.233}$	$1.44^{+1.10}_{-0.68}$				
GRB 061021	WT	$0.965^{+0.052}_{-0.047}$					
GRB 061028	PC	$0.53^{+0.21}_{-0.11}$	$1.08^{+0.11}_{-0.10}$	$1.052^{+0.066}_{-0.071}$			
	WT	$0.39^{+0.16}_{-0.15}$					
GRB 061102	PC	$0.73^{+0.18}_{-0.17}$	$9.0^{+2.3}_{-1.5}$				
	WT	$2.21^{+0.40}_{-0.35}$					
GRB 061110A	PC		$0.58^{+0.55}_{-0.51}$				
	WT	$2.071^{+0.094}_{-0.087}$	$2.24^{+0.14}_{-0.13}$				
GRB 061121	PC		$1.05^{+0.25}_{-0.20}$	$0.937^{+0.110}_{-0.098}$	$1.00^{+0.32}_{-0.32}$		
	WT	$-0.035^{+0.078}_{-0.075}$	$1.255^{+0.101}_{-0.097}$	$1.11^{+0.14}_{-0.13}$	$0.960^{+0.084}_{-0.081}$	$1.14^{+0.29}_{-0.28}$	
GRB 061126	PC				$0.86^{+0.18}_{-0.16}$	$0.935^{+0.077}_{-0.075}$	$0.899^{+0.065}_{-0.061}$
	WT	$0.86^{+0.16}_{-0.15}$					
GRB 061201	PC	$0.952^{+0.078}_{-0.075}$	$0.936^{+0.123}_{-0.075}$				
	WT	$-0.03^{+0.64}_{-0.26}$	$0.08^{+1.23}_{-0.54}$				
GRB 061202	PC	$0.33^{+0.11}_{-0.10}$	$1.26^{+0.40}_{-0.22}$				
	WT	$0.912^{+0.084}_{-0.082}$					
GRB 061222A	PC	$1.21^{+0.21}_{-0.20}$	$1.11^{+0.15}_{-0.15}$	$1.463^{+0.097}_{-0.163}$			
	WT	$1.203^{+0.079}_{-0.077}$	$1.24^{+0.39}_{-0.35}$	$1.49^{+1.27}_{-0.84}$			
GRB 070103	PC		$0.871^{+0.070}_{-0.067}$	$1.059^{+0.083}_{-0.080}$	$1.352^{+0.039}_{-0.123}$		
	WT		$1.81^{+1.21}_{-0.88}$				
GRB 070107	PC	$1.36^{+0.43}_{-0.39}$	$1.05^{+0.50}_{-0.44}$	$1.43^{+0.33}_{-0.31}$			
	WT	$0.904^{+0.060}_{-0.059}$					
	PC	$1.088^{+0.102}_{-0.099}$	$1.168^{+0.076}_{-0.055}$				

GRB	Mode	$\beta_1$	$\beta_2$	$\beta_3$	$\beta_4$	$\beta_5$	$\beta_6$
GRB 070110	WT	$0.906^{+0.090}_{-0.086}$	$1.25^{+0.21}_{-0.17}$				
	PC	$1.08^{+0.23}_{-0.19}$	$0.81^{+0.12}_{-0.11}$	$1.124^{+0.076}_{-0.073}$	$1.13^{+0.18}_{-0.15}$	$1.16^{+0.20}_{-0.16}$	
GRB 070125	PC	$1.14^{+0.21}_{-0.23}$	$1.17^{+0.25}_{-0.14}$				
GRB 070129	WT	$0.862^{+0.027}_{-0.027}$					
	PC	$1.46^{+0.11}_{-0.11}$	$1.53^{+0.28}_{-0.27}$	$1.29^{+0.13}_{-0.16}$	$1.65^{+1.26}_{-0.59}$		
GRB 070208	PC	$1.35^{+0.44}_{-0.26}$	$1.26^{+0.32}_{-0.31}$	$1.17^{+0.26}_{-0.37}$			
GRB 070219	WT	$1.1^{+4.4}_{-2.0}$					
	PC	$0.61^{+0.72}_{-0.56}$	$1.4^{+1.7}_{-1.3}$	$2.06^{+0.47}_{-0.31}$			
GRB 070220	WT	$0.446^{+0.098}_{-0.096}$	$0.44^{+0.13}_{-0.12}$				
	PC			$0.460^{+0.081}_{-0.080}$	$0.65^{+0.22}_{-0.22}$		
GRB 070223	WT	$0.56^{+0.14}_{-0.14}$	$1.08^{+0.17}_{-0.16}$				
	PC			$1.68^{+0.28}_{-0.19}$			
GRB 070224	WT	$1.43^{+0.20}_{-0.16}$					
	PC	$1.34^{+0.15}_{-0.15}$	$0.96^{+0.37}_{-0.20}$				
GRB 070306	WT	$1.137^{+0.092}_{-0.089}$	$1.366^{+0.091}_{-0.087}$				
	PC		$1.00^{+0.53}_{-0.24}$	$1.11^{+0.11}_{-0.11}$	$1.16^{+0.19}_{-0.18}$	$1.42^{+0.17}_{-0.12}$	
GRB 070311	PC	$1.01^{+0.23}_{-0.24}$	$1.22^{+0.19}_{-0.39}$	$1.14^{+0.98}_{-0.67}$			
GRB 070328	WT	$1.107^{+0.089}_{-0.084}$	$1.271^{+0.056}_{-0.055}$	$1.238^{+0.065}_{-0.064}$			
	PC			$1.22^{+0.61}_{-0.56}$	$1.219^{+0.037}_{-0.083}$		
GRB 070412	WT	$1.16^{+0.40}_{-0.34}$					
	PC		$0.86^{+0.19}_{-0.30}$	$1.74^{+0.55}_{-0.50}$			
GRB 070419A	WT		$1.15^{+0.13}_{-0.13}$				
	PC		$1.11^{+0.20}_{-0.19}$	$1.50^{+2.59}_{-0.58}$			
GRB 070419B	WT	$0.801^{+0.030}_{-0.029}$					
	PC	$0.520^{+0.044}_{-0.043}$	$0.77^{+0.14}_{-0.18}$				
GRB 070420	WT	$1.50^{+0.12}_{-0.11}$	$0.63^{+0.82}_{-0.40}$				
	PC		$1.023^{+0.081}_{-0.079}$	$0.91^{+0.12}_{-0.11}$	$1.07^{+0.18}_{-0.17}$	$1.25^{+0.20}_{-0.26}$	
GRB 070429A	WT	$2.83^{+0.25}_{-0.23}$	$2.08^{+0.67}_{-0.42}$				
	PC		$0.77^{+0.39}_{-0.17}$	$1.21^{+0.24}_{-0.26}$	$0.48^{+0.62}_{-0.40}$		
GRB 070508	WT	$0.892^{+0.047}_{-0.047}$	$0.905^{+0.063}_{-0.063}$				
	PC		$0.84^{+0.15}_{-0.14}$	$1.42^{+0.13}_{-0.30}$			
GRB 070517	PC	$1.15^{+0.26}_{-0.25}$	$0.98^{+0.49}_{-0.36}$				
GRB 070518	WT	$1.56^{+0.12}_{-0.12}$					
	PC	$1.17^{+0.27}_{-0.17}$	$2.09^{+0.31}_{-0.39}$				
GRB 070520A	WT	$2.14^{+0.20}_{-0.19}$					
	PC		$2.36^{+0.52}_{-0.33}$				
GRB 070520B	WT	$1.517^{+0.065}_{-0.062}$					
	PC	$1.05^{+0.63}_{-0.56}$	$1.97^{+0.56}_{-0.47}$				
GRB 070521	WT	$1.18^{+1.03}_{-0.83}$					
	PC	$0.86^{+0.40}_{-0.37}$	$0.83^{+0.13}_{-0.12}$	$1.52^{+0.11}_{-0.20}$			
GRB 070529	WT	$1.93^{+0.62}_{-0.62}$					
	PC	$1.08^{+0.92}_{-0.56}$	$0.81^{+0.12}_{-0.11}$	$1.38^{+0.26}_{-0.14}$			
GRB 070616	WT	$0.079^{+0.023}_{-0.023}$	$0.704^{+0.039}_{-0.039}$				
	PC		$0.90^{+0.25}_{-0.23}$	$1.56^{+0.15}_{-0.21}$			
GRB 070621	WT	$1.398^{+0.093}_{-0.091}$					
	PC	$1.39^{+0.37}_{-0.35}$	$1.69^{+0.26}_{-0.25}$	$2.13^{+0.30}_{-0.22}$			
GRB 070628	WT	$3.2^{+2.1}_{-1.3}$					
	PC	$0.94^{+0.15}_{-0.14}$	$1.076^{+0.099}_{-0.093}$				
GRB 070704	WT	$0.734^{+0.061}_{-0.061}$					
	PC	$0.49^{+0.92}_{-0.28}$	$1.16^{+0.31}_{-0.47}$				
GRB 070714B	WT	$0.154^{+0.100}_{-0.097}$	$0.78^{+0.21}_{-0.19}$				
	PC		$0.97^{+0.16}_{-0.15}$	$1.28^{+0.29}_{-0.28}$	$0.88^{+0.13}_{-0.14}$		
GRB 070721A	WT	$2.29^{+0.95}_{-0.61}$					
	PC	$1.66^{+0.23}_{-0.22}$	$1.96^{+0.34}_{-0.39}$				
GRB 070721B	WT	$0.72^{+0.17}_{-0.15}$	$0.302^{+0.107}_{-0.088}$				
	PC		$0.320^{+0.113}_{-0.047}$	$1.12^{+0.15}_{-0.19}$			
GRB 070724A	WT	$0.58^{+0.18}_{-0.18}$					
	PC	$0.82^{+0.27}_{-0.26}$	$1.57^{+0.60}_{-0.49}$				

GRB	Mode	$\beta_1$	$\beta_2$	$\beta_3$	$\beta_4$	$\beta_5$	$\beta_6$
GRB 070802	PC	$0.79^{+0.19}_{-0.17}$	$1.22^{+0.43}_{-0.41}$	$1.43^{+0.42}_{-0.43}$			
GRB 070808	WT	$0.61^{+0.66}_{-0.56}$					
	PC	$0.32^{+0.44}_{-0.40}$	$1.58^{+0.42}_{-0.34}$				
GRB 070810A	PC	$1.11^{+0.36}_{-0.33}$	$1.15^{+0.12}_{-0.15}$				
GRB 071001	WT	$1.95^{+0.24}_{-0.22}$					
	PC	$1.52^{+0.18}_{-0.24}$	$1.35^{+0.58}_{-0.29}$				
GRB 071010A	PC	$1.96^{+0.36}_{-0.38}$	$1.40^{+0.40}_{-0.33}$				
GRB 071011	PC	$1.47^{+0.13}_{-0.34}$	$0.73^{+0.50}_{-0.52}$				
GRB 071020	WT	$0.98^{+0.12}_{-0.11}$	$0.818^{+0.052}_{-0.047}$				
	PC		$0.742^{+0.041}_{-0.036}$				
GRB 071021	WT	$1.115^{+0.090}_{-0.088}$	$1.06^{+0.69}_{-0.58}$				
	PC		$1.288^{+0.052}_{-0.101}$				
GRB 071025	WT	$0.398^{+0.076}_{-0.074}$	$0.363^{+0.099}_{-0.058}$	$0.67^{+0.13}_{-0.12}$			
	PC			$1.28^{+1.80}_{-0.75}$	$1.278^{+0.045}_{-0.076}$		
GRB 071028A	WT	$1.10^{+0.25}_{-0.22}$					
	PC	$0.97^{+0.28}_{-0.19}$	$1.03^{+0.34}_{-0.23}$	$0.99^{+0.65}_{-0.33}$			
GRB 071031	WT	$0.849^{+0.026}_{-0.026}$					
	PC	$0.85^{+0.20}_{-0.12}$	$0.96^{+0.20}_{-0.23}$	$0.79^{+0.71}_{-0.47}$			
GRB 071112C	WT	$0.837^{+0.087}_{-0.083}$	$0.612^{+0.103}_{-0.088}$				
	PC		$0.66^{+0.17}_{-0.12}$	$0.95^{+0.18}_{-0.21}$			
GRB 071118	WT	$0.69^{+0.15}_{-0.14}$					
	PC	$0.81^{+0.33}_{-0.31}$	$0.654^{+0.075}_{-0.073}$	$0.67^{+0.23}_{-0.28}$			
GRB 071227	WT	$0.60^{+0.14}_{-0.14}$					
	PC		$0.76^{+0.30}_{-0.27}$	$1.97^{+1.91}_{-0.62}$			
GRB 080123	WT	$0.72^{+0.11}_{-0.10}$					
	PC		$1.37^{+0.38}_{-0.35}$	$2.28^{+0.42}_{-0.99}$			
GRB 080129	PC	$0.94^{+0.23}_{-0.16}$	$1.16^{+0.30}_{-0.28}$				
GRB 080205	WT	$1.09^{+0.16}_{-0.15}$	$1.49^{+0.43}_{-0.36}$	$0.77^{+0.55}_{-0.29}$			
	PC			$0.66^{+0.27}_{-0.26}$	$0.856^{+0.074}_{-0.153}$		
GRB 080207	WT	$0.300^{+0.090}_{-0.089}$					
	PC		$1.52^{+0.11}_{-0.15}$				
GRB 080212	WT	$2.371^{+0.092}_{-0.090}$	$1.689^{+0.060}_{-0.058}$				
	PC		$1.089^{+0.176}_{-0.087}$	$1.485^{+0.075}_{-0.185}$			
GRB 080229A	WT	$1.932^{+0.095}_{-0.090}$	$1.34^{+0.74}_{-0.64}$				
	PC		$0.86^{+0.13}_{-0.12}$	$0.769^{+0.046}_{-0.045}$	$0.82^{+0.14}_{-0.27}$		
GRB 080303	WT	$0.94^{+0.20}_{-0.13}$					
	PC	$0.957^{+0.076}_{-0.087}$	$1.10^{+0.27}_{-0.30}$				
GRB 080307	WT	$0.386^{+0.083}_{-0.079}$	$0.528^{+0.080}_{-0.078}$				
	PC		$0.647^{+0.110}_{-0.091}$	$1.15^{+0.32}_{-0.60}$			
GRB 080310	WT	$0.514^{+0.020}_{-0.020}$					
	PC		$1.381^{+0.076}_{-0.071}$	$0.960^{+0.141}_{-0.094}$			
GRB 080319B	WT	$0.722^{+0.035}_{-0.034}$	$0.764^{+0.013}_{-0.013}$				
	PC		$0.793^{+0.079}_{-0.078}$	$0.827^{+0.105}_{-0.099}$	$0.922^{+0.087}_{-0.084}$	$0.84^{+0.32}_{-0.18}$	
GRB 080319C	PC	$0.68^{+0.26}_{-0.25}$	$0.573^{+0.044}_{-0.043}$	$1.08^{+0.31}_{-0.18}$			
GRB 080319D	WT	$-3.36^{+2.36}_{-0.63}$					
	PC	$0.90^{+0.12}_{-0.11}$	$2.5^{+1.1}_{-1.7}$				
GRB 080320	PC	$0.84^{+0.13}_{-0.13}$	$1.040^{+0.076}_{-0.085}$	$1.50^{+0.24}_{-0.14}$			
GRB 080325	WT	$1.338^{+0.043}_{-0.042}$					
	PC		$1.45^{+0.14}_{-0.26}$				
GRB 080328	WT	$1.16^{+0.12}_{-0.11}$	$1.30^{+0.19}_{-0.18}$				
	PC		$0.833^{+0.068}_{-0.066}$	$1.055^{+0.098}_{-0.094}$			
GRB 080330	WT	$1.19^{+0.20}_{-0.18}$					
	PC		$0.87^{+0.18}_{-0.14}$	$1.19^{+0.58}_{-0.48}$			
GRB 080409	PC	$0.7^{+4.4}_{-4.6}$	$0.62^{+0.13}_{-0.26}$				
GRB 080411	PC	$1.00^{+0.12}_{-0.12}$	$1.027^{+0.040}_{-0.023}$	$0.62^{+0.15}_{-0.18}$			
GRB 080413A	WT	$2.13^{+0.16}_{-0.16}$					
	PC	$1.52^{+0.45}_{-0.36}$	$1.09^{+0.22}_{-0.26}$				

GRB	Mode	$\beta_1$	$\beta_2$	$\beta_3$	$\beta_4$	$\beta_5$	$\beta_6$
GRB 080413B	WT	$1.03^{+0.10}_{-0.10}$					
	PC	$0.94^{+0.32}_{-0.30}$	$0.889^{+0.051}_{-0.050}$	$1.16^{+0.13}_{-0.17}$			
GRB 080426	PC	$0.63^{+0.40}_{-0.30}$	$1.23^{+0.18}_{-0.27}$				
GRB 080430	WT	$1.39^{+0.20}_{-0.17}$					
	PC	$0.64^{+0.23}_{-0.22}$	$1.109^{+0.094}_{-0.063}$	$1.11^{+0.11}_{-0.10}$			
GRB 080503	WT	$0.114^{+0.062}_{-0.062}$	$0.724^{+0.099}_{-0.095}$	$1.39^{+0.42}_{-0.37}$			
	PC			$1.21^{+0.17}_{-0.10}$			
GRB 080506	WT	$0.285^{+0.085}_{-0.084}$	$0.85^{+0.12}_{-0.12}$	$1.22^{+0.12}_{-0.11}$			
	PC			$0.881^{+0.179}_{-0.083}$	$1.28^{+0.23}_{-0.13}$		
GRB 080516	PC	$1.37^{+0.50}_{-0.46}$	$1.18^{+0.26}_{-0.32}$				
GRB 080517	WT	$1.22^{+1.03}_{-0.79}$					
	PC	$0.72^{+0.33}_{-0.29}$	$1.54^{+0.63}_{-0.67}$				
GRB 080523	WT	$1.52^{+0.11}_{-0.10}$	$1.479^{+0.166}_{-0.082}$				
	PC		$0.78^{+0.17}_{-0.16}$	$1.33^{+0.43}_{-0.43}$			
GRB 080602	WT	$0.60^{+0.36}_{-0.33}$	$1.25^{+0.44}_{-0.38}$				
	PC		$0.90^{+0.14}_{-0.13}$	$0.775^{+0.080}_{-0.077}$			
GRB 080603B	WT	$0.49^{+0.13}_{-0.13}$	$0.788^{+0.084}_{-0.081}$	$0.95^{+0.17}_{-0.16}$			
	PC			$0.89^{+0.19}_{-0.18}$			
GRB 080604	WT	$1.069^{+0.068}_{-0.063}$					
	PC	$0.63^{+0.11}_{-0.13}$	$1.13^{+0.56}_{-0.43}$				
GRB 080605	WT	$0.737^{+0.052}_{-0.051}$	$0.772^{+0.049}_{-0.048}$				
	PC		$0.69^{+0.18}_{-0.18}$	$1.32^{+0.20}_{-0.22}$			
GRB 080607	WT	$1.00^{+0.13}_{-0.13}$	$1.045^{+0.041}_{-0.040}$	$1.155^{+0.098}_{-0.094}$			
	PC			$0.950^{+0.066}_{-0.046}$	$1.21^{+0.55}_{-0.50}$		
GRB 080613B	WT	$0.172^{+0.081}_{-0.079}$	$1.66^{+1.50}_{-0.61}$				
	PC			$1.22^{+0.77}_{-0.57}$			
GRB 080625	PC	$1.31^{+0.11}_{-0.22}$	$1.65^{+0.62}_{-0.65}$				
GRB 080703	PC	$0.618^{+0.098}_{-0.073}$	$0.38^{+0.19}_{-0.23}$				
GRB 080707	WT	$1.29^{+0.77}_{-0.47}$	$3.7^{+4.2}_{-3.4}$				
	PC	$0.79^{+0.41}_{-0.34}$	$1.44^{+0.38}_{-0.36}$	$1.00^{+0.15}_{-0.21}$			
GRB 080710	PC	$0.969^{+0.113}_{-0.081}$	$1.23^{+0.16}_{-0.23}$				
GRB 080714	WT	$0.54^{+0.22}_{-0.14}$	$0.54^{+0.17}_{-0.11}$				
	PC		$0.73^{+0.53}_{-0.47}$	$0.762^{+0.099}_{-0.208}$			
GRB 080721	WT	$0.834^{+0.028}_{-0.028}$	$0.87^{+0.12}_{-0.11}$	$0.831^{+0.019}_{-0.019}$			
	PC				$1.04^{+0.52}_{-0.43}$		
GRB 080723A	PC	$1.40^{+0.59}_{-0.52}$	$1.15^{+0.30}_{-0.29}$	$1.11^{+0.12}_{-0.24}$	$1.013^{+0.048}_{-0.035}$		

GRB	Mode	$N_{H,1}$	$N_{H,2}$	$N_{H,3}$	$N_{H,4}$	$N_{H,5}$	$N_{H,6}$
GRB 050126	PC	< 10.43	$5.5^{+37.1}_{-5.5}$				
GRB 050128	WT		< 123.27				
	PC	$6.3^{+3.0}_{-2.9}$	$4.0^{+1.6}_{-1.7}$				
GRB 050219A	WT	$15.3^{+5.2}_{-4.8}$	$15.2^{+8.9}_{-7.5}$				
	PC		$29.9^{+28.2}_{-20.7}$				
GRB 050315	WT		$112.5^{+85.2}_{-65.7}$				
	PC	$35.8^{+18.9}_{-17.8}$	$79.1^{+19.7}_{-17.1}$	$100.0^{+19.9}_{-14.3}$			
GRB 050318	WT	$15.9^{+84.8}_{-15.9}$					
	PC	$11.5^{+10.0}_{-9.6}$	$16.8^{+12.8}_{-10.8}$				
GRB 050319	WT			$97.3^{+167.0}_{-97.3}$			
	PC	< 16.50	$18.5^{+28.0}_{-18.5}$	$33.6^{+41.7}_{-23.3}$			$(7.0^{+11.1}) \times 10^3$
GRB 050401	WT	$155.6^{+19.2}_{-18.3}$	$120.7^{+115.2}_{-94.6}$				
	PC	$141.4^{+91.1}_{-78.5}$	$236.2^{+209.0}_{-97.6}$				
GRB 050406	WT	< 3.29					
	PC	$18.1^{+121.6}_{-9.0}$	$(3.2^{+unconstr.}_{-unconstr.}) \times 10^4$				
GRB 050410	WT	$10.1^{+19.3}_{-10.1}$					
	PC	$15.2^{+39.7}_{-15.2}$	$63.8^{+unconstr.}_{-unconstr.}$				
GRB 050416A	PC	$12.9^{+13.6}_{-12.2}$	$56.1^{+18.7}_{-16.0}$	$76.0^{+10.2}_{-10.6}$			
GRB 050421	WT	$80.0^{+35.3}_{-27.0}$	$19.4^{+45.9}_{-19.4}$				
	PC		$47.5^{+6.1}_{-14.6}$				
GRB 050422	PC	< 10.13	< 19.43				
GRB 050502B	WT	$7.05^{+0.67}_{-0.66}$					
	PC	$0.68^{+1.78}_{-0.68}$	$11.4^{+11.0}_{-11.3}$				
GRB 050505	PC	$119.7^{+117.7}_{-107.1}$	$212.7^{+54.6}_{-51.0}$	$136.7^{+55.8}_{-67.2}$			
GRB 050525A	PC	$20.8^{+20.4}_{-17.0}$	$97.1^{+36.5}_{-22.9}$				
GRB 050607	PC	$10.0^{+3.9}_{-3.7}$	< 2.18	$3.9^{+8.1}_{-3.9}$			$14.5^{+6.3}_{-14.0}$
GRB 050712	WT	$8.2^{+3.2}_{-3.0}$					
	PC	$5.3^{+3.1}_{-2.0}$	$11.9^{+8.5}_{-11.9}$				
GRB 050713A	WT	$43.0^{+8.9}_{-8.1}$	$22.6^{+2.2}_{-2.1}$	$15.8^{+16.6}_{-14.2}$			$38.7^{+33.8}_{-23.8}$
	PC						$26.3^{+2.9}_{-5.0}$
GRB 050713B	PC	$18.4^{+10.4}_{-9.2}$	$26.6^{+8.1}_{-7.4}$	$19.2^{+4.1}_{-4.5}$			
GRB 050714B	WT	$77.9^{+12.6}_{-11.1}$					
	PC	$45.1^{+26.5}_{-18.7}$	$31.7^{+6.1}_{-6.7}$				
GRB 050716	WT	$8.8^{+4.0}_{-3.7}$	$2.0^{+2.1}_{-2.0}$				
	PC		$5.7^{+7.1}_{-5.7}$	$9.5^{+4.1}_{-2.4}$			
GRB 050717	WT	$19.7^{+5.4}_{-5.0}$	< 78.34				
	PC		$11.2^{+5.6}_{-5.1}$	$3.4^{+37.7}_{-3.4}$			
GRB 050721	WT	$11.2^{+5.2}_{-4.7}$					
	PC	$9.8^{+3.9}_{-3.7}$	$14.6^{+12.1}_{-9.5}$				
GRB 050724	WT	$51.1^{+4.8}_{-4.7}$	$43.6^{+6.8}_{-6.1}$				
	PC			$26.8^{+13.0}_{-15.1}$			
GRB 050726	WT	$4.7^{+2.6}_{-2.4}$					
	PC	$0.48^{+2.14}_{-0.48}$	$6.5^{+3.9}_{-5.4}$				
GRB 050730	WT	$52.7^{+22.6}_{-21.8}$	$275.2^{+640.1}_{-275.2}$				
	PC	< 45.59	$43.0^{+31.5}_{-24.0}$				
GRB 050801	PC	< 1.98	< 6.33				
GRB 050802	WT	$4.0^{+3.4}_{-3.1}$					
	PC	$3.0^{+2.4}_{-2.3}$	$5.77^{+0.95}_{-1.42}$				
GRB 050803	WT	$13.5^{+4.5}_{-4.2}$	$40.0^{+33.5}_{-24.0}$				
	PC	< 9.71	$12.9^{+2.4}_{-2.3}$	$30.3^{+5.2}_{-7.5}$			
GRB 050814	WT	$73.0^{+61.8}_{-58.9}$	$432.7^{+1457.4}_{-432.7}$				
	PC	< 17.69	$183.0^{+113.4}_{-119.6}$	$27.2^{+256.7}_{-27.2}$			
GRB 050815	PC	< 18.21	$11.0^{+14.8}_{-11.0}$				

**Table 10.** Column densities (in excess of the Galactic value) for the time-resolved spectra, in units of  $10^{20} \text{ cm}^{-2}$ .  $N_{H,1}$  corresponds to the time during which the decay followed  $\alpha_1$  in Table 6. Spectral indices for these spectra are given in Table 9.

GRB	Mode	$N_{H,1}$	$N_{H,2}$	$N_{H,3}$	$N_{H,4}$	$N_{H,5}$	$N_{H,6}$
GRB 050819	WT	< 4.12					
	PC	< 4.11	$14.0^{+10.1}_{-6.5}$				
GRB 050820A	WT	$2.7^{+3.7}_{-2.7}$	< 1.29				
	PC		$2.2^{+1.8}_{-1.7}$	$52.7^{+9.3}_{-12.1}$			
GRB 050822	WT	$13.0^{+1.4}_{-1.3}$	< 18.67	< 44.94			
	PC	$3.6^{+9.7}_{-3.6}$	$3.5^{+3.5}_{-1.6}$	$18.8^{+3.6}_{-1.7}$			
GRB 050824	PC	$3.3^{+6.8}_{-3.3}$	$40.5^{+13.6}_{-11.4}$				
GRB 050826	PC	$99.9^{+46.8}_{-39.1}$	$39.1^{+39.1}_{-22.9}$	$51.0^{+50.0}_{-45.3}$			
GRB 050904	WT	$298.0^{+90.1}_{-86.9}$					
	PC	< 70.58	$135.7^{+52.7}_{-82.6}$				
GRB050915B	WT	$9.5^{+4.7}_{-4.4}$	$455.2^{+1910}_{-398.3}$				
	PC	$7.0^{+22.0}_{-7.0}$	$20.5^{+10.4}_{-15.3}$				
GRB050916	PC	< 104.78	$26.0^{+25.8}_{-14.1}$				
GRB 050922B	WT	$13.4^{+1.6}_{-1.5}$					
	PC	$9.0^{+1.5}_{-1.4}$	$7.2^{+4.6}_{-6.8}$	$18.1^{+11.0}_{-7.6}$			
GRB 050922C	WT	$17.7^{+14.1}_{-13.7}$					
	PC	$2.7^{+24.2}_{-2.7}$	$49.5^{+18.3}_{-17.8}$				
GRB 051001	WT	$12.5^{+3.6}_{-3.4}$	$14.2^{+2.3}_{-2.2}$				
	PC		$16.4^{+11.7}_{-9.8}$	$20.5^{+8.5}_{-8.3}$			
GRB 051008	PC	$32.4^{+4.3}_{-3.9}$	$36.2^{+5.1}_{-8.0}$				
GRB 051016A	WT	$27.4^{+21.7}_{-17.9}$					
	PC	$50.5^{+37.9}_{-29.7}$	$37.4^{+10.6}_{-12.2}$				
GRB 051016B	WT	$85.0^{+32.9}_{-28.3}$					
	PC	< 27.07	$55.7^{+23.5}_{-20.6}$	$87.6^{+17.5}_{-27.4}$			
GRB 051021B	WT	< 31.12					
	PC	$0.75^{+33.63}_{-0.75}$	$24.3^{+65.7}_{-24.3}$				
GRB 051022	PC	$315.2^{+35.0}_{-33.5}$	$275.0^{+166.2}_{-70.1}$				
GRB 051109A	WT	$15.3^{+49.5}_{-15.3}$	$118.3^{+543.8}_{-118.3}$				
	PC		$158.0^{+70.0}_{-62.1}$	$74.0^{+27.2}_{-18.8}$			
GRB 051109B	PC	< 4.50	$27.4^{+15.1}_{-12.9}$	$16.0^{+10.6}_{-9.5}$			
GRB 051117A	WT	$10.07^{+0.40}_{-0.39}$	$9.3^{+39.9}_{-9.3}$				
	PC	$8.4^{+2.7}_{-2.6}$		$10.4^{+1.6}_{-4.0}$			
GRB 051221A	PC	$16.6^{+9.2}_{-4.4}$	$7.4^{+9.8}_{-6.4}$	$35.2^{+10.2}_{-9.5}$			
GRB 051227	WT	$17.7^{+8.2}_{-7.3}$					
	PC	$6.3^{+6.9}_{-6.1}$	$9.1^{+7.5}_{-5.4}$				
GRB 060105	WT	$19.4^{+2.0}_{-1.9}$	$18.1^{+1.2}_{-1.1}$				
	PC			$18.8^{+2.6}_{-2.5}$	$16.5^{+3.9}_{-6.6}$	$16.5^{+2.9}_{-6.5}$	
GRB 060108	WT		< 69.31				
	PC	< 26.61	$54.8^{+58.4}_{-54.8}$	$94.3^{+39.1}_{-49.1}$			
GRB 060109	WT	$17.5^{+4.9}_{-4.5}$					
	PC	$2.9^{+11.4}_{-2.9}$	$22.8^{+7.6}_{-6.9}$	$28.2^{+6.8}_{-8.4}$			
GRB 060111A	WT	$18.64^{+0.97}_{-0.95}$					
	PC	$15.0^{+8.1}_{-7.4}$	$15.9^{+5.5}_{-5.7}$				
GRB 060111B	WT	$11.6^{+5.6}_{-5.1}$	$20.1^{+16.3}_{-14.7}$				
	PC		$18.4^{+6.4}_{-5.6}$	$25.4^{+6.3}_{-16.4}$			
GRB 060115	WT	$135.9^{+59.2}_{-55.7}$					
	PC	< 28.41	$0.99^{+54.33}_{-0.99}$				
GRB 060124	PC	$193.3^{+573.1}_{-192.9}$	$66.2^{+18.2}_{-17.2}$	$90.0^{+16.0}_{-15.5}$			
GRB 060202	WT	$43.1^{+1.9}_{-1.9}$	$38.4^{+1.8}_{-1.7}$	$37.1^{+3.6}_{-3.4}$			
	PC			$37.6^{+7.3}_{-6.7}$	$49.5^{+2.0}_{-4.5}$		
GRB 060204B	WT	$19.5^{+2.2}_{-2.2}$	$24.4^{+4.0}_{-3.8}$				
	PC	$12.9^{+8.2}_{-7.3}$	$10.0^{+3.4}_{-3.2}$	$20.7^{+5.5}_{-7.1}$			
GRB 060206	WT	< 265.06					
	PC	$20.5^{+11.6}_{-20.5}$	$49.2^{+56.1}_{-49.2}$				
GRB 060210	WT	$227.3^{+24.6}_{-24.0}$	$66.4^{+1909.0}_{-66.4}$				
	PC	$195.0^{+43.6}_{-41.0}$	$164.9^{+44.7}_{-44.3}$				
GRB 060211A	WT	$7.4^{+1.9}_{-1.8}$					
	PC	$1.9^{+12.0}_{-1.9}$	< 5.82	$20.4^{+9.1}_{-8.1}$			

GRB	Mode	$N_{H,1}$	$N_{H,2}$	$N_{H,3}$	$N_{H,4}$	$N_{H,5}$	$N_{H,6}$
GRB 060211B	WT	$2.0^{+17.6}_{-2.0}$					
	PC	$2.6^{+10.8}_{-2.6}$	$8.3^{+29.2}_{-8.3}$				
GRB 060218	WT	$26.34^{+0.44}_{-0.44}$					
	PC	$22.1^{+5.4}_{-5.0}$	$62.0^{+15.0}_{-7.4}$				
GRB 060219	PC	$14.6^{+19.3}_{-14.3}$	$39.8^{+12.2}_{-11.5}$	$34.6^{+15.7}_{-9.5}$			
GRB 060223A	WT		$605.4^{+1022.8}_{-506.2}$				
	PC	$56.1^{+313.1}_{-56.1}$	$319.2^{+284.3}_{-244.8}$				
GRB 060306	WT	$38.3^{+11.0}_{-9.8}$	$9.3^{+110.8}_{-9.3}$				
	PC	$9.2^{+23.4}_{-9.2}$	$35.3^{+6.6}_{-6.1}$	$37.7^{+4.2}_{-6.5}$			
GRB 060312	WT	$10.2^{+2.5}_{-2.4}$					
	PC	$< 2.55$	$1.9^{+2.6}_{-1.9}$				
GRB 060313	WT	$< 7.84$	$< 20.30$				
	PC	$0.52^{+9.34}_{-0.52}$	$< 5.61$	$< 1.27$	$5.4^{+2.4}_{-5.3}$		
GRB 060319	PC	$41.4^{+4.8}_{-4.3}$	$51.0^{+7.3}_{-10.4}$				
GRB 060403	WT	$19.2^{+15.9}_{-14.1}$					
	PC	$< 26.92$	$28.0^{+63.2}_{-28.0}$				
GRB 060413	WT	$126.9^{+16.0}_{-15.6}$					
	PC	$43.0^{+24.1}_{-22.0}$	$87.3^{+21.1}_{-20.2}$	$162.2^{+44.7}_{-37.5}$			
GRB 060418	WT	$61.6^{+6.7}_{-6.3}$	$42.8^{+15.9}_{-14.8}$	$2.8^{+59.3}_{-2.8}$			
	PC		$40.7^{+19.2}_{-17.7}$	$149.4^{+92.8}_{-95.3}$			
GRB 060427	WT	$10.4^{+3.0}_{-2.8}$					
	PC	$3.8^{+6.1}_{-3.8}$	$12.3^{+3.1}_{-1.5}$				
GRB 060428A	WT	$< 15.50$					
	PC	$35.5^{+142.8}_{-35.5}$	$16.8^{+11.7}_{-11.0}$	$0.013^{+10.099}_{-0.013}$	$70.3^{+32.1}_{-70.3}$		
GRB 060428B	WT	$6.5^{+1.5}_{-1.4}$					
	PC	$< 6.52$	$1.5^{+1.6}_{-1.5}$				
GRB 060502A	WT	$53.8^{+16.8}_{-15.3}$					
	PC	$< 6.72$	$41.9^{+17.9}_{-16.4}$	$39.0^{+14.2}_{-20.6}$			
GRB 060507	WT		$101.2^{+447.8}_{-101.2}$				
	PC	$< 6.06$	$7.5^{+3.3}_{-4.7}$				
GRB 060510A	WT	$< 4.31$					
	PC		$< 0.76$	$1.6^{+3.6}_{-1.6}$			
GRB 060510B	WT	$393.0^{+48.1}_{-47.3}$	$272.6^{+86.2}_{-82.1}$				
	PC		$122.3^{+219.2}_{-122.3}$	$240.6^{+166.7}_{-84.6}$			
GRB 060512	WT	$30.2^{+17.6}_{-15.1}$					
	PC	$2.3^{+9.1}_{-2.3}$	$< 3.55$				
GRB 060522	WT	$120.4^{+288.3}_{-120.4}$					
	PC	$< 187.92$	$96.9^{+202.5}_{-96.9}$	$944.0^{+2022.1}_{-434.9}$			
GRB 060526	WT	$55.0^{+15.4}_{-14.8}$					
	PC	$< 38.97$	$< 42.72$	$92.2^{+80.5}_{-92.2}$	$0.055^{+137.888}_{-0.055}$		
GRB 060604	WT	$159.1^{+18.0}_{-17.0}$					
	PC		$20.0^{+42.0}_{-20.0}$	$149.4^{+59.9}_{-96.6}$			
GRB 060605	WT	$< 183.29$					
	PC	$< 44.44$	$44.8^{+72.0}_{-44.8}$	$112.7^{+58.9}_{-58.6}$			
GRB 060607A	WT	$28.5^{+12.3}_{-11.8}$	$< 82.41$	$101.5^{+439.6}_{-101.5}$			
	PC		$4.9^{+16.0}_{-4.9}$	$59.0^{+26.7}_{-17.2}$			
GRB 060614	WT	$4.0^{+1.4}_{-1.4}$	$5.80^{+0.71}_{-0.69}$	$< 1.26$			
	PC			$< 1.56$	$6.5^{+3.1}_{-3.1}$		
GRB 060707	WT	$< 56.85$					
	PC	$< 46.13$	$52.0^{+84.3}_{-44.2}$	$209.3^{+370.5}_{-102.9}$			
GRB 060708	WT	$11.8^{+2.8}_{-2.6}$					
	PC		$2.7^{+2.7}_{-2.3}$	$5.2^{+3.2}_{-4.9}$			
GRB 060712	PC	$10.2^{+8.4}_{-7.0}$	$15.7^{+14.8}_{-10.7}$	$15.6^{+7.0}_{-6.7}$			
GRB 060714	WT	$136.9^{+19.8}_{-18.8}$					
	PC	$33.0^{+111.0}_{-33.0}$	$91.7^{+51.6}_{-47.4}$	$301.0^{+107.1}_{-117.5}$			
GRB 060719	WT	$26.2^{+6.7}_{-5.9}$					
	PC	$21.6^{+19.3}_{-15.6}$	$45.0^{+8.0}_{-7.4}$	$45.5^{+6.5}_{-11.6}$			

GRB	Mode	$N_{H,1}$	$N_{H,2}$	$N_{H,3}$	$N_{H,4}$	$N_{H,5}$	$N_{H,6}$
GRB 060729	WT	$40.1^{+4.0}_{-3.7}$	$18.8^{+3.7}_{-3.4}$				
	PC		< 3.76	$12.8^{+2.0}_{-1.9}$	$13.0^{+1.3}_{-1.6}$	$16.7^{+5.8}_{-8.2}$	
GRB 060801	PC	$48.0^{+42.0}_{-33.3}$	$7.8^{+22.0}_{-7.8}$	$(1.28^{+2.97}_{-0.64}) \times 10^3$			
GRB 060804	PC	< 7.21	$8.2^{+9.5}_{-8.2}$				
GRB 060805A	PC	$5.1^{+7.5}_{-2.9}$	$4.1^{+9.8}_{-4.1}$				
GRB 060807	PC	$1.6^{+10.9}_{-1.6}$	$10.9^{+5.4}_{-4.9}$	$13.3^{+2.9}_{-2.6}$	$17.0^{+8.0}_{-11.9}$		
GRB 060813	WT	$8.6^{+3.4}_{-3.3}$					
	PC		$5.8^{+3.6}_{-3.4}$	$13.8^{+14.8}_{-13.8}$			
GRB 060814	WT	$39.6^{+8.2}_{-7.5}$	$25.7^{+1.4}_{-1.4}$	$19.2^{+3.4}_{-3.3}$			
	PC			$22.4^{+6.9}_{-6.3}$	$30.8^{+3.1}_{-3.0}$	$29.3^{+3.0}_{-3.7}$	
GRB 060904A	WT	$17.8^{+1.6}_{-1.5}$	$18.1^{+2.5}_{-2.3}$				
	PC			$19.6^{+12.0}_{-9.5}$			
GRB 060904B	WT	$46.9^{+3.9}_{-3.7}$					
	PC	$31.8^{+22.0}_{-17.4}$	$49.6^{+13.9}_{-13.0}$				
GRB 060906	WT	$166.2^{+408.2}_{-166.2}$	$325.1^{+728.8}_{-270.9}$				
	PC		$312.6^{+189.8}_{-171.0}$	$263.8^{+212.5}_{-186.1}$			
GRB 060908	WT	$43.9^{+40.1}_{-36.9}$	$169.9^{+226.9}_{-165.3}$				
	PC	$92.7^{+72.1}_{-62.8}$	$60.7^{+37.2}_{-48.1}$				
GRB 060912A	PC	$20.0^{+11.8}_{-10.9}$	$40.5^{+8.1}_{-14.2}$				
GRB 060923A	WT	$10.8^{+8.9}_{-7.5}$	$3.7^{+27.7}_{-3.7}$	$10.8^{+8.9}_{-7.4}$			
	PC	$14.2^{+14.8}_{-11.2}$	< 9.31	$32.4^{+8.8}_{-14.0}$			
GRB 060923C	WT	$0.78^{+4.40}_{-0.78}$					
	PC	< 1.68	$27.8^{+11.9}_{-10.1}$	$5.7^{+13.8}_{-5.7}$			
GRB 060926	WT	$0.11^{+294.31}_{-0.11}$	$246.7^{+205.7}_{-155.3}$				
	PC			$453.6^{+274.2}_{-254.6}$			
GRB 060927	PC	$52.5^{+320.0}_{-52.5}$	$176.5^{+518.5}_{-176.5}$				
GRB 060929	WT		$12.1^{+1.4}_{-1.4}$				
	PC	$16.2^{+16.2}_{-12.4}$	$11.2^{+4.4}_{-3.6}$				
GRB 061002	WT	$16.2^{+9.4}_{-8.5}$	$8.7^{+17.1}_{-8.7}$				
	PC		$20.2^{+16.0}_{-14.8}$				
GRB 061004	WT	< 11.41					
	PC	< 6.83	$6.3^{+6.7}_{-5.9}$	$5.7^{+7.5}_{-5.7}$			
GRB 061007	WT	$44.8^{+7.2}_{-6.9}$	$45.0^{+2.8}_{-2.7}$				
	PC		$71.4^{+45.1}_{-36.8}$	$57.2^{+19.3}_{-17.3}$	$64.0^{+15.1}_{-8.6}$		
GRB 061019	PC	$67.6^{+11.0}_{-11.5}$	$76.5^{+55.5}_{-34.2}$				
GRB 061021	WT	< 0.20					
	PC	< 4.93	$5.4^{+2.3}_{-2.1}$	$6.0^{+1.0}_{-1.3}$			
GRB 061028	WT	$10.0^{+6.3}_{-5.7}$					
	PC	< 3.28	$114.5^{+22.2}_{-17.7}$				
GRB 061102	WT	$8.6^{+5.4}_{-4.7}$					
	PC		< 10.28				
GRB 061110A	WT	$16.2^{+1.6}_{-1.5}$	$5.9^{+1.8}_{-1.7}$				
	PC		< 1.20	< 0.49	$9.0^{+8.3}_{-9.0}$		
GRB 061121	WT	$83.2^{+26.0}_{-22.8}$	$70.4^{+12.3}_{-11.5}$	$40.5^{+14.6}_{-13.5}$	$60.5^{+11.3}_{-10.6}$	$102.1^{+56.9}_{-47.2}$	
	PC				$37.8^{+22.6}_{-20.1}$	$55.2^{+10.9}_{-10.3}$	$66.1^{+13.5}_{-18.7}$
GRB 061126	WT	$9.5^{+4.6}_{-4.2}$					
	PC	$14.5^{+2.6}_{-2.4}$	$12.0^{+3.3}_{-4.7}$				
GRB 061201	WT	< 19.16	< 71.80				
	PC	$1.7^{+3.2}_{-1.7}$	$13.2^{+16.0}_{-9.9}$				
GRB 061202	WT	$45.3^{+4.7}_{-4.5}$					
	PC	$52.7^{+11.4}_{-10.3}$	$47.7^{+8.0}_{-7.4}$	$48.9^{+5.6}_{-7.4}$			
GRB 061222A	WT	$32.6^{+3.0}_{-2.9}$	$27.9^{+14.3}_{-11.9}$	$18.7^{+30.2}_{-18.7}$			
	PC		$27.3^{+2.9}_{-2.8}$	$25.9^{+3.1}_{-2.9}$	$36.0^{+3.3}_{-5.0}$		
GRB 070103	WT		$40.6^{+55.5}_{-27.9}$				
	PC	$30.1^{+13.9}_{-12.1}$	$23.0^{+16.4}_{-13.2}$	$26.3^{+8.2}_{-8.4}$			
GRB 070107	WT	$3.5^{+2.3}_{-2.2}$					
	PC	$5.7^{+3.8}_{-3.6}$	$9.8^{+2.1}_{-5.5}$				

GRB	Mode	$N_{H,1}$	$N_{H,2}$	$N_{H,3}$	$N_{H,4}$	$N_{H,5}$	$N_{H,6}$
GRB 070110	WT	$10.6^{+17.4}_{-10.6}$	< 9.18				
	PC	< 12.20	< 11.15	$13.8^{+14.1}_{-13.3}$	$7.8^{+32.2}_{-7.8}$	$17.3^{+24.0}_{-14.3}$	
GRB 070125	PC	$5.8^{+2.8}_{-4.9}$	$3.5^{+3.6}_{-3.5}$				
GRB 070129	WT	$11.66^{+0.77}_{-0.76}$					
	PC	< 2.31	$16.3^{+6.9}_{-6.4}$	$14.2^{+1.9}_{-4.0}$	$11.5^{+12.5}_{-11.5}$		
GRB 070208	PC	$48.9^{+40.2}_{-24.5}$	$66.1^{+36.3}_{-30.9}$	$89.6^{+38.0}_{-43.9}$			
GRB 070219	WT	$23.6^{+110.6}_{-23.6}$					
	PC	$8.2^{+21.2}_{-8.2}$	$19.3^{+40.1}_{-19.3}$	$48.8^{+22.2}_{-18.7}$			
GRB 070220	WT	$11.7^{+6.1}_{-5.7}$	$8.5^{+7.3}_{-6.7}$				
	PC			$15.8^{+5.2}_{-4.9}$	$13.1^{+7.7}_{-8.4}$		
GRB 070223	WT	$55.5^{+9.8}_{-8.8}$	$49.7^{+7.7}_{-7.1}$				
	PC			$57.4^{+14.3}_{-19.2}$			
GRB 070224	WT	< 2.16					
	PC	< 1.60	$3.2^{+6.6}_{-3.2}$				
GRB 070306	WT	$40.8^{+3.7}_{-3.6}$	$37.4^{+3.1}_{-3.0}$				
	PC		$34.1^{+20.8}_{-18.1}$	$31.6^{+4.0}_{-3.8}$	$38.1^{+7.6}_{-4.1}$	$32.9^{+5.1}_{-3.8}$	
GRB 070311	PC	$19.9^{+10.0}_{-11.0}$	$11.5^{+11.8}_{-11.5}$	$18.5^{+26.9}_{-18.5}$			
GRB 070328	WT	$16.8^{+2.2}_{-2.1}$	$19.0^{+1.4}_{-1.4}$	$21.2^{+1.7}_{-1.7}$			
	PC			$32.4^{+21.2}_{-17.5}$	$21.7^{+1.2}_{-1.8}$		
GRB 070412	WT	$12.9^{+9.2}_{-7.4}$					
GRB 070419A	PC		$10.5^{+8.3}_{-7.6}$	$21.6^{+9.7}_{-10.9}$			
	WT		$22.2^{+8.2}_{-7.8}$				
GRB 070419B	PC		$26.7^{+14.1}_{-12.9}$	$23.5^{+24.1}_{-23.5}$			
	WT	$12.30^{+0.88}_{-0.86}$					
GRB 070420	PC	$5.7^{+1.3}_{-1.3}$	$8.4^{+5.5}_{-5.6}$				
	WT	$3.5^{+3.4}_{-3.3}$	< 40.65				
GRB 070429A	PC		$5.5^{+3.3}_{-3.2}$	$9.2^{+5.4}_{-5.1}$	$10.1^{+9.1}_{-9.2}$	$18.1^{+10.8}_{-16.7}$	
	WT	$41.9^{+5.3}_{-4.9}$	$17.4^{+10.9}_{-7.9}$				
GRB 070508	PC		$2.2^{+10.0}_{-2.2}$	$19.6^{+7.7}_{-8.5}$	$3.2^{+22.4}_{-3.2}$		
	WT	$24.7^{+1.8}_{-1.8}$	$27.2^{+2.5}_{-2.5}$				
GRB 070517	PC	$4.3^{+5.2}_{-2.4}$	$26.1^{+6.0}_{-5.6}$	$29.2^{+6.6}_{-5.7}$			
	WT	$7.3^{+1.9}_{-1.8}$	$2.2^{+11.2}_{-2.2}$				
GRB 070518	PC	< 3.49	$24.5^{+8.0}_{-16.3}$				
	WT	$20.3^{+3.6}_{-3.4}$					
GRB 070520A	PC		$33.7^{+9.0}_{-8.5}$				
	WT	$19.4^{+1.5}_{-1.4}$					
GRB 070520B	PC	$12.0^{+17.3}_{-12.0}$	$37.8^{+19.2}_{-20.2}$				
	WT	$56.7^{+79.4}_{-39.7}$					
GRB 070521	PC	$77.5^{+32.4}_{-26.2}$	$56.2^{+7.7}_{-7.1}$	$63.8^{+9.5}_{-5.2}$			
	WT	$481.5^{+484.3}_{-314.3}$					
GRB 070529	PC	< 409.06	$99.0^{+69.8}_{-62.0}$	$601.1^{+349.8}_{-244.7}$			
	WT	$6.8^{+1.6}_{-1.6}$	$3.2^{+1.8}_{-1.8}$				
GRB 070616	PC		$18.4^{+12.7}_{-11.1}$	$9.8^{+4.8}_{-7.6}$			
	WT	$35.0^{+3.0}_{-2.9}$					
GRB 070621	PC	$35.4^{+12.7}_{-11.1}$	$38.9^{+8.3}_{-7.6}$	$40.4^{+8.8}_{-14.9}$			
	WT	$40.5^{+73.8}_{-40.5}$					
GRB 070628	PC	$6.4^{+9.3}_{-6.4}$	$12.1^{+3.2}_{-5.7}$				
	WT	$33.8^{+5.9}_{-5.7}$					
GRB 070704	PC	< 75.75	$80.7^{+35.6}_{-40.6}$				
	WT	$26.2^{+15.1}_{-12.6}$	$41.8^{+29.1}_{-20.1}$	$24.3^{+21.0}_{-18.5}$	$31.1^{+16.3}_{-19.5}$		
GRB 070714B	PC		$46.4^{+17.3}_{-15.2}$				
	WT	$4.5^{+10.7}_{-4.5}$					
GRB 070721A	PC	< 2.65	$25.0^{+8.5}_{-17.7}$				
	WT	$2.5^{+3.3}_{-2.5}$	$1.0^{+2.5}_{-1.0}$				
GRB 070721B	PC		< 2.09	$20.5^{+8.7}_{-8.6}$			
	WT	$19.0^{+6.2}_{-5.7}$					
GRB 070724A	PC	$25.5^{+10.1}_{-8.9}$	$56.3^{+20.7}_{-25.8}$				

GRB	Mode	$N_{H,1}$	$N_{H,2}$	$N_{H,3}$	$N_{H,4}$	$N_{H,5}$	$N_{H,6}$
GRB 070802	PC	< 33.71	$161.6^{+150.9}_{-116.6}$	$162.5^{+351.7}_{-81.5}$			
GRB 070808	WT	$79.7^{+53.2}_{-39.6}$					
	PC	$57.8^{+38.9}_{-29.4}$	$95.0^{+24.5}_{-22.2}$				
GRB 070810A	PC	$49.5^{+72.6}_{-49.5}$	$74.0^{+32.9}_{-35.3}$				
GRB 071001	WT	< 5.06					
	PC	< 3.07	< 30.90				
GRB 071010A	PC	$44.6^{+14.0}_{-12.9}$	$48.4^{+13.2}_{-30.1}$				
GRB 071011	PC	$49.8^{+26.8}_{-15.5}$	$21.5^{+57.0}_{-21.5}$				
GRB 071020	WT	$7.2^{+2.6}_{-2.5}$	$0.65^{+2.26}_{-0.65}$				
	PC		$5.6^{+1.0}_{-1.3}$				
GRB 071021	WT	$14.4^{+2.3}_{-2.2}$	$12.4^{+22.3}_{-12.4}$				
	PC		$15.4^{+2.8}_{-3.3}$				
GRB 071025	WT	$6.0^{+2.2}_{-2.1}$	$3.6^{+1.7}_{-1.6}$	$7.5^{+3.4}_{-3.1}$			
	PC			$0.34^{+29.63}_{-0.34}$	$9.2^{+1.3}_{-1.2}$		
GRB 071028A	WT	$4.1^{+4.9}_{-4.1}$					
	PC	$1.4^{+6.0}_{-1.4}$	< 4.29	< 11.74			
GRB 071031	WT	$88.8^{+8.9}_{-8.7}$					
	PC	$0.093^{+52.872}_{-0.093}$	$48.5^{+53.9}_{-41.0}$	$128.3^{+237.9}_{-128.3}$			
GRB 071112C	WT	$10.0^{+5.4}_{-5.2}$	< 4.25				
	PC		$1.6^{+12.0}_{-1.6}$	$24.0^{+16.6}_{-15.8}$			
GRB 071118	WT	$19.5^{+5.5}_{-5.2}$					
	PC	$19.8^{+12.9}_{-11.0}$	$13.9^{+2.7}_{-2.6}$	$20.9^{+6.9}_{-10.1}$			
GRB 071227	WT	$12.9^{+4.2}_{-3.9}$					
	PC		$4.6^{+6.7}_{-4.6}$	$36.4^{+607.5}_{-15.6}$			
GRB 080123	WT	$7.9^{+2.6}_{-2.5}$					
	PC		$7.1^{+7.1}_{-6.1}$	$30.9^{+20.7}_{-24.8}$			
GRB 080129	PC	$1.8^{+15.1}_{-1.8}$	$24.5^{+14.8}_{-12.7}$				
GRB 080205	WT	$14.6^{+4.2}_{-3.9}$	$6.6^{+7.8}_{-6.6}$	< 11.28			
	PC			$5.7^{+7.9}_{-5.7}$	$12.4^{+3.6}_{-4.5}$		
GRB 080207	WT	$88.2^{+9.4}_{-8.8}$					
	PC		$69.7^{+8.6}_{-7.6}$				
GRB 080212	WT	$31.9^{+2.1}_{-2.0}$	$16.6^{+1.3}_{-1.3}$				
	PC		$8.3^{+4.4}_{-4.1}$	$18.3^{+3.3}_{-4.9}$			
GRB 080229A	WT	$22.1^{+2.1}_{-2.0}$	$15.8^{+19.3}_{-15.5}$				
	PC		$16.4^{+4.4}_{-4.2}$	$16.3^{+1.7}_{-1.6}$	$12.8^{+8.7}_{-8.2}$		
GRB 080303	WT	$1.1^{+5.2}_{-1.1}$					
	PC	< 1.92	$11.6^{+8.1}_{-11.6}$				
GRB 080307	WT	$2.2^{+2.0}_{-1.8}$	$2.1^{+1.8}_{-1.7}$				
	PC		$6.4^{+2.7}_{-2.5}$	$7.4^{+6.6}_{-7.4}$			
GRB 080310	WT	$47.3^{+6.4}_{-6.2}$					
	PC		< 3.27	$46.7^{+25.6}_{-38.3}$			
GRB 080319B	WT	$5.8^{+2.2}_{-2.1}$	$12.73^{+0.85}_{-0.85}$				
	PC		$9.5^{+5.2}_{-4.9}$	$9.6^{+6.7}_{-6.3}$	$13.6^{+5.2}_{-7.8}$	< 7.88	
GRB 080319C	PC	$50.9^{+59.9}_{-50.2}$	$73.5^{+11.8}_{-11.2}$	$74.0^{+41.5}_{-53.0}$			
GRB 080319D	WT	$(7.4^{+23.4}_{-4.0}) \times 10^3$					
	PC	$6.5^{+4.2}_{-4.0}$	$41.4^{+35.1}_{-39.7}$				
GRB 080320	PC	$3.2^{+2.7}_{-2.5}$	$4.5^{+1.7}_{-1.4}$	$13.8^{+2.0}_{-5.7}$			
GRB 080325	WT	$26.0^{+1.3}_{-1.2}$					
	PC		$24.3^{+8.0}_{-8.7}$				
GRB 080328	WT	$11.7^{+4.7}_{-4.4}$	$12.6^{+7.6}_{-7.0}$				
	PC		$7.3^{+3.1}_{-3.0}$	$11.0^{+4.4}_{-4.1}$			
GRB 080330	WT	$3.7^{+3.3}_{-3.0}$					
	PC		$1.5^{+3.4}_{-1.5}$	$9.0^{+12.9}_{-9.0}$			
GRB 080409	PC	< 98.04	$14.1^{+13.8}_{-12.3}$				
GRB 080411	PC	$42.2^{+12.9}_{-12.0}$	$46.8^{+4.5}_{-2.5}$	$31.6^{+11.9}_{-24.9}$			
GRB 080413A	WT	$163.5^{+38.5}_{-36.0}$					
	PC	< 62.49	$121.5^{+95.5}_{-105.5}$				

GRB	Mode	$N_{H,1}$	$N_{H,2}$	$N_{H,3}$	$N_{H,4}$	$N_{H,5}$	$N_{H,6}$
GRB 080413B	WT	$27.7^{+9.2}_{-8.6}$					
	PC	$21.4^{+27.8}_{-21.4}$	$23.4^{+4.6}_{-4.5}$	$38.2^{+15.0}_{-19.5}$			
GRB 080426	PC	< 15.79	$21.4^{+5.2}_{-12.5}$				
GRB 080430	WT	$13.4^{+6.9}_{-6.3}$					
	PC	$7.9^{+13.6}_{-7.9}$	$36.1^{+6.4}_{-3.3}$	$43.5^{+7.8}_{-9.5}$			
GRB 080503	WT	$2.5^{+2.0}_{-1.9}$	$8.6^{+2.8}_{-2.6}$	$11.5^{+8.9}_{-7.5}$			
	PC			< 1.09			
GRB 080506	WT	$5.0^{+3.7}_{-3.5}$	$4.6^{+3.7}_{-3.5}$	$2.6^{+2.8}_{-2.6}$			
	PC			$0.098^{+5.072}_{-0.098}$	< 2.68		
GRB 080516	PC	$71.4^{+37.3}_{-30.9}$	$51.9^{+24.3}_{-12.5}$				
GRB 080517	WT	$17.0^{+28.0}_{-17.0}$					
	PC	$9.8^{+10.4}_{-8.9}$	$40.1^{+22.6}_{-21.6}$				
GRB 080523	WT	$9.0^{+1.8}_{-1.7}$	< 2.13				
	PC		< 1.51	$7.1^{+9.5}_{-7.1}$			
GRB 080602	WT	$11.0^{+10.2}_{-8.5}$	$13.2^{+10.3}_{-7.9}$				
	PC		$9.2^{+3.4}_{-3.2}$	$12.5^{+2.3}_{-2.2}$			
GRB 080603B	WT	$144.6^{+70.4}_{-57.8}$	$79.0^{+25.3}_{-24.2}$	$116.8^{+56.7}_{-49.8}$			
	PC			$85.2^{+66.7}_{-57.4}$			
GRB 080604	WT	< 2.62					
	PC	$6.6^{+14.6}_{-6.6}$	$0.21^{+36.53}_{-0.21}$				
GRB 080605	WT	$51.2^{+10.3}_{-9.8}$	$82.4^{+11.7}_{-11.2}$				
	PC		$49.7^{+40.2}_{-34.7}$	$474.2^{+283.1}_{-156.4}$			
GRB 080607	WT	$558.9^{+115.1}_{-103.0}$	$369.1^{+26.2}_{-24.7}$	$345.2^{+53.7}_{-50.5}$			
	PC			$258.9^{+38.6}_{-22.5}$	$99.0^{+206.4}_{-99.0}$		
GRB 080613B	WT	$2.8^{+2.4}_{-2.2}$	< 18.28				
	PC			$9.8^{+16.0}_{-9.8}$			
GRB 080625	PC	$10.2^{+5.0}_{-5.9}$	$44.4^{+53.9}_{-15.4}$				
GRB 080703	PC	$0.93^{+2.39}_{-0.93}$	$3.4^{+9.5}_{-3.4}$				
GRB 080707	WT	$13.8^{+51.7}_{-13.8}$	$101.1^{+1444.1}_{-101.1}$				
	PC	< 32.12	$54.0^{+46.5}_{-36.7}$	$39.3^{+28.0}_{-24.4}$			
GRB 080710	PC	$7.4^{+6.9}_{-3.5}$	$28.5^{+14.4}_{-17.3}$				
GRB 080714	WT	< 11.72	< 6.55				
	PC		$30.1^{+49.2}_{-30.1}$	$20.0^{+16.5}_{-16.3}$			
GRB 080721	WT	$51.3^{+9.5}_{-9.3}$	$28.4^{+35.5}_{-28.4}$	$75.2^{+7.4}_{-7.3}$	$141.5^{+196.2}_{-141.5}$		
	PC				$99.7^{+14.1}_{-16.5}$		
GRB 080723A	PC	$48.5^{+42.5}_{-32.2}$	$55.7^{+24.3}_{-20.9}$	$68.2^{+12.3}_{-13.6}$			

Type of burst	Bursts
No breaks	050408, 050520, 051021A, 051028, 051211B, 060121, 060123, 060805B, 060901, 060928 061025, 061122, 070309, 070724B, 070925, 071104, 080120, 080229B, 080405, 080507 080514B, 080603A, 080613A, 080723B, 041223, 050124, 050215B, 050219B, 050223, 050326 050412, 050509A, 050603, 050701, 050827, <b>050908</b> , <b>050915A</b> , 051006, 051111 051117B, 051210, 051221B, 060110, <b>060116</b> , 060203, 060323, 060421, 060505, 060515 060602A, 060602B, 060717, 060825, 060919, 060923B, 061006, 061110B, 061210, <b>061222B</b> 070227, <b>070318</b> , <b>070330</b> , 070411, 070506, 070509, 070531, 070611, 070612B, 070714A 070809, 070911, 070917, 071003, 071010B, 071028B, 071101, 071117, 071122, <b>080210</b> 080218B, 080319A, 080515, 080520, 080623, 080701, 080702A
One break	051022, 070125, 080625, 050126, 050128, 050219A, 050318, <b>050401</b> , 050406, 050410 050421, 050422, <b>050502B</b> , <b>050525A</b> , <b>050712</b> , <b>050714B</b> , <b>050721</b> , <b>050726</b> , <b>050730</b> , <b>050801</b> 050802, 050815, <b>050819</b> , 050824, <b>050904</b> , <b>050915B</b> , 050916, <b>050922C</b> , 051008, <b>051016A</b> 051021B, <b>051227</b> , <b>060111A</b> , <b>060115</b> , <b>060206</b> , <b>060210</b> , 060211B, <b>060218</b> , 060223A, <b>060312</b> <b>060319</b> , <b>060403</b> , <b>060427</b> , 060428B, 060507, <b>060512</b> , <b>060804</b> , 060805A, <b>060904B</b> , <b>060908</b> <b>060912A</b> , 060927, <b>060929</b> , 061002, 061019, 061028, 061102, 061126, <b>061201</b> , <b>070107</b> <b>070224</b> , <b>070419B</b> , <b>070517</b> , <b>070518</b> , <b>070520A</b> , 070520B, <b>070628</b> , <b>070704</b> , 070721A, <b>070724A</b> <b>070808</b> , 070810A, 071001, 071010A, 071011, <b>071020</b> , <b>071021</b> , 080129, <b>080207</b> , <b>080303</b> <b>080319D</b> , <b>080325</b> , 080409, 080413A, 080426, 080516, 080517, <b>080604</b> , <b>080703</b> , 080710
Canonical	070311, <b>050315</b> , 050319, <b>050416A</b> , <b>050607</b> , <b>050713A</b> , <b>050713B</b> , <b>050803</b> , <b>050814</b> , <b>050820A</b> <b>050822</b> , 050922B, <b>051016B</b> , <b>051109A</b> , <b>051109B</b> , <b>051221A</b> , <b>060105</b> , <b>060108</b> , <b>060109</b> , <b>060204B</b> <b>050826</b> <b>060219</b> , <b>060313</b> , <b>060413</b> , <b>060418</b> , <b>060428A</b> , <b>060502A</b> , <b>060510A</b> , <b>060526</b> , <b>060604</b> , <b>060605</b> <b>060607A</b> , <b>060614</b> , <b>060707</b> , <b>060708</b> , <b>060712</b> , <b>060714</b> , <b>060719</b> , <b>060729</b> , <b>060807</b> , <b>060814</b> <b>060904A</b> , <b>060906</b> , <b>060923A</b> , 060923C, <b>060926</b> , <b>061004</b> , <b>061021</b> , <b>061121</b> , <b>061202</b> , <b>061222A</b> <b>070129</b> , 070219, <b>070220</b> , <b>070306</b> , <b>070328</b> , <b>070420</b> , <b>070429A</b> , <b>070529</b> , <b>070714B</b> , <b>070721B</b> 070802, <b>071028A</b> , <b>071112C</b> , <b>071118</b> , <b>080205</b> , <b>080212</b> , <b>080229A</b> , <b>080310</b> , <b>080320</b> , 080328 <b>080330</b> , <b>080430</b> , 080602, <b>080707</b> , <b>080723A</b>
Oddball	050505, <b>050716</b> , <b>050717</b> , <b>050724</b> , <b>051001</b> , <b>051117A</b> , <b>060111B</b> , <b>060124</b> , <b>060202</b> , <b>060211A</b> <b>060306</b> , <b>060510B</b> , <b>060522</b> , 060801, <b>060813</b> , <b>061007</b> , <b>061110A</b> , <b>070103</b> , <b>070110</b> , <b>070208</b> <b>070223</b> , <b>070412</b> , <b>070419A</b> , <b>070508</b> , <b>070521</b> , <b>070616</b> , <b>070621</b> , <b>071025</b> , <b>071031</b> , <b>071227</b> 080123, <b>080307</b> , <b>080319B</b> , 080319C, 080411, <b>080413B</b> , <b>080503</b> , 080506, <b>080523</b> , 080603B <b>080605</b> , <b>080607</b> , <b>080613B</b> , <b>080714</b> , <b>080721</b>

**Table 11.** Classification of GRB light curves. Bursts in bold are those for which a canonical light curve would be discernable. See text for details.

## REFERENCES

- Abbey, A.F., et al., 2005, in ESA-SP 604, 'The X-ray Universe 2005', 943
- Anders E., Grevesse N., *Geochimica et Cosmochimica Acta* 53, 197
- Barthelmy S.D., et al., 2005a, *Sp. Sci. Rev.*, 120, 143
- Barthelmy S.D., et al., 2005b, *ApJ*, 635, L133
- Burrows, D.N., et al., 2005, *Sp. Sci. Rev.*, 120, 165
- Butler N.R., 2007, *AJ*, 133, 1027
- Butler N.R., Kocevski D., 2007a, 668, 400
- Butler N.R., Kocevski D., 2007b, 663, 407
- Campana S., et al., 2006, *Nature*, 442, 100
- Chincarini G., et al., 2007, *ApJ*, 671, 1903
- Cusumano G., et al., 2007, *A&A*, 462, 73
- Curran P.A., van der Horst A.J., Wijers R.A.M.J., 2008a, *MNRAS*, 386, 859
- Curran P.A., Starling R.L.C., O'Brien P.T., Godet, O., van der Horst A.J., Wijers R.A.M.J., 2008b, *A&A*, 487, 533
- de Pasquale et al., 2008, *MNRAS*, in press (arXiv: 0809.4688)
- Evans P.A., et al., 2007, *A&A*, 469, 379
- Evans P.A., Beardmore A.P., Osborne J.P., Goad M.R., Kennea J., Burrows D.N., Gehrels N., 2008a, *GCN Circ* 7328
- Evans P.A., Osborne J.P., Burrows D.N. and Barthelmy S.D., 2008b, *GCN Circ* 7955
- Falcone A.D., et al., 2006, *ApJ*, 641, 1010
- Falcone A.D., et al., 2007, *ApJ*, 671, 1912
- Gehrels N., et al. 2004, *ApJ*, 611, 1005
- Ghisellini G., Ghirlanda G., Nava L., Firmani C., 2007, *ApJ*, 658, L75
- Ghisellini G., Nardini M., Ghirlanda G., Celotti A., 2008, *MNRAS*, in press (arXiv:0811.1038)
- Goad M.R., et al., 2006, *A&A*, 449, 89
- Goad M.R., et al., 2007, *A&A*, 476, 1401 (G07)
- Godet O., et al., 2009, *A&A*, in press (arXiv:0811.4246)
- Hill J.E., et al., 2005, *SPIE*, 5898, 313
- Kalberla, P.M.W., Burton W.B., Hartmaan, D., Arnal E.M., Bajaja E., Morras R., Pöppel W.G.L., 2005, *A&A*, 440, 775
- Kennea J.A., et al., 2005, *SPIE*, 5898, 329
- Kocevski D., Butler N., Bloom J.S., 2007, *ApJ*, 667, 1024
- Kraft, R.P., Burrows, D.N., Nousek, J.A., et al. 1991, *ApJ*, 374, 344
- Liang E., et al., 2006, *ApJ*, 646, 351
- Moretti, A., et al., 2005, *SPIE*, 5898, 360
- Nousek J.A., et al., 2006, *ApJ*, 642, 389
- O'Brien P.T., et al., 2004, *ApJ*, 647, 1213
- Panaitescu A., Mészáros P., Gehrels N., Burrows D., Nousek J., 2006, *MNRAS*, 366, 1357
- Piran T., 1999, *Rev. Mod. Phys.* 76, 1143
- Rees M.J., Mészáros P., 1994, *ApJ*, 430, L93
- Romano, P., et al., 2006, *A&A*, 456, 917
- Roming P.W.A. et al., 2005, *Sp. Sci. Rev.*, 120, 95
- Roming P.W.A. et al., 2009, *ApJ*, 690, 163
- Sakamoto T., 2008, *ApJS*, 175, 179
- Sala G., Greiner J., McBreen S., Kruehler T., Esquej P.M., 2008, *GCN Circ* 8078
- Sari R., Piran T., Narayan R., 1998, *ApJ*, 497, L17
- Shao L., Dai Z.G., 2007, *ApJ*, 660, 1319
- Shen R.-F., Willingale R., Kumar P., O'Brien P.T., Evans P.A., 2008, *MNRAS*, in press (arXiv:0806.3541)
- Starling R.L.C., van der Horst A.J., Rol E., Wijers R.A.M.J., Kouveliotou C., Wiersema K., Curran P.A., Weltevrede P., 2008, *ApJ*, 672, 433
- Tagliaferri G., et al., 2005, *Nature*, 436, 985
- Uhm Z., Beloborodoc A.M., 2007, *ApJ*, 665, L93
- Vaughan, S., et al., 2006, *ApJ*, 638, 920
- Willingale R., 2007, *ApJ*, 662, 1093
- Zhang B., 2007, *Chin. J. Astron. Astrophys.* 7, 1
- Zhang B., Fan Y.Z., Dyks J., Kobayashi S., Mészáros, P., Burrows D.N., Nousek J.A., Gehrels N., 2006, *ApJ*, 642, 354
- Zhang B., Mészáros P., 2004, *IJMPA*, 19, 2385